Modular molecular gels

Control over design, formation and properties

Poolman, Jos

DOI
10.4233/uuid:5dac3509-019c-40c8-a1bf-7db9b7b41f6d

Publication date
2017

Document Version
Final published version

Citation (APA)
Poolman, J. (2017). *Modular molecular gels: Control over design, formation and properties*. [Dissertation (TU Delft), Delft University of Technology]. https://doi.org/10.4233/uuid:5dac3509-019c-40c8-a1bf-7db9b7b41f6d

Important note
To cite this publication, please use the final published version (if applicable).
Please check the document version above.

Modular molecular gels:
control over design, formation and properties

Proefschrift

Ter verkrijging van de graad van doctor
aan de Technische Universiteit Delft,
op gezag van Rector Magnificus
prof. ir. K.C.A.M. Luyben,
voorzitter van het College voor Promoties,
in het openbaar te verdedigen op

vrijdag 17 maart 2017 om 15:00 uur
door

Jozef Marie POOLMAN

Master of Science in Chemistry
geboren te Schiedam, Nederland

Dit proefschrift is goedgekeurd door:

Promotor: Prof. dr. J.H. van Esch

Copromotor: Dr. R. Eelkema

Samenstelling promotiecommissie:

Rector Magnificus	Technische Universiteit Delft	voorzitter
Prof. dr. J.H. van Esch	Technische Universiteit Delft	promotor
Dr. R. Eelkema	Technische Universiteit Delft	copromotor

Onafhankelijke leden:

Prof. dr. E.J.R. Sudhölter	Technische Universiteit Delft
Prof. dr. U. Hanefeld	Technische Universiteit Delft
Prof. dr. N.H. Katsonis	Universiteit Twente
Prof. dr. A. Kros	Universiteit Leiden
Prof. dr. A. Pich	RWTH Aachen University

The work described in this thesis was carried out in the Advanced Soft Matter group (formerly known as Self-Assembling Systems) at the Delft University of Technology. Fund was provided by an ECHO Project grant received from the Netherlands Organisation for Scientific Research (NWO).

ISBN:

Gedrukt door: Gildeprint BV, Enschede

Cover design: Maarten Ebbelinghaus

“It is only through deliberate practice at what you cannot do, that you will turn into the expert you desire to become.”

-Brian Buirge, Creative director at Good Fucking Design Advice

Table of contents

General introduction 1

Abstract

Self-assembly is a key tool in the design of smart materials. The research of low-molecular-weight gels research as smart materials has largely focused on the final assembly and its resulting properties. One major problem in this field is the lack of understanding of the relation between the initial gelator molecule and the final assembled hydrogel. Moreover, the rate of assembly towards the hydrogel has proven to be of major influence on the mechanical properties as well, but its relation is not well understood.

This thesis describes the research of using covalent bond formation in making new low-molecular-weight gelators. This new approach allows us to control the rate of building block formation and the molecular design of the gelator molecule more effectively. The use of this new approach is therefore an interesting addition in the design towards new smart materials and creates an improved approach towards the design of smart materials.

Introduction

In recent years we have witnessed the emergence of smart materials.[1] Applications can be found in various fields such as, neuronal networks[2], drug delivery[3], explosive detection[4], tissue engineering[5] and optoelectronics[6]. Many of these applications are based on molecular materials which share a key tool, namely self-assembly. It is because of self-assembly that these fields have been able to progress in recent years.[7]

Self-assembly is the spontaneous formation of large organized structures starting from small components.[8] These small components can interact with each other by means of attractive and repulsive forces such as Vanderwaals forces, electrostatic interactions, dipole-dipole interactions and π-π stacking. These forces result from functionalities that are present in the structure of each of these small components. According to this precept, the small components are embedded with 'instructions' that drives them towards its assembled state which corresponds to thermodynamic equilibrium.[9–11]

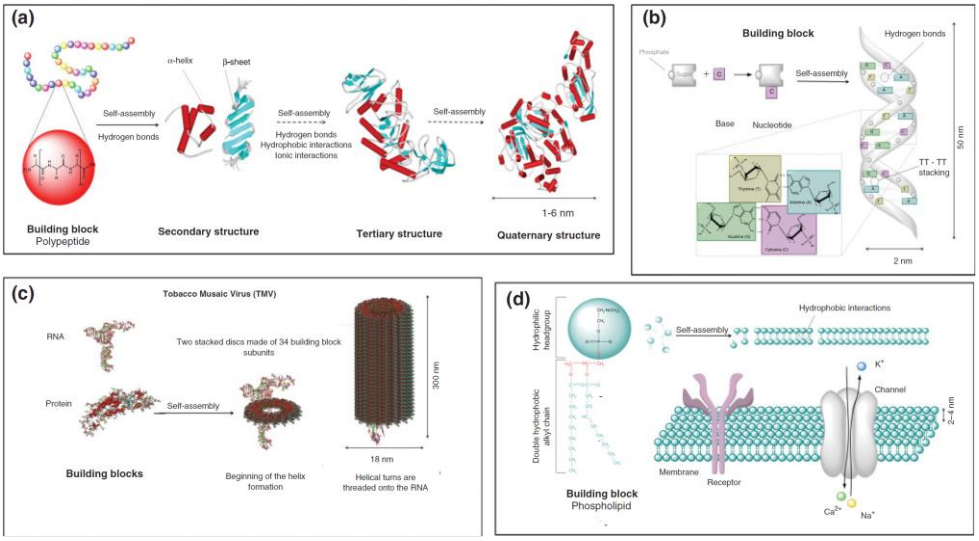

Figure 1 | Examples of biological self-assembled structures showing the building blocks and the relevant interactions involved in the self-assembly process. (a) Protein folding (b) double-stranded DNA (c) Tobacco mosaic virus (TMV). (d) Cell membrane. Reproduced from reference.[12]

Examples of self-assembly are widespread in nature where small components in the form of biomolecules are used for a multitude of self-assembling processes **(Fig. 1)**. [12] Science eventually followed by creating artificial systems. The field of chemistry has successfully applied self-assembly for the design of a wide array of supramolecular structures such as monolayers[13], metal-organic frameworks[14], DNA-origami[15], amphiphiles[16] and gelators[17] **(Fig. 2)**.

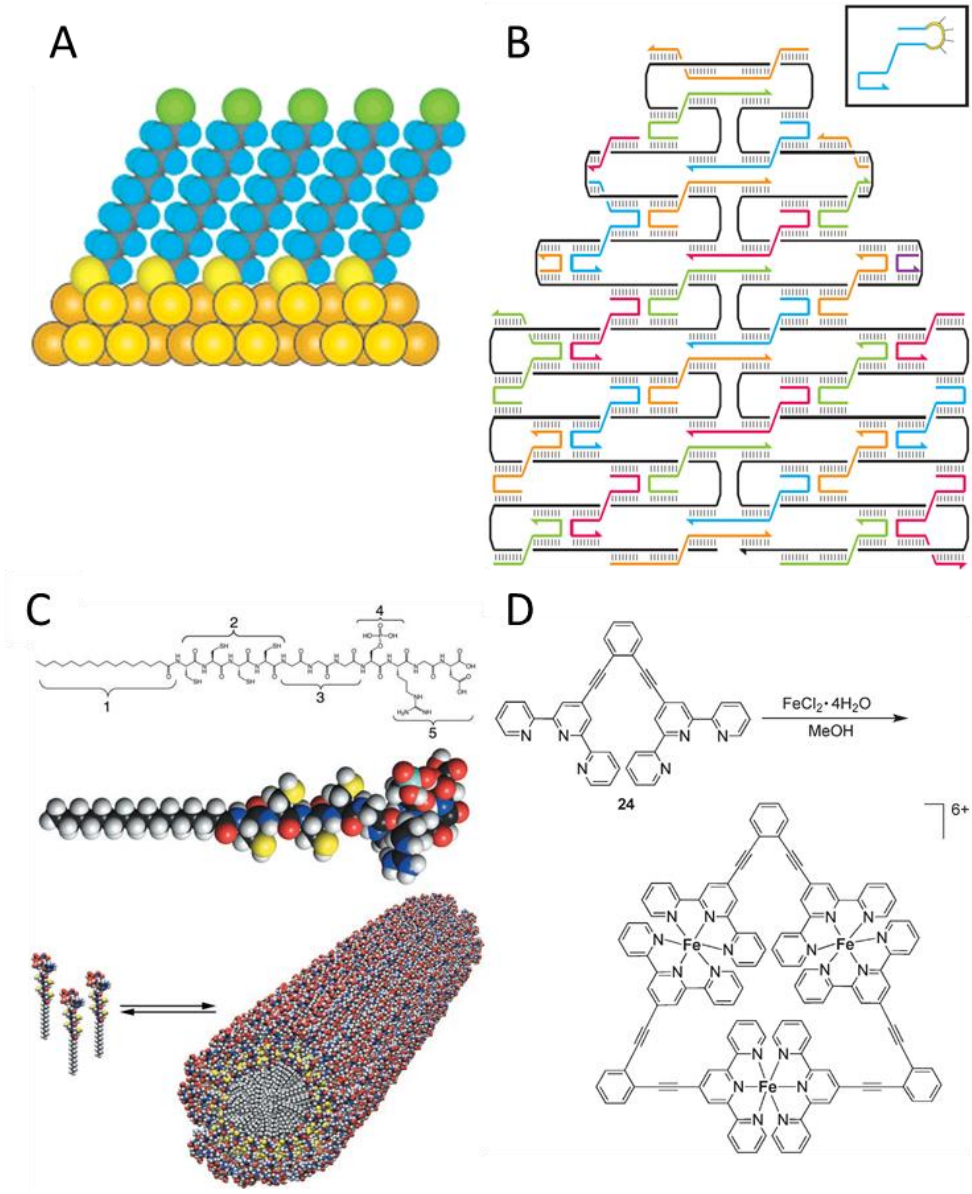

Figure 2 | Examples of molecular self-assembled structures showing the building blocks of the self-assembly process. **(A)** Thiol-functionalized alkyl chains absorb and align on a gold surface. **(B)** DNA origami assembled from a single strand moved into shape by smaller strands. **(C)** Peptide amphiphile assembling into a rod-like structure. **(D)** Ter-pyridine building block coordinates to iron forming a triangular metal-organic framework.

As shown in the examples above, the use of weak non-covalent interactions make it possible for components to assemble. These interactions can be broken reversibly due to the small difference between the energy levels of the assembled state and disassembled state. This means that when the assembled state is disturbed thermodynamics are able to drive the systems to return to its assembled state.[18]

Instead of reaching the original thermodynamic equilibrium, another so-called "metastable" state can be obtained, usually described as a kinetic trap. Such kinetic traps are states different from thermodynamic equilibrium, yet they are able to exist for a period of time.[19] Thermodynamic equilibrium will eventually be reached. The ability to obtain different states from one self-assembling system makes it possible to obtain different properties depending on the current state. The ability to switch between these states is described as dynamic behaviour, which can result in properties such as responsiveness, self-healing or adaptation .[20,21]

Low-molecular-weight gels

Low-molecular-weight gels (LMWGs) are excellent proven platforms for the application of self-assembly.[22] They are constituted of small components, also known as gelator molecules, which self-assemble and subsequently form into fibres in solution.[23] Above a certain concentration, the formed fibres entangle into a continuous network which interacts with the solvent and fixating it, resulting in a gel.

LMWGs can be obtained from various categories of gelator molecules **(Fig. 3)**. Derivatives of urea, sugars and peptides to name only a few, have successfully demonstrated their ability to gelate in water.[17] These examples provide us with a general explanation of how LMWGs are constituted and as such are able to gelate in water. A gelator molecule should feature hydrophilicity to interact with the aqueous phase and prevent crystallization. Also, hydrophobicity is required in order to promote cohesion and directionality to induce one-dimensional alignment to form fibres. The assembled fibres result in exposure of the hydrophilic part and shielding of the hydrophobic part.

Despite the plurality and ubiquity of different LMWG designs, the relation between the molecular design and the gelation properties is not properly understood. Rational design, such as the guidelines described above, is currently used in the design of new LMWGs.[24] This method of trial and error leaves much to unpredictability. Minor changes of the molecular design can either result in entirely different assemblies with different properties or, in the worst case, no self-assembly at all. The lack of understanding between molecular design and final assembly creates a major obstacle in the development of new gelator molecules.

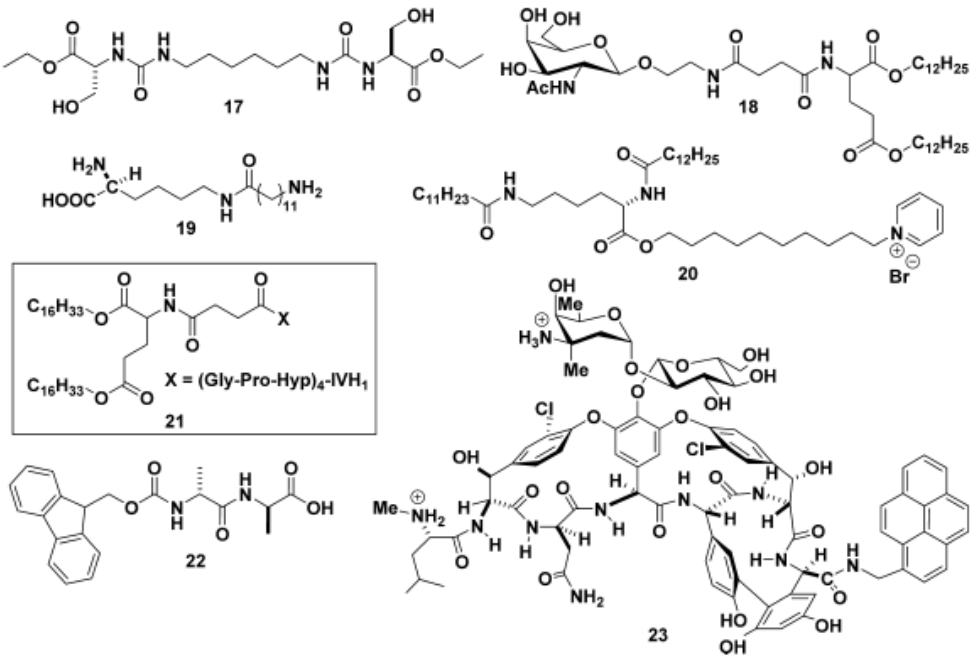

Figure 3 | Examples of molecular structures of hydrogelators. Reproduced from reference.[17]

A gel is constituted of a fibre network which determines its mechanical properties.[25] Cryo-transmission electron microscopy (cryo-TEM) gives us direct insight into the morphology of the fibre network.[26] From this direct imaging, we can observe morphological properties at the level of individual fibres such as fibre thickness, bundling, chirality, or the presence of micro-domains. These morphological properties contribute to the mechanical properties presented by the bulk material.

Mechanical properties of the fibre network, such as elasticity, stiffness and self-healing properties are determined using rheology.[27,28] These properties contribute to the applicability of a hydrogel. For example, a hydrogel must be stiff enough and able to support itself. Also, applying stress determines self-healing capabilities e.g. after a gel is moulded into shape.

The major drawback of LMWGs are their poor mechanical performance.[29,30] Since LMWGs are based on physical bonds, there is little flexibility in the fibre structure without breaking of these bonds. The functional groups are stacked in order to enforced directionality which form the fibres, meaning that disturbance of the gelator molecules would break the fibres. On the other hand, polymer gels generally rely more on chemical bonds in the form of long stretchable polymer chains.[29,31,32] Polymer gels have shown more resistance to mechanical deformation as compared to LMWGs.[27] However, it is more laborious to modify polymers then small molecules. Therefore, any mechanical improvement on LMWGs is considered of interest in increasing their application.

Triggers & kinetics

Although self-assembly is a spontaneous process, the assembly of LMWGs requires a form of initiation. The most common process is called a heat-cool cycle. It consists of heating and cooling, inducing supersaturation followed by gelation **(Fig. 4a, T2)**. First, the gelator molecules are dissolved by heating. Subsequently, the gelator molecules are forced to self-assemble by the shift from high solubility to poor solubility due to the decreasing temperature, yielding the assembled structure.[33] This procedure is but one of the many triggers which is used in order to initiate gelation.

The gelation process can also be initiated using a wide range of other triggers. Physical triggers exist such as sonication or UV-Vis irradiation. Chemical triggers such as changes in pH or salt concentrations and enzymes are used as well.[34] In these cases, the gelator molecule is obtained by converting a non-assembling precursor molecule into a gelator molecule **(Fig. 4a, T1)**. The concentration of gelator molecules increases and gelation takes place.

The majority of triggers activate all the building blocks at once. For example, a large excess of acid is introduced in order to protonate all the precursor molecules, converting them into building blocks and shifting towards the thermodynamic equilibrium of the self-assembled state **(Fig. 4b)**.

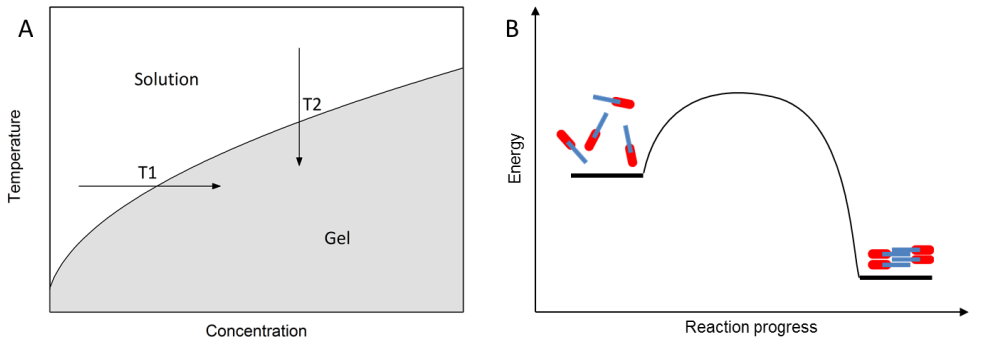

Figure 4 | Transition diagrams of the gelation process. **(A)** Sol-gel phase diagram. **T1** depicts the increase of gelator molecule concentration by conversion of a precursor. **T2** depicts the decrease in temperature of a heat-cool cycle. In both cases, gelation occurs upon crossing of the phase boundary, shifting towards the gel phase. **(B)** Energy diagram depicting the self-assembly of separate building blocks. The self-assembled state is energetically more favourable but an energy barrier must be overcome first.

However, this is not always the case. The trigger does not only initiate the gelation process, it can also determine the rate at which the entire gelation process takes place. The trigger has direct effect on the rate of building block formation which in turn affects the subsequent gelation process and final gel structure. [35,36] In this case, gelation becomes a kinetically controlled process. By influencing the kinetics, different properties can be obtained by reaching different kinetically trapped states.

The use of enzymes to trigger gelation is one way to control the rate of formation.[37,38] For example, Ulijn et al. demonstrated that by varying the amount of enzyme the rate of gelation could be controlled **(Fig. 5)**.[39–41] Similar results were obtained by varying the pH for the gelation of Fmoc-diphenylalanine. [42] Xu et al. demonstrated that varying of the pH not only changed the rate at which gelation took place but also influenced the mechanical properties of the final assembly. Different gels with different storage moduli were obtained, resembling different kinetically trapped states which can be reached.[43]

Control over kinetics proves to be a useful tool in creating different material properties starting from one gelator molecule. However, few examples exist in the field of hydrogels. In the field of self-assembly in general, examples of controlling the kinetics of self-assembly processes have been very sparse. [44,45]

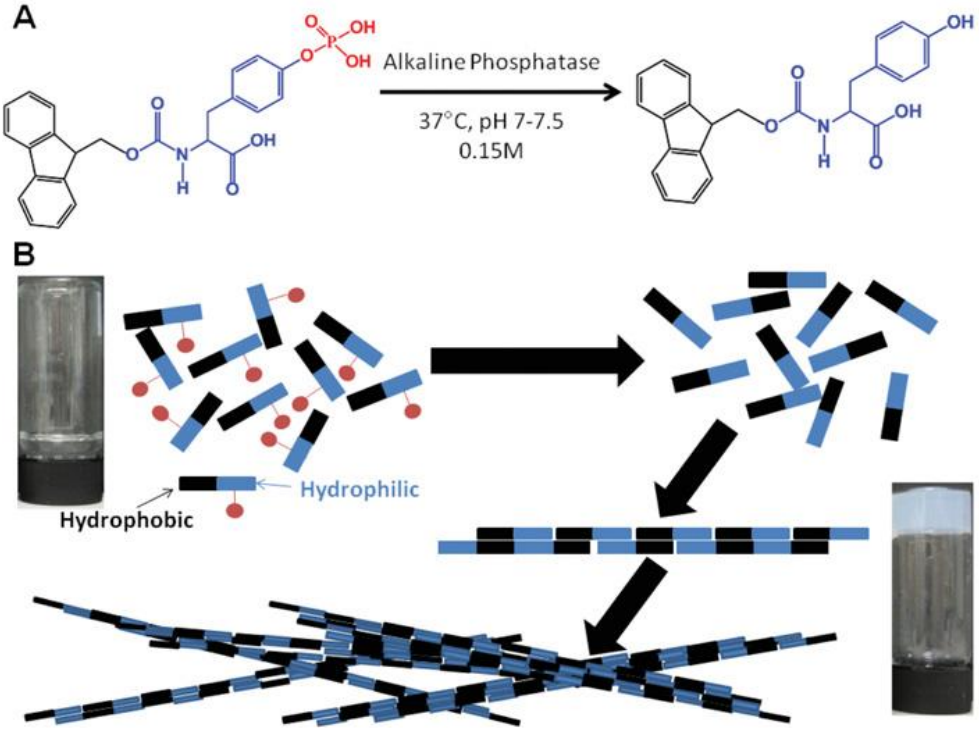

Figure 5 | Enzyme triggered self-assembly of Fmoc-tyrosine. (**A**) Schematic representation of Fmoc-tyrosine phosphate by alkaline phosphatase. (**B**) Proposed reaction and self-assembly of Fmoc-tyrosine following dephosphorylation. Insets show the solution of Fmoc-tyrosine phosphate before enzyme addition and the stable self-supporting hydrogel of Fmoc-tyrosine following dephosphorylation. Reproduced from reference.[43]

Research aim

LMWGs are a useful material with many different applications. However, the relation between the initial building block and the final assembled structure and its properties is not fully understood.

How does the initial building block influence the final assembled structure and its properties? New designs for new molecular materials are continuously confronted with unpredictability. For an initial building block, it is important to understand how the structure influences the properties of the final assembled structure.

How does the rate of building block formation influence the final assembled structure and its properties? The effect of the rate of building block formation on the assembled structure is not yet fully understood. In order to have more understanding, control over the rate of formation is necessary.

If we wish to progress in the design of new materials, we have to tackle a challenge which is twofold: control over the molecular design and control over the rate of building block assembly.

We propose the design of new LMWGs by means of covalent bond formation. Covalent bonds are an excellent candidate for catalysis, giving us control over building block formation. Simultaneously, we can form larger structures in-situ from multiple reactive precursor molecules, allowing to perform a systematic library approach of different gelator designs.[46,47]

Through this approach we can use control over catalysis to improve control over material properties while keeping the molecular design intact. [38,48,49] According to this strategy, we can change the material properties while avoiding unpredictability up to a certain level.

Covalent bond formation requires the use of multiple reactive precursor molecules in order to form a gelator molecule. Designs of reactive precursor molecules with systematic variations will allow us to better understand the effects of gelator designs on the material properties. Instead having to design completely new gelator molecules, we now have a design which can easily be tuned using different reactive precursor molecules. The use of this approach allows us to modify our gelator design more gradually by mixing in different ratios of reactive precursor molecules. New functionalities can be introduced more easily as well. This approach introduces an increased level of control which brings us closer to tailor made smart materials in the form of LMWGs.

Outline of this thesis

This thesis describes the experimental work of a LMWG system based on dynamic hydrazone bond formation. This system is able to form different aggregates from the same gelator molecule as well as functionalized hydrogels through the introduction of multiple precursor molecules.

Chapter 2 elaborately describes the synthetic steps towards the preparation of the hydrogelator precursor molecules. Next, we explain various analytical experiments such as rheology and microscopy in order to characterize the gel network and its mechanical properties. This protocol is written in detail including a troubleshooting section, making it a comprehensive tutorial article for fellow scientists who are working in this field.

Chapter 3 describes the results obtained from using a chemically catalysed hydrogelator system. The hydrogelator is subjected to different catalytic conditions revealing different rates of gelation. The different rates of gelation yield large differences in mechanical properties and fibre morphology.

Chapter 4 investigates the combination of different functional molecules in obtaining different hydrogelator systems. First, a library approach is perceived over a range of corresponding gelator precursors, revealing trends in dependence of the gelator structure. Secondly, functionalities are introduce by adding chemically functional molecules, creating an entire toolbox in which the hydrogel network as a whole can be used for a wide range of applications.

Chapter 5 explores the functionalization of the gel network by using functionalized polymers. PEG-polymers are added to induce chemical crosslinking of the gel network resulting in control over the physical properties such as the storage modulus as well as resistance towards mechanical strain.

Chapter 6 is an exploratory study into the use of functionalized dextran to enhance the hydrogel network's mechanical properties. The introduction of dextran enables the use of top-down design of functionalized commercial polymers.

References

1. Lutz, J.-F., Lehn, J.-M., Meijer, E. W. & Matyjaszewski, K. From precision polymers to complex materials and systems. *Nat. Rev. Mater.* **1,** 16024 (2016).
2. Avizienis, A. V. *et al.* Neuromorphic Atomic Switch Networks. *PLoS ONE* **7,** e42772 (2012).
3. Swaminathan, S. *et al.* Intracellular Guest Exchange between Dynamic Supramolecular Hosts. *J. Am. Chem. Soc.* **136,** 7907–7913 (2014).
4. Dey, N., Samanta, S. K. & Bhattacharya, S. Selective and Efficient Detection of Nitro-Aromatic Explosives in Multiple Media including Water, Micelles, Organogel, and Solid Support. *ACS Appl. Mater. Interfaces* **5,** 8394–8400 (2013).
5. Skilling, K. J. *et al.* Insights into low molecular mass organic gelators: a focus on drug delivery and tissue engineering applications. *Soft Matter* **10,** 237 (2014).
6. Kaafarani, B. R. Discotic Liquid Crystals for Opto-Electronic Applications † ‡. *Chem. Mater.* **23,** 378–396 (2011).
7. Busseron, E., Ruff, Y., Moulin, E. & Giuseppone, N. Supramolecular self-assemblies as functional nanomaterials. *Nanoscale* **5,** 7098 (2013).
8. Whitesides, G. M. Self-Assembly at All Scales. *Science* **295,** 2418–2421 (2002).
9. Whitesides, G., Mathias, J. & Seto, C. Molecular self-assembly and nanochemistry: a chemical strategy for the synthesis of nanostructures. *Science* **254,** 1312–1319 (1991).
10. Rubenstein, M., Cornejo, A. & Nagpal, R. Programmable self-assembly in a thousand-robot swarm. *Science* **345,** 795–799 (2014).
11. Zhang, S. Fabrication of novel biomaterials through molecular self-assembly. *Nat. Biotechnol.* **21,** 1171–1178 (2003).
12. Mendes, A. C., Baran, E. T., Reis, R. L. & Azevedo, H. S. Self-assembly in nature: using the principles of nature to create complex nanobiomaterials: Self-assembling in nature. *Wiley Interdiscip. Rev. Nanomed. Nanobiotechnol.* **5,** 582–612 (2013).
13. Love, J. C., Estroff, L. A., Kriebel, J. K., Nuzzo, R. G. & Whitesides, G. M. Self-Assembled Monolayers of Thiolates on Metals as a Form of Nanotechnology. *Chem. Rev.* **105,** 1103–1170 (2005).
14. Chakrabarty, R., Mukherjee, P. S. & Stang, P. J. Supramolecular Coordination: Self-Assembly of Finite Two- and Three-Dimensional Ensembles. *Chem. Rev.* **111,** 6810–6918 (2011).
15. Rothemund, P. W. K. Folding DNA to create nanoscale shapes and patterns. *Nature* **440,** 297–302 (2006).
16. Hartgerink, J. D. Self-Assembly and Mineralization of Peptide-Amphiphile Nanofibers. *Science* **294,** 1684–1688 (2001).
17. Du, X., Zhou, J., Shi, J. & Xu, B. Supramolecular Hydrogelators and Hydrogels: From Soft Matter to Molecular Biomaterials. *Chem. Rev.* **115,** 13165–13307 (2015).
18. Aida, T., Meijer, E. W. & Stupp, S. I. Functional Supramolecular Polymers. *Science* **335,** 813–817 (2012).
19. Mattia, E. & Otto, S. Supramolecular systems chemistry. *Nat. Nanotechnol.* **10,** 111–119 (2015).
20. White, S. R. *et al.* Restoration of Large Damage Volumes in Polymers. *Science* **344,** 620–623 (2014).
21. Wojtecki, R. J., Meador, M. A. & Rowan, S. J. Using the dynamic bond to access macroscopically responsive structurally dynamic polymers. *Nat. Mater.* **10,** 14–27 (2011).
22. Weiss, R. G. The Past, Present, and Future of Molecular Gels. What Is the Status of the Field, and Where Is It Going? *J. Am. Chem. Soc.* **136,** 7519–7530 (2014).
23. Terech, P. & Weiss, R. G. Low Molecular Mass Gelators of Organic Liquids and the Properties of Their Gels. *Chem. Rev.* **97,** 3133–3160 (1997).
24. van Esch, J. H. We Can Design Molecular Gelators, But Do We Understand Them? †. *Langmuir* **25,** 8392–8394 (2009).
25. Chen, L. *et al.* Tuneable mechanical properties in low molecular weight gels. *Soft Matter* **7,** 9721 (2011).
26. Boekhoven, J., van Rijn, P., Brizard, A. M., Stuart, M. C. A. & van Esch, J. H. Size control and compartmentalization in self-assembled nano-structures of a multisegment amphiphile. *Chem. Commun.* **46,** 3490 (2010).
27. Yan, C. & Pochan, D. J. Rheological properties of peptide-based hydrogels for biomedical and other applications. *Chem. Soc. Rev.* **39,** 3528 (2010).
28. Menger, F. M. & Caran, K. L. Anatomy of a Gel. Amino Acid Derivatives That Rigidify Water at Submillimolar Concentrations. *J. Am. Chem. Soc.* **122,** 11679–11691 (2000).

29. Cornwell, D. J. & Smith, D. K. Expanding the scope of gels – combining polymers with low-molecular-weight gelators to yield modified self-assembling smart materials with high-tech applications. *Mater Horiz* **2,** 279–293 (2015).
30. Way, A. E. *et al.* Enhancing the Mechanical Properties of Guanosine-Based Supramolecular Hydrogels with Guanosine-Containing Polymers. *Macromolecules* **47,** 1810–1818 (2014).
31. Dai, X. *et al.* A Mechanically Strong, Highly Stable, Thermoplastic, and Self-Healable Supramolecular Polymer Hydrogel. *Adv. Mater.* **27,** 3566–3571 (2015).
32. Deng, C. *et al.* Mechanically strong and stretchable polyurethane–urea supramolecular hydrogel using water as an additional in situ chain extender. *RSC Adv.* **4,** 24095 (2014).
33. Weiss, R. & Terech, P. *Molecular Gels*. (Springer, 2006).
34. Segarra-Maset, M. D., Nebot, V. J., Miravet, J. F. & Escuder, B. Control of molecular gelation by chemical stimuli. *Chem Soc Rev* **42,** 7086–7098 (2013).
35. Yang, Z., Liang, G. & Xu, B. Enzymatic control of the self-assembly of small molecules: a new way to generate supramolecular hydrogels. *Soft Matter* **3,** 515 (2007).
36. Toledano, S., Williams, R. J., Jayawarna, V. & Ulijn, R. V. Enzyme-Triggered Self-Assembly of Peptide Hydrogels via Reversed Hydrolysis. *J. Am. Chem. Soc.* **128,** 1070–1071 (2006).
37. Yang, Z. *et al.* Enzymatic Formation of Supramolecular Hydrogels. *Adv. Mater.* **16,** 1440–1444 (2004).
38. Yang, Z. & Xu, B. A simple visual assay based on small molecule hydrogels for detecting inhibitors of enzymes. *Chem. Commun.* 2424 (2004). doi:10.1039/b408897b
39. Schnepp, Z. A. C., Gonzalez-McQuire, R. & Mann, S. Hybrid Biocomposites Based on Calcium Phosphate Mineralization of Self-Assembled Supramolecular Hydrogels. *Adv. Mater.* **18,** 1869–1872 (2006).
40. Tang, C., Smith, A. M., Collins, R. F., Ulijn, R. V. & Saiani, A. Fmoc-Diphenylalanine Self-Assembly Mechanism Induces Apparent p K_a Shifts. *Langmuir* **25,** 9447–9453 (2009).
41. Thornton, K., Smith, A. M., Merry, C. L. R. & Ulijn, R. V. Controlling stiffness in nanostructured hydrogels produced by enzymatic dephosphorylation. *Biochem. Soc. Trans.* **37,** 660–664 (2009).
42. Raeburn, J., Zamith Cardoso, A. & Adams, D. J. The importance of the self-assembly process to control mechanical properties of low molecular weight hydrogels. *Chem. Soc. Rev.* **42,** 5143 (2013).
43. Yang, Z., Liang, G. & Xu, B. Enzymatic Hydrogelation of Small Molecules. *Acc. Chem. Res.* **41,** 315–326 (2008).
44. Stano, P. & Luisi, P. L. Achievements and open questions in the self-reproduction of vesicles and synthetic minimal cells. *Chem. Commun.* **46,** 3639 (2010).
45. Takakura, K., Toyota, T. & Sugawara, T. A Novel System of Self-Reproducing Giant Vesicles. *J. Am. Chem. Soc.* **125,** 8134–8140 (2003).
46. Lehn, J.-M. Dynamic Combinatorial Chemistry and Virtual Combinatorial Libraries. *Chem. - Eur. J.* **5,** 2455–2463 (1999).
47. Rowan, S. J., Cantrill, S. J., Cousins, G. R. L., Sanders, J. K. M. & Stoddart, J. F. Dynamic Covalent Chemistry. *Angew. Chem. Int. Ed.* **41,** 898–952 (2002).
48. Williams, R. J., Mart, R. J. & Ulijn, R. V. Exploiting biocatalysis in peptide self-assembly. *Biopolymers* **94,** 107–117 (2010).
49. Williams, R. J. *et al.* Enzyme-assisted self-assembly under thermodynamic control. *Nat. Nanotechnol.* **4,** 19–24 (2008).

Variable gelation time and stiffness of low-molecular-weight hydrogels through catalytic control over self-assembly

2

Abstract

This protocol details the preparation of LMWGs in which the gelation time and mechanical stiffness of the final gel can be tuned with the concentration of the catalyst used in the *in situ* formation of the hydrogelator. By altering the rate of formation of the hydrazone-based gelator from two water soluble compounds-an oligoethylene functionalized benzaldehyde and a cyclohexane-derived trishydrazide in the presence of acid or aniline as catalyst, the kinetics of gelation can be tuned from hours to minutes. The resulting materials display controllable stiffness in the 5-50 kPa range. This protocol works at ambient temperatures in water, at either neutral or moderately acidic pH (phosphate buffer, pH 5) depending on the catalyst used. The hydrazide and aldehyde precursors take a total of five days to prepare. The final gel is prepared by mixing aqueous solutions of the two precursors and can take between minutes and hours to set, depending on the catalytic conditions. We also describe analysis of the hydrogels by critical gel concentration (CGC) tests, rheology and confocal laser-scanning microscopy (CLSM).

Published as:

Variable gelation time and stiffness of low-molecular-weight hydrogels through catalytic control over self-assembly

Jos M. Poolman, Job Boekhoven, Anneke Besselink, Alexandre G. Olive, Jan H. van Esch and Rienk Eelkema

Nature Protocols **9,** 977–988 (2014)

Introduction

Low-molecular-weight gels (LMWGs) or supramolecular gels are typically constructed from small molecules that assemble through non-covalent interactions into fibrous structures in solution[1,2]. Once these fibres form a network, the surrounding solvent is trapped and a gel is formed. These gels show great potential for many fields of application, including tissue engineering[3], controlled drug release[4] and the petrochemical industry. LMWGs are often prepared by heating a suspension of the gelator in the solvent until dissolution; subsequent slow cooling inducing supersaturation, which is followed by nucleation of fibre growth leading to gelation. Other methods include sonication, the protonation or deprotonation of charged groups in the gelator[5–8], the use of photolabile protecting groups[9] or the use of photochromic gelators[10]. In some cases, these methods are prohibitive to their application. For example, sonication, high temperatures or large changes in pH are not compatible with *in situ* gelation of tissue culture medium containing living cells. Also, such triggers are simply not available in some applications such as the gelation of oil spills or *in situ* formation in living tissue, which require spontaneous gelation under ambient conditions. Moreover, it can be difficult to control the mechanical strength of the resulting gel other than by changing the initial gelator concentration. Control over the stiffness of hydrogel materials is of great importance in tissue-engineering applications, in which these materials are used as cell growth scaffolds.[11]

The mechanical properties of a LMWG largely depend on the fibre density of the network and the number of cross-links between these fibres[12]. In a recent publication, we showed how the network morphology and resulting mechanical properties of a LMWG can depend on the rate of gelator formation, which in turn can be controlled by catalysis[13]. The use of catalysis in soft materials has recently shown great promise in actuator[14], controlled release[15] and self-healing[16] materials. In this protocol, we describe the preparation of these LMWGs with controllable mechanical properties and speed of gelation depending on the catalytic conditions. This protocol covers the synthesis of the building blocks of the hydrogelator, the preparation of the gels and characterization of their properties.

Central to the concept described in this paper are low-molecular-weight building blocks that by themselves are soluble in aqueous environments and do not assemble into gels. These building blocks, however, can react with each other to form a new species that does assemble into larger structured assemblies (**Fig. 1**). On a larger length scale, such assemblies can interact with each other, giving rise to a variety of material properties. The rate of formation of the covalent chemical bond between these initial building blocks can be controlled using a suitable catalyst. If the self-assembly process is faster than or comparable to the rate of assembler formation, the rate of assembly can be controlled by catalysis.

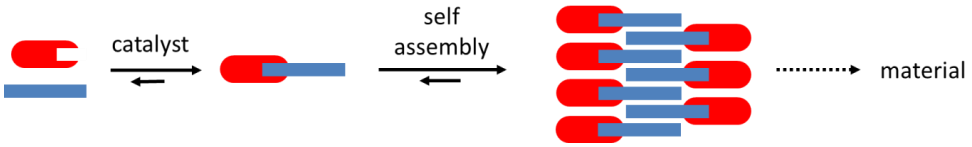

Figure 1 | Scheme of the general concept. Two building blocks react with each other under influence of a catalyst to form a self-assembling moiety that subsequently assembles into a larger assembly, ultimately leading to the formation of a material.

Although widespread in nature, reports of catalytic control over self-assembly processes are scarce in synthetic systems. Amongst the few reported cases are examples that deal with the (mostly) biocatalytic formation of hydrogels[17–26]and surfactant assemblies[27–29]. Only recently Ulijn and co-workers showed how fibre morphology of peptide-based gelators can be affected using biocatalysis.[18]

Development of the protocol

This protocol was developed to prepare LMWGs with precisely controlled mechanical properties and gelation kinetics by using catalysis. The design of the hydrogelator is based on a class of C_3-symmetric hydrogelators that were previously developed in our group[30]. These hydrogelators are based on a *cis,cis*-cyclohexane-1,3,5-triamide core (**Fig. 2**), with hydrophobic phenyl functionalities and hydrophilic oligoethylene glycols in the peripheral groups. The *cis,cis*-conformation of the central cyclohexanetriamide core induces a planar, discotic shape in the molecule. Owing to the directionality of the hydrogen-bonding amides and the hydrophobic cyclohexane and phenyl substituents, these molecules have a tendency to stack on top of one another, forming long 1D fibrous structures.

The hydrophilic oligoethylene glycol groups on the periphery of the gelator promote water solubility and interfibre repulsion, thereby preventing precipitation. In the current design, the original amide-based hydrogelator is split up into four separate molecular segments that by themselves do not assemble. *In situ* formation of a covalent bond between these precursors restores the general gelator design and induces gelation. In this design, we chose for hydrazones as the newly formed covalent bonds. This functional group has the required hydrogen-bonding amide functionality, and its formation can be controlled with either acid or nucleophilic catalysis, both in aqueous environments.

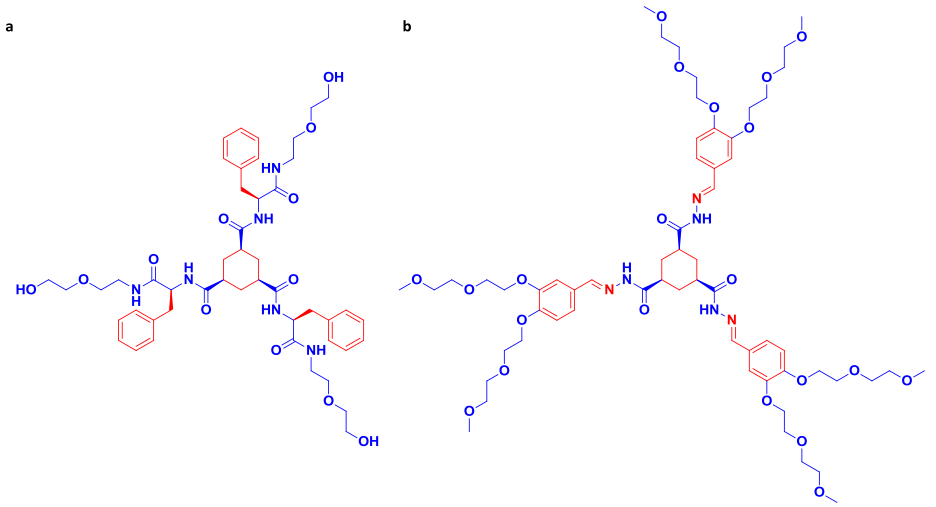

Figure 2 | Cyclohexane core gelator designs. (**a**) Original *cis,cis*-cyclohexane-1,3,5-triamide core gelator design. (**b**), Design of gelator **3** formed out of one hydrazide and three aldehyde building blocks by the formation of hydrazone bonds. Blue: Hydrophilic functional groups, Red: Hydrophobic functional groups.

Replacing the three amides by three hydrazone bonds and a slight redesign results in a hydrogelator (**3, Fig. 2b**) that can be formed by condensation of one tri-hydrazide core (hydrazide **1**) and three aldehyde functionalised side groups (aldehyde **2**) (**Fig. 3**). The rate of hydrazone formation can be enhanced by acid catalysts, or nucleophilic catalysts such as aniline[31]. Aniline can be used at physiological pH[32]. Acid catalysis of hydrazone formation works most effectively between pH 4 and 6[33]. Above pH 6, the rate enhancement is very small. Below pH 4, the equilibrium of the reaction is shifted back toward the starting materials owing to protonation of the hydrazide.

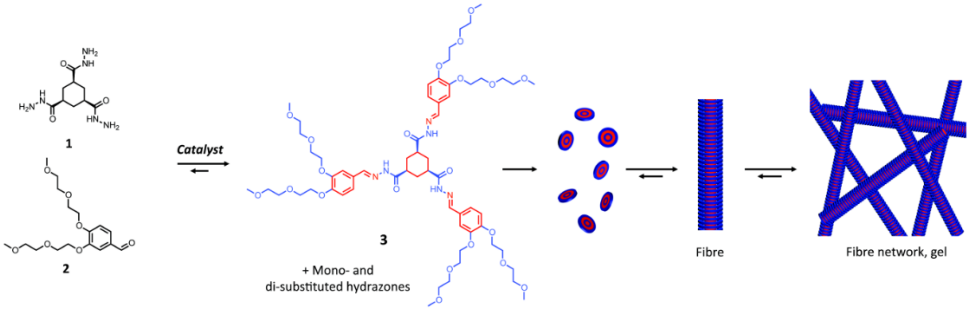

Figure 3 | Catalytic formation of trishydrazone hydrogelator **3** from soluble building blocks **1** and **2** leads to supersaturation followed by formation of fibres, which eventually cross-link to form a network that traps the surrounding solvent, leading to gelation. Blue: Hydrophilic functional groups, Red: Hydrophobic functional groups.

The two starting compounds (compounds **1** and **2** in **Fig. 3**) are both water soluble, which ensures homogeneity of the initial mixture. In a 0.1 M sodium phosphate buffer, the

hydrazide as well as the aldehyde can be dissolved up to 50 mM and at least up to 480 mM, respectively. Over time, formation of **3** leads to the formation of fibres through self-assembly at room temperature (22 ± 2°C). Above a certain threshold concentration, the CGC, these fibres eventually gel the surrounding solvent. In the current system, the rate of gel formation depends heavily on the concentration of the catalyst, being either aniline or acid (pH) (**Fig. 4**). For example, the gelation time, which is the time needed to reach a constant storage modulus G' (the storage modulus (G') and loss modulus (G") of the viscoelastic material are measures for the elastic and viscous behaviour, respectively, as determined by rheology), changed from 4.5 h at pH 7 to 10 min at pH 5. Similarly, the addition of aniline at pH 7 resulted in a substantial and aniline concentration-dependent, reduction of the gelation time (**Fig. 4**).

The CGC is a first indication of the quality of the formed network, and was found to change markedly with the catalyst content. The CGC is here defined as the threshold minimum concentration to form a gel that withstands gravity when turned upside down. Typically, the higher the quality of the network, the lower the CGC will be. In the current system, it is lowest in the pH 4-6 window, where the catalysis is most efficient (**Fig. 4e**). Both above pH 6 and below pH 4, an increase of the CGC is observed, in the latter case presumably because of an unfavourable shift in the hydrazone equilibrium. Previous studies showed that both acid and aniline do not change the CGC by simply changing the solvent quality or acting as an additive, thereby again pointing towards a relation between catalysis and the material properties.[13]

Rheology measurements showed a sharp increase in stiffness for gels prepared in the presence of catalyst (**Fig. 4c,d**). Although uncatalyzed gel at pH 7 yielded a storage modulus (G') close to a mere 6 kPa after 275 min a marked increase to 50 kPa was obtained at pH 5 in only 8 min, and an increase to 55 kPa for 10 mM of aniline was observed after less than 70 min. Any further increase of the aniline concentration resulted in a higher gelation speed, but a decrease in storage modulus was observed. HPLC analysis revealed the formation of the imine of aniline and aldehyde at high concentrations of aniline, which may be at the origin of the worsening mechanical properties.

A CLSM study showed that the morphology of the gel fibres differs substantially between pH 7 and pH 5 (**Fig. 5**). The morphology of the network changes from a poorly connected network with a marked degree of bundling of fibres at pH 7 to a well-connected and evenly distributed, dense network of heavily branched fibres at pH 5. Similar effects were observed when aniline was used as a catalyst at pH 7, up to an aniline concentration of 10 mM. In both the aniline- and the acid-catalysed scenarios, the formation of these denser networks leads to increasing mechanical stability of the gels, giving control over the gel strength by using catalysis. It should be noted that, within these experimental conditions and catalyst concentrations, the overall conversion to gelator **3** is the same in all scenarios (>95% **3** as determined by HPLC).

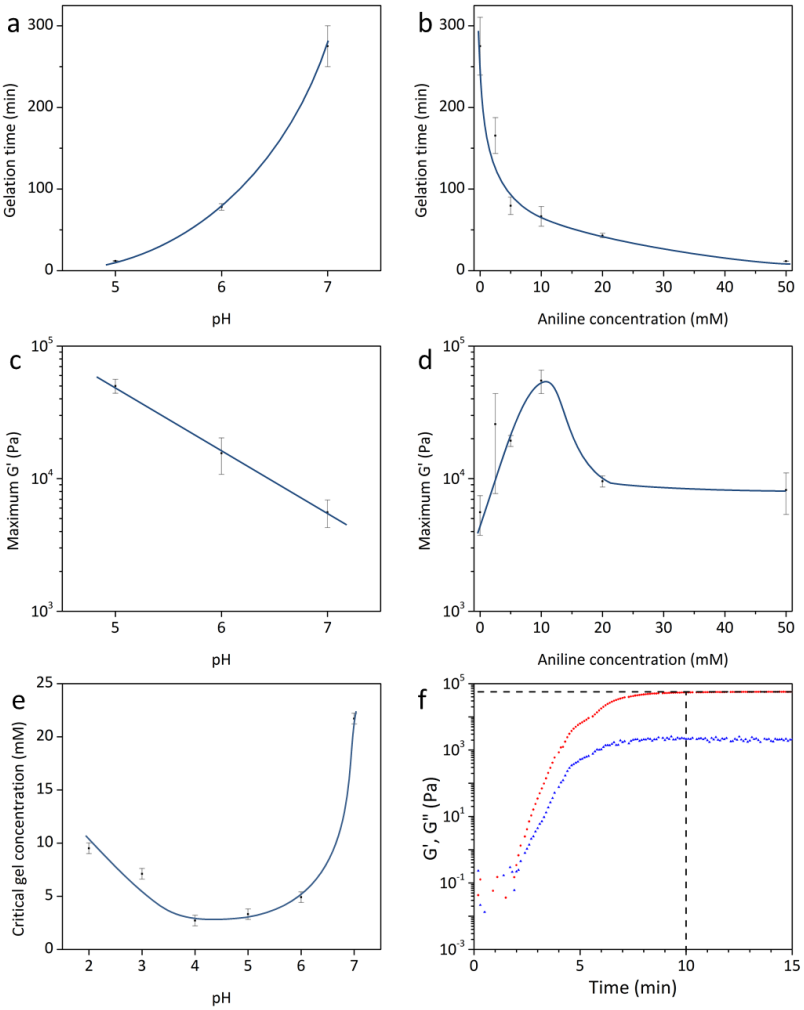

Figure 4 | Gel formation and formation dynamics depend on catalyst loading. (**a-d**) Gel formation measured by rheology: the dependence on catalyst concentration of gelation time (**a,b**) and the maximum storage modulus (G') at equilibrium (**c,d**). Errors are the standard deviation from duplicate experiments; the lines are to guide the eye. Both gelation time and maximum storage modulus show a strong dependence on the amount of added catalyst: in the acid-catalyzed scenario (**a,c**) the gelation time is reduced and the storage modulus increases with increasing catalyst concentration. (**b,d**) The aniline-catalysed samples at pH 7 show a more complex behaviour. Gelation time is reduced with increasing aniline concentration (**b**). The maximum attained storage modulus initially increases with increasing aniline concentration, but decreases again at very high aniline concentrations, most probably because of the formation of a surface-active adduct of aniline, to **2**. All samples: **1**:**2** = 1:6, [**1**] = 20 mM; 0.1 M phosphate buffer. (**e**) Dependence of the CGC on pH. The CGC is expressed as the initial concentration of **1**. A sample will flow at concentrations below the CGC, and behave as a viscoelastic solid above the CGC. (**f**) An example of a rheology measurement to determine the maximum G' and gelation time. The storage modulus (G', red) and loss modulus (G", blue) increase over time and eventually reach a plateau value. We define the gelation time as the moment that G'measures >95% of the plateau value (horizontal dashed line). In this example the plateau value is reached after 10 min (vertical dashed line).

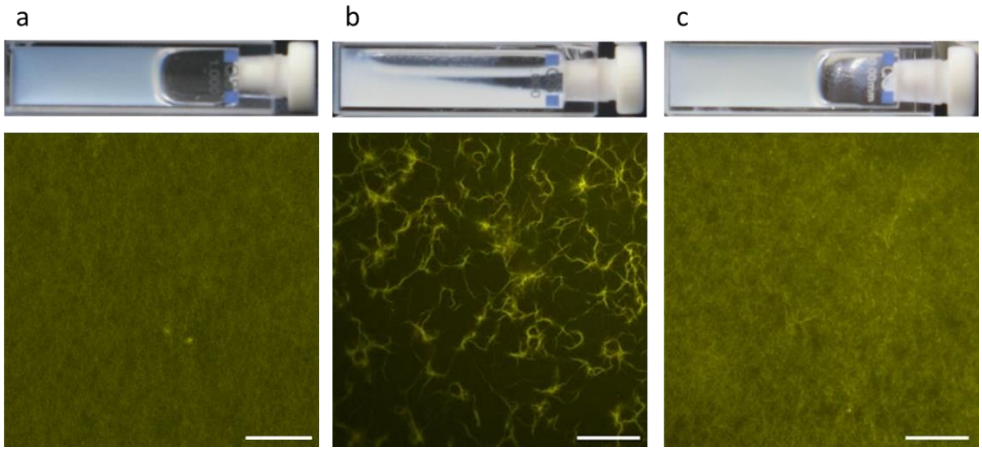

Figure 5 | Influence of catalysis on material morphology. (**a-c**)Examples of gels and their corresponding confocal laser-scanning fluorescence micrographs show differences in network morphology and fibre thickness that depend on catalyst loading during gel formation: acidic catalysis pH 5.0 (**a**); uncatalyzed pH 7.0 (**b**); and nucleophilic catalysis with 10 mM aniline at pH 7.0 (**c**). (**a**,**c**) Both catalysed samples show thin highly branched fibres forming a dense network. (**b**) In the uncatalyzed scenario, thick less-branched fibres form a poorly connected network. All samples were prepared by mixing solutions of **1** and **2** ([**1**] = 4 mM, **1**:**2** = 1:6, 0.1 M phosphate buffer) and 30 µM fluorescein-derived probe **8 (Fig. 7c)** at room temperature. Scale bars, 20 µm.

Experimental design

Synthesis of the precursors.

Compound **1** was synthesized from commercially available chemicals in three steps **(Fig. 6)**[34]. It is worth noting that the first step can be skipped by purchasing compound **4**, which is commercially available, but it is much more expensive to do so. The synthesis of the aldehyde-functionalized fluorescein-derivative **8** (**Fig. 7**), required for fluorescent labeling in the CLSM experiments, is described in ref. 13.

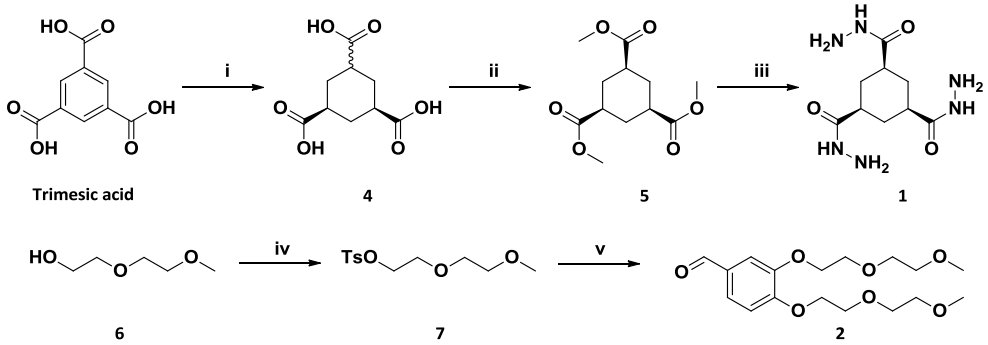

Figure 6 | Synthesis of the gelator building blocks. Reagents and conditions: (i) Pd/C, H_2O, 150°C, 60 bar, 2 h; (ii) *p*-TsOH, MeOH, reflux, 36 h, 70% isolated yield over two steps; (iii) N_2H_4, MeOH, RT, 3 h, quant; (iv) TsCl, Et_3N, THF, 0→RT, 2 h, quant; (v) 3,4-dihydroxybenzaldehyde, K_2CO_3, THF, reflux, 18 h, 83%.

Tuning gelation time and mechanical properties

Both gelation time and the mechanical properties of the gels can be controlled with the concentration and nature of the catalyst added (**Fig. 4a–d** can be used as a guide). The acid catalyst concentration is set with the pH of the phosphate buffer medium. For aniline catalysis, stock solutions of aniline pH 7.0 phosphate buffer are mixed with stock solutions of **1** and **2** to initiate gel formation.

Preparation of gels

When preparing any kind of gel, the stock solution of **1** is always added as the last ingredient to maintain an excess of **2** at all times during the process. In our hands, gels were always prepared in a 1:6 molar ratio between **1** and **2**. This means that there is an initial 1:2 functional group molar ratio of the hydrazide and aldehyde. For example, starting with 20 mM of **1** and 120 mM of **2** would yield 20 mM of hydrogelator in the final mixture accompanied by 60 mM free aldehyde in solution, which was not removed. The 1:2 functional group ratio is maintained to ensure the complete conversion of all hydrazide groups. This ratio and order of addition were originally used to prevent any possible assembly of mono- or disubstituted hydrazone products, although none was ever observed, even at lower stoichiometries. Product analysis of these mixtures by HPLC after equilibration showed >95% conversion to gelator **3**. Changing the ratio between **1** and **2** (between 3:1 and 1:1 aldehyde:hydrazide) had no major effect on the overall conversion. It did, however, affect the kinetics of gelator formation, showing the expected faster kinetics at higher ratios by maintaining pseudo–first-order conditions for the second-order hydrazone formation reaction. Gelation times increased on decreasing the concentration of catalyst or the molarity of the gelator precursors. To ensure that all samples had reached complete conversion to gelator **3** before measurement (CGC, CLSM), they were allowed to stand overnight, irrespective of their catalyst content. Mechanical perturbation of the system during formation has a detrimental influence on the mechanical stability of the final material, and should be avoided. In rheological measurements, G' can be followed over time and therefore this technique can be used during gel formation (vide infra).

CGC test

The CGC can serve as a first indication of the quality of the obtained gel network. CGCs were determined by an inverted tube test to determine the minimal amount of gelator needed to trap the solvent and form a stable gel. In the current reactive system, the CGC is expressed as initial concentration of **1**, and it is always determined by using a mixture with a 1:6 ratio of **1** and **2**. In an inverted tube test, the capped vials were turned upside down to visually observe any gravitationally induced flow. The inverted tube test was performed on samples in a range of building-block concentrations and the CGC value was determined by taking the average of the lowest concentration value at which gelation occurred and the highest value at which no gelation occurred. For example, if a hydrogelator gelated at a

concentration of 5 mM **1** but did not do so at 4 mM, the CGC is 4.5 ± 0.5 mM, where the margin of error is the difference between the CGC and its upper or lower value.

Rheology

Rheology is essential in quantifying the mechanical properties of the obtained materials. To determine the rheological properties, a sample was poured onto the bottom rheometer plate and distributed evenly by having the top plate rotate on descending. When the sample is smeared out, a meniscus is formed along the edge between both the plates. Although a pipette would give a more exact sample volume, a marked variation of final G' values was observed when pipetting the gelation mixture directly after mixing. The constant plate-plate gap distances (500 µm ± 10%) can serve as a rough indication of having the same amount of sample volume between the plates at each measurement. A strict consistency of the gap distance is not considered to be crucial for obtaining reproducible results because the gap distance is much larger than the typical dimensions of the fibres. Depending on the catalytic conditions of the sample, gels of different mechanical stiffnesses were formed. Gel formation was followed over time by plate-plate rheology to determine the evolution of the storage (G') and loss moduli (G") of the material (**Fig. 4c,d**). Gel stiffnesses were measured while applying 0.05% strain. This strain percentage is in the linear strain regime, which was determined by a strain sweep. By definition, a gel should have a markedly higher storage than loss modulus. In the systems described here, G' is typically ±100 times higher than G" on completion of the reaction, and G' typically exceeds G" (the 'gel point') early in the reaction. Once the storage modulus of a gel sample had reached a plateau value, the gel strength was determined on the basis of the average value of the plateau region.

Confocal Laser Scanning Microscopy

From simple macroscopic observation (visual appearance, turbidity, CGC) of the gels, it was clear that the morphology of the gel network changed when changing the catalytic conditions of gelator formation. These gel networks were subsequently imaged using CLSM. For this purpose, an aldehyde functionalised fluorescein-derived fluorescent probe **8** was incorporated into the fibre formation process[13]. We synthesized probe **8** from fluorescein isothiocyanate (FITC, which is commercially available) in one step, as describe in ref 13. Probe **8** was bound covalently to hydrazide **1** thereby allowing imaging of the gel and its composing fibres without disrupting its native state (**Fig. 5**). For this purpose, special polydimethylsiloxane (PDMS) cuvettes were prepared using a prefabricated polytetrafluoroethylene (PTFE) mould (**Fig. 7**). The gel samples were prepared as before, but now including 30 µM (replacing that amount of aldehyde **2**) of the fluorescent probe, and placed inside of the cuvette closed off by a glass cover slide. Samples were allowed to stand overnight in order to ensure complete conversion and gelation. After imaging was completed, the cuvettes could be washed and reused.

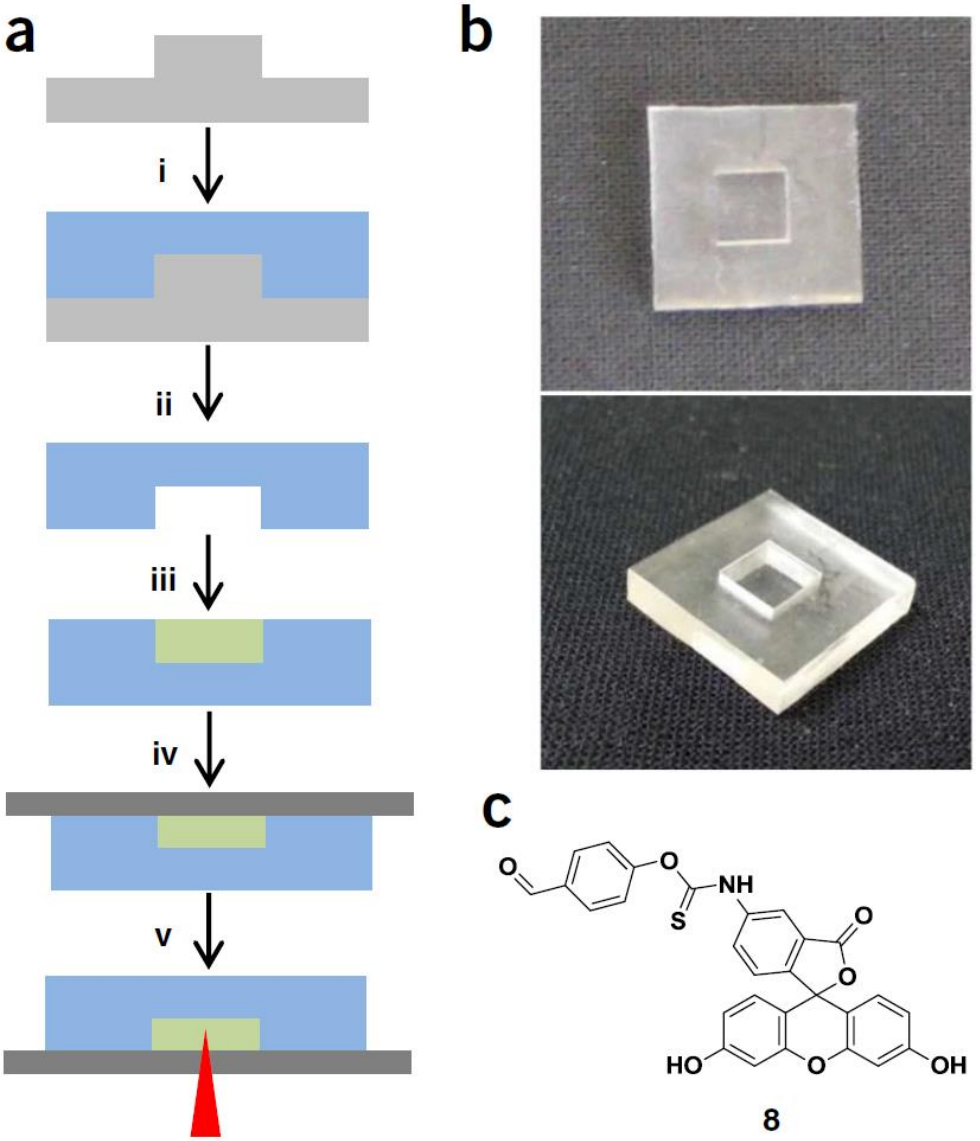

Figure 7 | Confocal Microscopy. (**a**) Preparation of a PDMS cuvette and its use in confocal microscopy: (i) A PTFE mold with a 0.5 x 0.5 x 0.2 cm protrusion was covered with PDMS elastomer + 10% (wt/wt) curing agent and heated at 70 °C for 12 h. (ii) Once cured, the PDMS was peeled off and placed in a plasma oven for 3 min to create hydroxyl groups on the surface needed for proper fixation of the cover slide in step iv. (iii) The cuvette was filled with freshly prepared mixture of building blocks **1** and **2**. (iv) Directly after the mixture was poured into the cuvette, it was closed with a 0.13 mm glass cover slide. (v) After overnight gelation, the sample was ready to be measured by CLSM. Light gray, PTFE mold; blue. PDMS cuvette; dark gray, glass slide; green, sample; red, confocal laser. (**b**) Example of the resulting PDMS cuvette (without cover slide). (**c**) Molecular structure of fluorescent probe **8** used to image the gel fibres under CLSM.

Materials

Reagents

- Trimesic acid (99%, AK Scientific, Cat. no. 165103)
- Demineralised water
- Palladium on activated charcoal (Pd/C, 10% Pd basis; Sigma-Aldrich, cat. No. 75990)
- Hydrazine hydrate, 64% (wt/wt) in water (Acros Organics, Cat. No.: 19671)
  ! CAUTION This reagent is carcinogenic and corrosive and should be handled with extreme caution in a fume hood wearing water-resistant gloves. The reagent needs be stored at 5°C.
- Hydrogen gas (Linde Gas)
  ! CAUTION This gas is highly flammable and should be handled using proper equipment; it should be kept away from open ignition sources.
- Hydranal-methanol Dry (Fluka, Cat. No.:34741)
- *para*-Toluenesulfonic acid monohydrate, ≥98,5% (Sigma-Aldrich, Cat. No. 402885)
- 2-(2-Methoxyethoxy)ethanol, 99% (Acros, Cat. No. 14937)
- 3,4-Dihydroxybenzaldehyde, 98% (AK Scientific, Cat. No. 365356)
- Triethylamine, 99% (Acros, Cat. No. 15791)
- *para*-Toluenesulfonyl chloride. 99+% (Acros, Cat. No. 13903)
- Potassium carbonate, 99% (Alfa Aesar, Cat. No. 16625)
- Tetrahydrofuran, 99.9% (Sigma-Aldrich, Cat. No. 186562)
- Petroleum ether (40-60 °C Fraction, Brenntag)
- Deuterated chloroform ($CDCl_3$; Cambridge Isotope Laboratories, cat. No. DLM-7-100)
- Sodium phosphate, dibasic, 99+% (Acros Organics, Cat. No.: 42437)
- Sodium phosphate, monobasic, 99+%(Acros Organics, Cat. No.: 38987)
- Acetone (Brenntag)
- Ethanol (Brenntag)
- Ethyl acetate (Brenntag)
- Hydrochloric Acid
- Dish soap (for cleaning glassware)

Equipment

- Buchner funnel
- Syringe filters
- Disposable syringes
- Qualitative filter paper
- Glassware (round-bottom flasks, Erlenmeyer flasks, beakers and so on)
- Glass slides

- Plasma oven
- PDMS cuvette
- Magnetic stirrer and stir bars
- Sintered funnel
- Rotary evaporator
- Separatory funnel
- Heat gun
- Vacuum pump
- Parr autoclave
- Flexible gas tubing (Swagelok)
- Utensils
- Balances
- NMR instrument (Bruker 400 MHz NMR spectrometer)
- Rheometer (TA Instruments, AR-G2 Magnetic Bearing Rheometer)
- Confocal laser scanning microscope (Carl Zeiss, LSM 700)

Equipment setup

Autoclave

In our laboratory we use a Parr autoclave with a 236HC10 1-liter cylinder, featuring a mechanical stirrer a gas inlet at the bottom and a gas outlet at the top. Gas was led into the setup using SwageLok tubing for high-pressure gases.

NMR spectrometry

For recording ^{1}H NMR spectra, we use a Bruker DMX 400 MHz NMR spectrometer. Chemical shifts are given in ppm (δ) relative to tetramethylsilane as internal standard or the signal of the deuterated solvent. Coupling constants (*J*) are given in Hz.

Rheology

Oscillatory experiments were performed using a rheometer in a strain-controlled mode; equipped with a steel plate-and-plate geometry of diameter 40 mm and a water trap. In our lab, we use an AR G2 rheometer from TA Instruments. The temperature of the plates was controlled at 25 ± 0.2 °C. Measurements were performed at a frequency of 1 Hz while applying 0.05% strain. During measurement, the storage and loss moduli G' and G" were followed as a function of the time. This measurement is called a "time sweep".

Confocal Laser Scanning Microscopy

To record confocal laser-scanning micrographs, we used a Zeiss LSM 700 confocal laser-scanning microscope equipped with a Zeiss LSM 700 Observer inverted microscope and a

x40 PlanFluor oil-immersion objective lens (Numerical Aperture 1.3) that uses incident wavelengths of 458 and 488 nm. The applied wavelength does not matter for the experimental outcome, but it does have to match the absorption and emission spectra of the applied fluorescent probe. We used probe 8 (Fig. 7), but other aldehyde-functionalized probes can be used as well. The confocal pinhole was set to 1.0 airy unit. Data files were processed using ZEN 2011 software. Image dimensions were 95.35 µm x 95.35 µm with a resolution of 1024 x 1024 pixels. Exposition time per pixel was 1.58 µs.

Procedure

Synthesis of 1,3,5-cyclohexanetricarboxylic acid 4 (timing 4 hours)

1. The synthesis of hydrazide **1** and aldehyde **2** are shown above (**Fig. 6**) and are described in steps 1-29 and steps 30-54 respectively. For hydrazide **1**, suspend trimesic acid (50.0 g, 238 mmol) and 10% palladium on activated charcoal (1.27 g, 11.9 mmol) in water (300 mL) in a Parr autoclave with a 1-liter volume.
2. Close the Parr vessel and stir mechanically.
   ! **CAUTION** To avoid the risk of an explosion, make sure that the autoclave is sealed properly.
3. Flush the autoclave with nitrogen gas by bringing it up to a pressure of 10 bar and then release the pressure. Repeat this step twice more.
4. Add hydrogen gas to the autoclave and bring it up to a pressure of 50 bar.
   ! **CAUTION** Hydrogen gas is highly explosive. Make sure the autoclave is not leaking any gas by checking the edges of the lid with a soap solution.
5. Stir the autoclave and heat to 150 °C. The pressure will increase to 70 bar.
6. When the pressure decreases over the course of the reaction to a pressure of ±50 bar, increase the pressure to 60 bar by addition of hydrogen gas while maintaining the temperature at 150 °C.
7. When the pressure finally stabilises around 60 bar, allow the autoclave to cool down to around 75 °C. **(? Troubleshooting)**
8. Release the pressure.
9. Flush the autoclave with nitrogen gas by bringing it up to a pressure of 10 bar and then releasing the pressure.
10. Open the autoclave and take a sample (±300 µl) from the reaction mixture with a Pasteur pipette. The disappearance of the suspended white solid material (trimesic acid) is a rough indication of complete conversion. Concentrate the sample in a rotary evaporator (40 mbar, 45 °C, ±10 min).
11. Dissolve the dried solids in deuterated methanol and filter off the palladium on activated charcoal by using a syringe filter. Complete conversion of the starting material is observed when singlet peak of trimesic acid at 8.811 ppm has

disappeared on the ^{1}H NMR spectrum (**Fig. 8**). The *cis,cis* and *cis,trans* isomers are observed in an approximate 6:1 ratio.

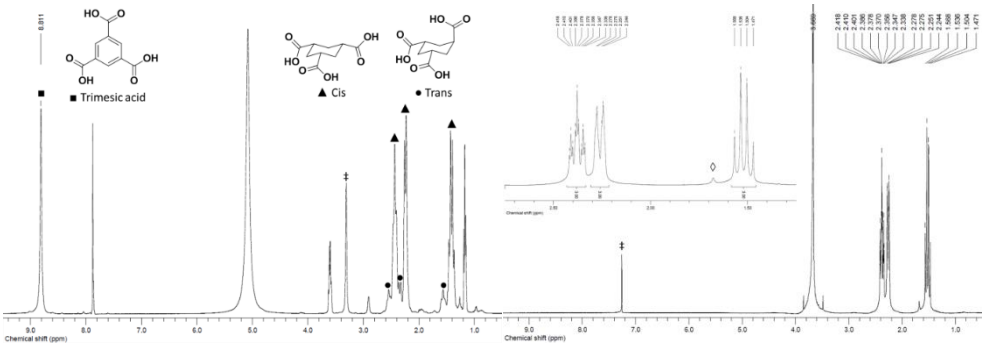

Figure 8 | ^{1}H NMR spectra of intermediate products **4** and **5**. Left, ^{1}H NMR spectrum (D_2O) of a reaction sample from the hydrogenation reaction. The singlet peak at 8.811 ppm reveals the presence of remaining trimesic acid and should disappear before proceeding. Right, ^{1}H NMR spectrum ($CDCl_3$) of methyl ester **5** after recrystallization (‡ = $CHCl_3$, ◊ = Water).

12. Filter the reaction mixture through a sintered funnel to remove the palladium on activated charcoal while applying vacuum with a vacuum pump.
13. Concentrate the mother liquor on a rotary evaporator (40 mbar, 45 °C, ±1 h) to obtain the solid product as a mixture of *cis,cis* and *cis,trans* isomers of 1,3,5-cyclohexanetricarboxylic acid **4**.
14. Dry the solids in a vacuum oven at 40 °C. Typical yield is quantitative based on both isomers.
    (**Pause point**: 1,3,5-cyclohexanetricarboxylic acid **4** can be stored in the dark for >1 year.)

Synthesis of *cis,cis*-trimethylcyclohexane-1,3,5-tricarboxylate 5 (Timing 48 h)

15. Dissolve compound **4** (37.2 g, 172 mmol) in methanol (1 liter) in a single-necked round-bottom flask equipped with a reflux condenser and stir the solution using a stirring magnet.
16. Add *p*-toluenesulfonic acid monohydrate (1.48 g, 8.61 mmol, 5 mol%) and heat it to reflux (80 °C) for 36 h.
17. Take a sample from the reaction mixture (±400 µl) using a Pasteur pipette, quench the reaction with triethylamine (0.5 mL) and concentrate it under vacuum (200 mbar, 45 °C, ±10 min). Dissolve it in $CDCl_3$ and record a ^{1}H NMR spectrum.
18. When all of the starting material has been converted according to ^{1}H NMR spectroscopy, add triethylamine (10 mL) to the reaction mixture and concentrate until 150 mL of the total volume is left (200 mbar, 45 °C).

19. Dilute the reaction mixture with diethyl ether (1 liter), and wash it with water (1 liter) and brine (1 liter).
20. Dry the organic layer by adding magnesium sulfate (enough to observe free-flowing crystallites when swirled). Filter off the magnesium sulfate using a sintered funnel mounted on an Erlenmeyer flask connected to a vacuum pump.
21. Concentrate the organic layer with the rotary evaporator (800-200 mbar, 45 °C, ±1 h) to obtain a yellow oil; add petroleum ether (1 liter).
22. Heat the mixture to reflux by using a heating mantle, and then pour the saturated solution into a beaker. Put the beaker in a refrigerator for 2 hours to obtain colourless crystals of *cis,cis*-trimethylcyclohexane-1,3,5-tricarboxylate **5** in the top of the beaker and a yellowish cake on the bottom of the beaker. **? TROUBLESHOOTING**
23. Filter off the colourless crystals and subject the yellowish cake to another round of recrystallization (go to step 1). Typical total yield after crystallisation is 70%.
24. Use ^{1}H NMR spectroscopy ($CDCl_3$) to determine purity.
    ▪**PAUSE POINT** When stored dark and dry *cis,cis*-trimethylcyclohexane-1,3,5-tricarboxylate can be kept for >1 year)

Synthesis of *cis,cis*-cyclohexane-1,3,5-tricarbohydrazide (1) (timing 4 h)

25. Dissolve compound **5** (40.2 g, 156 mmol) in methanol (600 mL) in a single-necked round-bottom flask and add hydrazine hydrate (141 mL, 64% in water).
    ! CAUTION Use proper safety measures when handling hydrazine. Hydrazine is carcinogenic and a strong reducing agent.
26. Stir the solution at room temperature for 3 h.
27. Take a sample from the reaction mixture (±300 µl), concentrate it by rotary evaporation and check the progress of the reaction by ^{1}H NMR spectroscopy (DMSO-*d*6).
28. When the reaction is complete, concentrate the reaction mixture under vacuum using a rotary evaporator (200 mbar, 45 °C, ±1 h).
    ! CAUTION Hydrazine vapours are formed. When evaporating hydrazine, preferably use a rotary evaporator inside of a fume hood.
29. Dry the white solids using an oil pump to obtain 39.7 g of *cis,cis*-cyclohexane-1,3,5-tricarbohydrazide **1**; typical yield is quantitative.
    ▪**PAUSE POINT** *cis,cis*-cyclohexane-1,3,5-tricarbohydrazide (**1**) can be stored in the dark for >1 year.

Synthesis of 2-(2-methoxyethoxy)ethyl tosylate 7 (timing 6 h)

30. Dissolve ethylene glycol monomethyl ether **6** (121.7 g, 1.013 mol) in THF (500 mL), add triethyl amine (205 g, 2.03 mol, 282 mL) and then stir.

31. Cool the solution to 0°C in an ice bath.
32. Dissolve *p*-toluenesulfonyl chloride (173.7 g, 911.3 mmol) in THF (500 mL) and add to the reaction over 30 min with a pressure-equalizing dropping funnel.
33. Take a sample (±400 µL) from the reaction using a Pasteur pipette and concentrate under reduced pressure using the rotary evaporator (200 mbar, 45 °C, ±10 min).
34. Dissolve the dry sample in deuterated chloroform and determine by ^{1}H NMR whether all p-toluenesulfonyl chloride has been consumed.
35. Concentrate the reaction on the rotary evaporator to a volume of ~100 mL (200 mbar, 45 °C).
36. Dilute the mixture with water (1 liter) and extract with DCM (two washes of 1 liter each) in a separatory funnel.
37. Combine the organic layers and dry with magnesium sulfate (add enough to observe free-flowing crystallites when swirled).
38. Filter off the magnesium sulfate using a Buchner funnel while applying vacuum.
39. Evaporate the DCM using a rotary evaporator (600 mbar, 45 °C, ±30 min).
40. Remove traces of DCM by applying vacuum to product **7** on an oil pump. Typical yield is quantitative.

    ▪ **PAUSE POINT** When stored dark and in the refrigerator (4 °C), 2-(2-methoxyethoxy)ethyl tosylate **7** can be kept for at least 2 months.

Synthesis of 3,4-bis(2-(2-methoxyethoxy)ethoxy)benzaldehyde 2 (timing 24 h)

41. Dissolve product **7** (200 g, 729 mmol) in dry DMF (600 mL).
42. Add potassium carbonate (183 g, 1.33 mol) and 3,4-dihydroxybenzaldehyde (45.8 g, 331 mmol) to the reaction mixture.
43. Stir the mixture while heating at 90°C.
44. Take a sample (±400 µL) from the reaction with a Pasteur pipette and concentrate under reduced pressure using the rotary evaporator (10 mbar, 70 °C, ±30 min).
45. Dissolve the dry sample in deuterated chloroform and determine by ^{1}H NMR whether all 3,4-dihydroxybenzaldehyde has been consumed.
46. Concentrate the reaction using a rotary evaporator (10 mbar, 70 °C, ±2 h).
47. Dilute the slurry with an aqueous 1 M solution of hydrochloric acid (1 liter).
48. Extract the aqueous layer with ethyl acetate (two washes of 1 liter each).
49. Combine the organic layers and wash them with a saturated aqueous solution of sodium bicarbonate (1 L).

    ? TROUBLESHOOTING
50. Dry the organic layer on magnesium sulfate (add enough to observe free-flowing crystallites when swirled).
51. Filter off the magnesium sulfate using a Buchner funnel while applying vacuum.
52. Evaporate the ethyl acetate using a rotary evaporator (150 mbar, 45 °C, ±30 min).

53. Remove traces of ethyl acetate by applying vacuum to product **2** using an oil pump. Typical yield is 83%. No traces of excess product **7** were detected by ^{1}H NMR.
    ? TROUBLESHOOTING
    PAUSE POINT Aldehyde **2** can be stored in the freezer (-20 °C), in the dark for >1 year.

Preparation of hydrogel (20 mM, 2 mL) and subsequent critical gel concentration (CGC) test series (timing 30 min)

54. Prepare 1.0 liter of a 100 mM phosphate buffer (Na_2HPO_4/NaH_2PO_4) of pH 5 by dissolving Na_2HPO_4 (89.0 mg) and NaH_2PO_4 (11.92 g) in 1.0 liter of demineralized water inside of a volumetric flask.
55. Check the pH of the phosphate buffer using a pH meter, and if necessary adjust the pH with a minimal amount of saturated sodium hydroxide if it is too acidic, or concentrated phosphoric acid (85%, (wt/vol) aq.) if it is too basic.
56. Suspend 41.3 mg of hydrazide **1** in 4 mL of phosphate buffer to obtain a 40 mM stock solution.
57. Sonicate and heat until hydrazide **1** is dissolved, and then allow it to cool to room temperature.
58. Dissolve 328.7 mg aldehyde **2** in 4 ml of phosphate buffer to obtain a 240 mM stock solution.
59. Put 1 mL of the aldehyde stock solution in a 4 mL glass vial.
60. If aniline is used as a catalyst instead of acid, use a solution buffered at pH 7.0 in steps 54-61. Add a stock solution of aniline in pH 7.0 phosphate buffer to the vial.
61. Add 1 ml of the hydrazide stock solution to the vial, cap the vial and shake it vigorously by vortexing for 3 s.
62. Allow the vial to stand overnight at room temperature to ensure that in any sample at any concentration or amount of catalyst formation of hydrogelator **3** and gelation are finished. (Do not touch the vial.)
63. Turn the vial upside down. If the sample does not slide toward the cap of the vial within 30 s, it is defined as a gel.
    ? TROUBLESHOOTING
64. Repeat this test from step 57 while decreasing the concentration of building blocks, until a concentration is reached on which no gel is formed. This can also be performed in parallel.
65. The CGC value is derived from the average of the highest concentration on which no gel is formed and the lowest concentration on which a gel is formed. The margin of error is based on the difference between the two values.

Rheological measurements (timing 30 min)

66. Prepare a mixture of **1** and **2** as described in steps 57 to 61.
67. After mixing the solutions of **1** and **2**, directly pour the mixture onto the rheometer plate.
    CRITICAL STEP Make sure the time between mixing and initiating the actual measurement is as short as possible as gelation of the sample is already taking place.
68. Bring down the top plate of the rheometer while it is slowly rotating. Lower the top plate onto the mixture until a meniscus is formed (**Fig. 9**).
    CRITICAL STEP Make sure the meniscus runs exactly along the edges of the plates of the rheometer.
69. Place a water trap over the top-plate
    CRITICAL STEP Make sure the water trap does not touch the top plate.

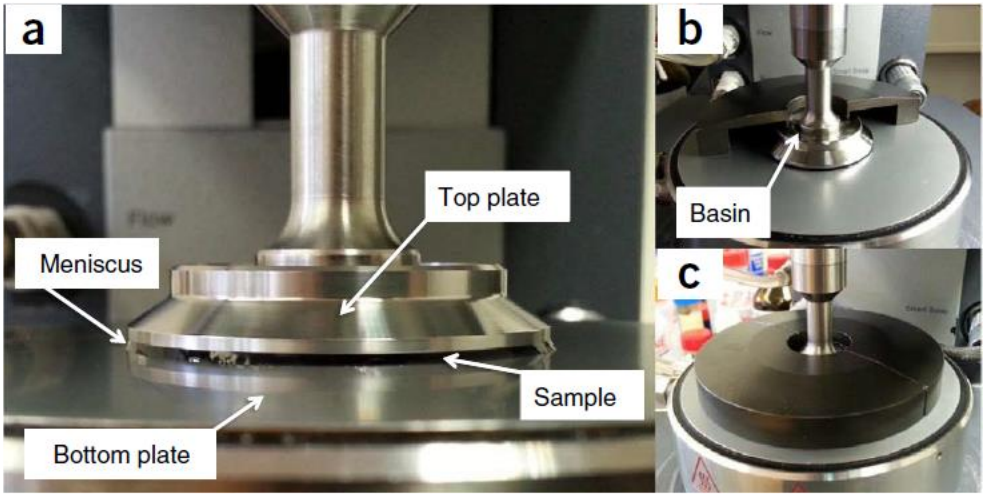

Figure 9 | Demonstration of applying a rheometer sample. (**a**) The top plate of the rheometer is lowered until a meniscus is formed along the edges of the top plate. (**b**) The basin on top of the top plate is filled with a layer of water. The first half of the water trap is placed, touching only the layer of water in the basin. (**c**) The second half of the water trap is placed in a similar fashion, preventing the sample from drying out.

70. Fill the basin on the top plate with water so that a meniscus is formed with the water trap.
71. Initiate the time sweep
    CRITICAL STEP Rheometers are sensitive to mechanical perturbations. Make sure not to touch the rheometer, and preferably not the table supporting it, during measurements.
72. When G' is maintaining a constant value, continue the measurement for 5 min to record the plateau value and then stop the measurement.

? TROUBLESHOOTING

CLSM (timing 20 h)

73. Prepare a mixture as described in steps 57-61 containing 0.1 mol% of fluorescent probe **8** and directly pour the mixture into a PDMS cuvette (**Fig. 7**). Cover the cuvette with a glass slide.
74. Allow the sample to gelate overnight inside of the cuvette.
75. Place the sample on the microscope and irradiate at 458 nm in order to observe the fibres.

TROUBLESHOOTING

Step	Problem	Possible reason	Solution
7	Pressure has dropped again to 50 bar or below	Not all the trimesic acid has reacted	Increase the hydrogen pressure to 60 bar again. If the pressure remains stable, proceed as normal
22	Compound **4** phase separates	Not enough petroleum ether has been used or solution was not cooled fast enough	Add more petroleum ether, heat to reflux again and cool down in the freezer
49	Layers do not phase separate	Product **2** is acting as a surfactant, mixing both the organic and the aqueous layers	Add some ethanol (100-200 mL) to the separatory funnel to break the hydrogen bonds formed with the aqueous layer
53	Compound **2** does not dissolve in water	Hydrophobic contamination present	Suspend compound **2** in water and filter over activated charcoal. Recover **2** by extraction with ethyl acetate, drying over magnesium sulphate and evaporation of the solvent
63	No gelation has occurred	The concentration of gelator is below the CGC	Repeat the experiment with a higher concentration of gelator
		Compounds have precipitated	Repeat the experiment with fresh stock solutions and make sure the compounds are dissolved properly using sonication and/or heating
			Check the starting compounds by ^{1}H NMR to check whether there are impurities present
72	The measured G' value is too low or too high	The compound has not gelated properly	Repeat the experiment with fresh stock solutions and make sure the compounds are dissolved properly using sonication and/or heating.
			Check the starting compounds by ^{1}H NMR to check whether there are impurities present

Table 1 | Troubleshooting table.

Timing

- Steps 1-14, Synthesis of 1,3,5-cyclohexanetricarboxylic acid **4**: 4 h
- Steps 15-24 Synthesis of *cis,cis*-1,3,5-tricyclohexylmethylcarboxylate **5**: 48 h
- Steps 25-29 Synthesis of hydrazide **1**: 4 h
- Steps 30-40 Synthesis of 2-(2-methoxyethoxy)ethyl tosylate **7**: 6 h
- Steps 41-53 Synthesis of aldehyde **2**: 24 h
- Steps 54-65 Preparation of hydrogel and subsequent CGC test: 30 min
- Steps 66-72 Rheological measurements: 30 min
- Steps 73-75 CLSM: 20 h

Anticipated results

This protocol details the procedure for the preparation of self-assembling LMWGs based on the catalytically controlled formation of hydrazone bonds between two water-soluble non-gelating precursors. The synthesis of these precursors is described along with the anticipated ^{1}H NMR data given below. The method of gel preparation to control gel strength and gelation time is described. The relation between the catalyst concentration versus gelation time and gel strength are detailed in **Fig. 4**. Analytical procedures for CGC test, rheology and CLSM have also been described showing the anticipated results of the gel strength (**Fig. 4**) and morphology (**Fig. 5**).

1,3,5-Cyclohexanetricarboxylic acid cis,cis/cis,trans mixture, hydrogenation (Reaction i, product 4)

White solid, ^{1}H NMR (300 MHz, CD_3OD) *cis*-product: δ 2.45 (t, *J* = 12.2, 3H), 2.24 (d, *J* = 12.8, 3H) 1.41 (q, *J* = 12.7, 3H), *trans*-product: δ 2.54 (t, *J* = 12.5, 3H), 2.34 (d, *J* = 13.5, 3H), 1.52-1.62 (m, 3H).

***cis,cis*-Trimethylcyclohexane-1,3,5-tricarboxylate, esterification (Reaction ii, product 5)**

White crystals, ^{1}H NMR (300 MHz, $CDCl_3$) δ 3.67 (s, 9H), 2.38 (tt, *J* = 12.7, 3.4, 3H), 2.24 (d, J = 12.8, 3H), 1.52 (q, *J* = 12.9, 3H); ^{1}H NMR (300 MHz, DMSO) δ 3.62 (s, 9H), 2.54 (tt, *J* = 12.5, 3.3, 3H) , 2.13 (d, *J* = 12.4, 3H), 1.31 (q, *J* = 12.8, 3H).

***cis,cis*-Cyclohexane-1,3,5-tricarbohydrazide, hydrazide synthesis (Reaction iii, product 1)**

White powder: ^{1}H NMR (300 MHz, DMSO) δ 8.98 (s, 3H), 4.17 (bs, 6H), 2.11 (t, *J* = 11.8, 3H), 1.57 (d, *J* = 11.7, 3H), 1.45 (q, *J* = 12.6, 3H).

2-(2-methoxyethoxy)ethyl tosylate, tosylation (Reaction iv, product 7)

Yellow oil: ^{1}H NMR (300 MHz, $CDCl_3$) δ 7.79, (d, *J* = 8.2, 2H), 7.33 (d, *J* = 8.0, 2H), 4.16 (t, *J* = 4.8, 2H), 3.68 (t, *J* = 4.8, 2H), 3.55-3.59 (m, 2H), 3.45-3.49 (m, 2H), 3.34 (s, 3H), 2.44 (s, 3H).

Williamson ether synthesis (Reaction v, product 2)

Yellow oil: ^{1}H NMR (300 MHz, $CDCl_3$) δ 9.82 (s, 1H), 7.42 (m, 2H), 6.98 (d, *J* = 11.6, 1H), 4.19-4.27 (m, 4H), 3.89 (t, *J* = 6.8, 2H), 3.88 (t, *J* = 6.4, 2H), 3.70-3.75 (m, 4H), 3.53-3.58 (m, 4H), 3.37 (s, 6H).

References

1. van Esch, J. H. & Feringa, B. L. New Functional Materials Based on Self-Assembling Organogels: From Serendipity towards Design. *Angewandte Chemie International Edition* **39,** 2263–2266 (2000).
2. Sangeetha, N. M. & Maitra, U. Supramolecular gels: Functions and uses. *Chemical Society Reviews* **34,** 821 (2005).
3. Lee, S. S. *et al.* Bone regeneration with low dose BMP-2 amplified by biomimetic supramolecular nanofibers within collagen scaffolds. *Biomaterials* **34,** 452–459 (2013).
4. Li, J. *et al.* Self-Delivery Multifunctional Anti-HIV Hydrogels for Sustained Release. *Advanced Healthcare Materials* n/a-n/a (2013). doi:10.1002/adhm.201300041
5. Adams, D. J., Mullen, L. M., Berta, M., Chen, L. & Frith, W. J. Relationship between molecular structure, gelation behaviour and gel properties of Fmoc-dipeptides. *Soft Matter* **6,** 1971 (2010).
6. Howe, R. C. T. *et al.* A family of simple benzene 1,3,5-tricarboxamide (BTA) aromatic carboxylic acid hydrogels. *Chemical Communications* **49,** 4268 (2013).
7. Jayawarna, V. *et al.* Nanostructured Hydrogels for Three-Dimensional Cell Culture Through Self-Assembly of Fluorenylmethoxycarbonyl–Dipeptides. *Advanced Materials* **18,** 611–614 (2006).
8. Ding, B. *et al.* Two approaches for the engineering of homogeneous small-molecule hydrogels. *Soft Matter* **9,** 4672 (2013).
9. Muraoka, T., Cui, H. & Stupp, S. I. Quadruple Helix Formation of a Photoresponsive Peptide Amphiphile and Its Light-Triggered Dissociation into Single Fibers. *Journal of the American Chemical Society* **130,** 2946–2947 (2008).
10. de Jong, J. J. D. *et al.* Light-Driven Dynamic Pattern Formation. *Angewandte Chemie International Edition* **44,** 2373–2376 (2005).
11. Engler, A. J., Sen, S., Sweeney, H. L. & Discher, D. E. Matrix Elasticity Directs Stem Cell Lineage Specification. *Cell* **126,** 677–689 (2006).
12. Weiss, R. & Terech, P. *Molecular Gels*. (Springer, 2006).
13. Boekhoven, J. *et al.* Catalytic control over supramolecular gel formation. *Nature Chemistry* **5,** 433–437 (2013).
14. He, X. *et al.* Synthetic homeostatic materials with chemo-mechano-chemical self-regulation. *Nature* **487,** 214–218 (2012).
15. Boekhoven, J., Koot, M., Wezendonk, T. A., Eelkema, R. & van Esch, J. H. A Self-Assembled Delivery Platform with Post-production Tunable Release Rate. *Journal of the American Chemical Society* **134,** 12908–12911 (2012).
16. Montarnal, D., Capelot, M., Tournilhac, F. & Leibler, L. Silica-Like Malleable Materials from Permanent Organic Networks. *Science* **334,** 965–968 (2011).
17. Williams, R. J. *et al.* Enzyme-assisted self-assembly under thermodynamic control. *Nature Nanotechnology* **4,** 19–24 (2008).
18. Hirst, A. R. *et al.* Biocatalytic induction of supramolecular order. *Nature Chemistry* **2,** 1089–1094 (2010).
19. Zhao, F. *et al.* β-Galactosidase-instructed formation of molecular nanofibers and a hydrogel. *Nanoscale* **3,** 2859 (2011).
20. Gao, Y. *et al.* Enzyme-instructed self-assembly of peptide derivatives to form nanofibers and hydrogels. *Biopolymers* **94,** 19–31 (2010).
21. Webber, M. J., Newcomb, C. J., Bitton, R. & Stupp, S. I. Switching of self-assembly in a peptide nanostructure with a specific enzyme. *Soft Matter* **7,** 9665 (2011).
22. Kühnle, H. & Börner, H. G. Biotransformation on Polymer-Peptide Conjugates: A Versatile Tool to Trigger Microstructure Formation. *Angewandte Chemie International Edition* **48,** 6431–6434 (2009).
23. John, G., Zhu, G., Li, J. & Dordick, J. S. Enzymatically Derived Sugar-Containing Self-Assembled Organogels with Nanostructured Morphologies. *Angewandte Chemie International Edition* **45,** 4772–4775 (2006).
24. Gao, J. *et al.* Enzyme Promotes the Hydrogelation from a Hydrophobic Small Molecule. *Journal of the American Chemical Society* **131,** 11286–11287 (2009).
25. Hahn, M. E. & Gianneschi, N. C. Enzyme-directed assembly and manipulation of organic nanomaterials. *Chemical Communications* **47,** 11814 (2011).
26. Gao, Y., Shi, J., Yuan, D. & Xu, B. Imaging enzyme-triggered self-assembly of small molecules inside live cells. *Nature Communications* **3,** 1033 (2012).

27. Bachmann, P. A., Luisi, P. L. & Lang, J. Autocatalytic self-replicating micelles as models for prebiotic structures. *Nature* **357,** 57–59 (1992).
28. Budin, I. & Devaraj, N. K. Membrane Assembly Driven by a Biomimetic Coupling Reaction. *Journal of the American Chemical Society* **134,** 751–753 (2012).
29. Xing, Y., Wang, C., Han, P., Wang, Z. & Zhang, X. Acetylcholinesterase Responsive Polymeric Supra-Amphiphiles for Controlled Self-Assembly and Disassembly. *Langmuir* **28,** 6032–6036 (2012).
30. van Bommel, K. J. C. *et al.* Responsive Cyclohexane-Based Low-Molecular-Weight Hydrogelators with Modular Architecture. *Angewandte Chemie International Edition* **43,** 1663–1667 (2004).
31. Dirksen, A., Dirksen, S., Hackeng, T. M. & Dawson, P. E. Nucleophilic Catalysis of Hydrazone Formation and Transimination: Implications for Dynamic Covalent Chemistry. *Journal of the American Chemical Society* **128,** 15602–15603 (2006).
32. Bhat, V. T. *et al.* Nucleophilic catalysis of acylhydrazone equilibration for protein-directed dynamic covalent chemistry. *Nature Chemistry* **2,** 490–497 (2010).
33. Ramström, O., Lohmann, S., Bunyapaiboonsri, T. & Lehn, J.-M. Dynamic Combinatorial Carbohydrate Libraries: Probing the Binding Site of the Concanavalin A Lectin. *Chemistry - A European Journal* **10,** 1711–1715 (2004).
34. Boudjouk, P., Kapfer, C. A. & Cunico, R. F. Synthesis and reactivity of 1-silaadamantyl systems. *Organometallics* **2,** 336–343 (1983).

Catalytic control over supramolecular gel formation

3

Abstract

LMWGs show great potential for application in fields ranging from the petrochemical industry to healthcare and tissue engineering. The supramolecular gels are often metastable materials, which implies that their properties are, at least partially, kinetically controlled. Here we show how the mechanical properties and structure of these materials can be controlled directly by catalytic action. We show how *in situ* catalysis of the formation of gelator molecules can be used to accelerate the formation of supramolecular hydrogels, which drastically enhances their resulting mechanical properties. Using acid or nucleophilic aniline catalysis, it is possible to make hydrogels with tunable gel-strength in a matter of minutes, under ambient conditions, starting from simple soluble building blocks. By changing the rate of formation of the gelator molecules using a catalyst, the overall rate of gelation and the resulting gel morphology are affected, providing access to metastable gel states with improved mechanical strength and appearance despite an identical gelator composition.

Published as:

Variable gelation time and stiffness of low-molecular-weight hydrogels through catalytic control over self-assembly

Jos M. Poolman, Job Boekhoven, Anneke Besselink, Alexandre G. Olive, Jan H. van Esch and Rienk Eelkema

Nature Protocols **9,** 977–988 (2014)

Introduction

Catalytic control over the formation of supramolecular structures is widespread in nature, directing vital processes such as cell motility, intracellular transport and muscle contraction, and resulting in the rapid turnover of self-assembled structures by acting on feedback-controlled processes.[1] In recent years, self-assembly of synthetic systems has seen major advances, particularly directed at the formation of dynamic and non-equilibrium structures.[2–4] However, in these artificial systems only a few specific examples of catalytic control over self-assembly exist in (auto)catalytic amphiphile formation and assembly[5–7], and in enzyme controlled peptide and surfactant assembly.[8–17] Vice versa, enzymatic catalysis of the disassembly of peptide-based gelators and dendrimer-based amphiphilic nanocontainers has been described.[18,19] Because material properties often depend on the rate of building-block assembly, they can potentially be controlled using chemical catalysis, thereby providing access to alternative self-assembly pathways and kinetically controlled non-equilibrium states. Moreover, catalysis of the formation of organic architectures offers the possibility to control the spatial and temporal distribution of soft materials and their associated properties. As such, catalytically controlled soft materials may find application in self-healing materials[20], for controlled-release purposes[21] and as actuators[22].

Here, we show how to control the rate of formation of supramolecular gels, and how this affects their material properties, by exploiting the susceptibility of formation of the gel monomers to catalytic action. Central to this concept are building blocks capable of self-assembling into fibrous structures, which form only on construction from smaller non-assembling fragments through the formation of a covalent bond. Catalytic action on the formation of this covalent bond can control the rate of assembly formation, which ultimately affects the morphology of the resulting materials and thus provides access to non-equilibrium metastable self-assembled materials.

The formation of molecular gels generally occurs through the self-assembly of LMWG molecules into elongated fibrous structures, which in turn form an entangled network in their solvent.[23,24] In such gels, the rate of formation of the fibres has a pronounced effect on fibre morphology and hence their macroscopic properties, but typically it is controlled via supersaturation levels, cooling rates and triggers such as light and pH.[25–27] Only very recently was it shown that the rate of enzyme-catalysed LMWG formation affects gel morphology.[9] Designing and applying LMWGs that are capable of forming from non-gelating precursors through the creation of a covalent bond will enable us to investigate the influence of catalysis on self-assembly and material properties. In the past, *in situ* formation of supramolecular gelators has been reported, typically using two-component systems that form the gelating monomer either by covalent[28,29] or non-covalent[30,31] interactions.

Remarkably, despite the prospects, so far the influence of catalysis on the formation and properties of these supramolecular materials has not been explored.

Results and discussion

The current study required a catalysis-responsive gelator, which was designed analogously to a highly efficient modular class of LMWGs based on a tris-functionalised cyclohexane scaffold,[32] further developed in our labs in recent years.[33] In the current design, the three original hydrogen-bonding amide linkages are replaced by hydrazone links (**3** in Fig. 1). Low and high molecular weight gels that contain hydrazone bonds have been reported, which underlines the compatibility of the hydrazone bond with the aggregation process.[34–36]

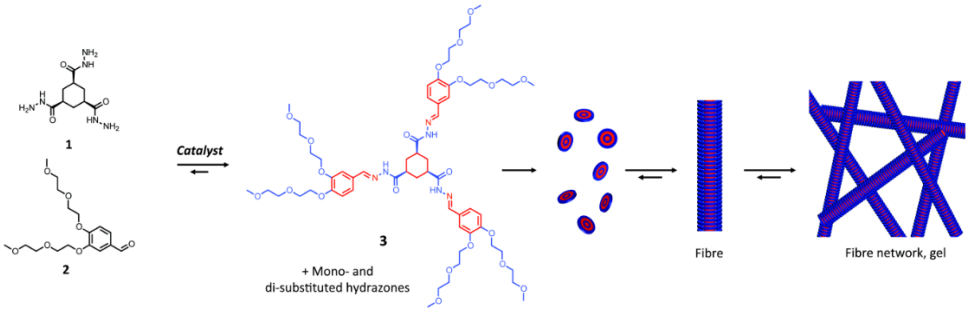

Figure 1 | Concept of a catalysed gelator and gel formation. Catalytic formation of trishydrazone hydrogelator **3** from soluble building blocks **1** and **2** leads to superstaturation followed by fibre formation, which eventually crosslink to form a network that traps the surrounding solvent, leading to gelation. Blue = hydrophilic functional groups, red = hydrophobic functional groups.

Structurally similar to amides, hydrazones are good hydrogen-bond acceptors and donors, and thereby provide the non-covalent interactions necessary for self-assembly. Hydrazone gelator **3** consists of a hydrophobic alkane core and three hydrogen-bonding hydrazone groups flanked by hydrophobic phenyl substituents. The phenyl moieties are decorated with oligoethylene glycol tails, which enhance the solubility of the building blocks (**2**) and prevent crystallization of the gelator (**Fig. 1**). Crucially, the gelator can be formed *in situ* by the reaction of the cyclohexane trishydrazide building block **1** and three molecules of aldehyde **2**. The rate of formation of the hydrazone bond, a prototypical reversible bond between a hydrazide and an aldehyde extensively applied in dynamic covalent chemistry[37,38], can be increased through both acid and nucleophilic aniline catalysis.[39,40]

Mixing clear aqueous solutions of trishydrazide **1** and aldehyde **2** in a 1:6 molar ratio at pH 7.0 (1:2 ratio of hydrazide to aldehyde functional groups, [**1**] = 8 mM, 0.1 M phosphate buffer) at room temperature resulted in the formation of turbid solutions. Interestingly, at pH 5.0, mixing these solutions resulted in the formation of stable opalescent gels, with a

critical gelation concentration (CGC) of 4.5 ± 0.5 mM (expressed in starting concentration of **1**). Similarly, the same mixture at pH 7.0 in the presence of 10 mM aniline afforded a stable turbid gel with a CGC of 3.8 ± 0.5 mM (**Fig. 2**). Increasing the concentration of starting material **1** to 20 mM at pH 7.0 without catalyst did eventually result in the formation of weak crystalline gels, which indicated a significantly higher CGC in the absence of catalysts. High-peformance liquid chromatography (HPLC) experiments showed, in all cases, the formation of >95% of the trishydrazone **3** and <5% of the bishydrazone, whereas no monohydrazone was observed. Gel formation could be reversed by applying strong acid (pH<1, gel → sol), and reinstated using base (pH>4, sol → gel), but the gels were stable to temperature increase (up to 120 °C), possibly as a result of a lower critical solution temperature of the oligoethylene glycol side chains. Clear differences were visible in the development of sample turbidity over time between catalyzed and uncatalyzed samples when studied by ultraviolet-visible spectroscopy (**Fig. 2**). The final turbidity (measured as absorbance of 500 nm light) was highest for the uncatalyzed sample and lowest for the acid-catalyzed sample. Moreover, the rate of turbidity increase was drastically higher in the catalysed samples, with the highest rate observed for the acid-catalyzed sample, reaching a maximum absorbance within 60 minutes. A somewhat lower but comparable rate was observed for the aniline-catalyzed sample, whereas the uncatalyzed sample took roughly nine hours to reach its final absorbance level. These results suggest a strong relationship between the rate of turbidity increase, and therefore of structure formation, and the morphology of the resulting material.

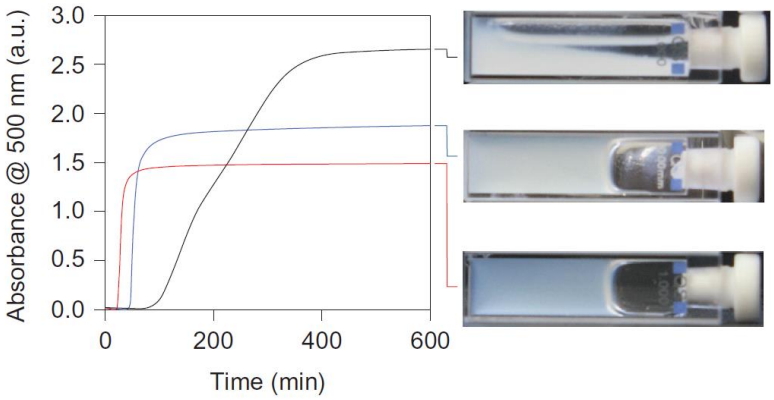

Figure 2 | Influence of catalysis on material formation and appearance. Turbidity measurements show the time-dependent absorbance of 500 nm light as a measure of structure formation (red line, pH 5.0; blue line, 10 mM aniline at pH 7.0; black line, pH 7.0 (**1**:**2**=1:6, [**1**]=8 mM; 0.1 M phosphate buffer)). The two catalysed samples (red and blue lines) show structure formation on significantly shorter time scales than the uncatalysed sample (black line). The resulting materials are shown on the right: the acidcatalysed gel (bottom) is more transparent than the aniline-catalysed gel (middle). The uncatalysed mixture cannot support the solvent and shows precipitation (top). a.u. = arbitrary units.

Indeed, both confocal laser scanning fluorescence microscopy and scanning electron microscopy showed the formation of dense homogeneous networks that consisted of heavily branched interconnecting fibres in both catalysed scenarios, whereas the uncatalysed system was made up of single poorly connected unbranched bundles of fibres and networks of thick fibre bundles (**Fig. 3**). Despite the differences in network morphology, cryotransmission electron microscopy showed that in all systems the gel networks consist of fibres up to a 1 μm in length 5.5 ± 1 nm thick fibres, which in the uncatalysed case sometimes appeared to assemble into slightly thicker bundles (**Supplementary Fig. S2**). Wide-angle x-ray powder diffraction patterns of catalysed and uncatalysed gels showed main reflections at 27.0 and 4.1 Å, which are probably associated with the intercolumn distance and the intermolecular stacking distance within the columns, respectively, when compared to related single-crystal X-ray structures (**Supplementary Fig. S4**).[33] No significant differences were observed between catalysed and uncatalysed samples, which indicates equivalent molecular organization in all cases.

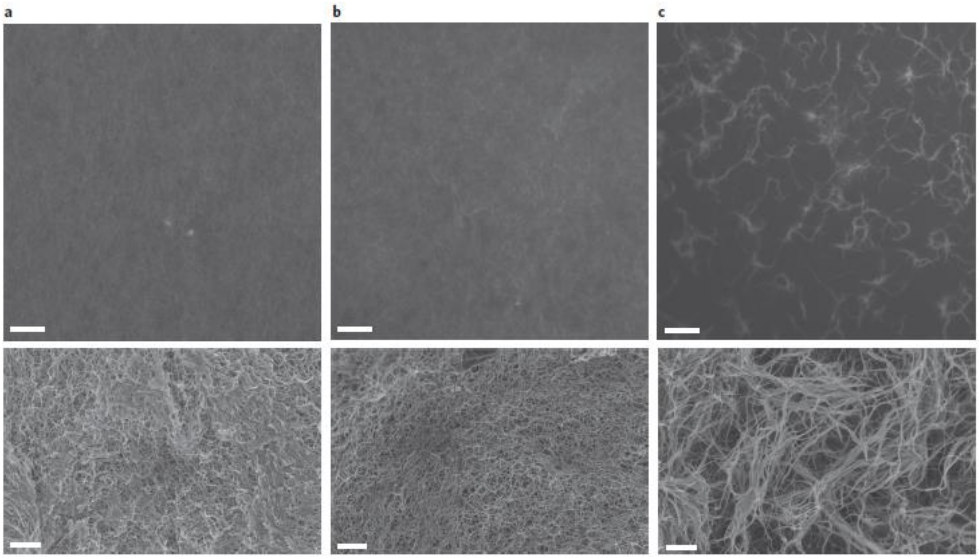

Figure 3 | Influence of catalysis on material morphology. **a–c**, Confocal laser scanning fluorescence micrographs (top) and scanning electron micrographs (bottom) show differences in network morphology and fibre thickness that depend on catalyst loading at pH 5.0 (**a**) and pH 7.0 with 10 mM aniline (**b**), and uncatalysed at pH 7.0 (**c**). Both catalysed samples (**a,b**) show thin highly branched fibres forming a dense network. In the uncatalysed scenario (**c**) thick less-branched fibres form a poorly connected network. All samples were prepared by mixing solutions of **1** and **2** ([**1**] = 4mM, **1**:**2** = 1:6, 0.1 M phosphate buffer) and a 30 μM fluorescent probe at room temperature. Scale bars = 10μm (top) and 500 nm (bottom).

The influence of catalysis on the material properties was studied by rheology, at [**1**]=20 mM to ensure the formation of gels in all mixtures. Again, distinct differences between catalysed and uncatalysed samples were observed. Lowering the pH resulted in a drastic reduction of

the gelation time, changing from 275 minutes at pH 7 to less than eight minutes at pH 5 (**Fig. 4a**). Addition of aniline to a pH 7 mixture had a similar effect, reducing the gelation time to less than 12 minutes with 50 mM aniline (**Fig. 4b**). Moreover, the catalysis greatly influenced the mechanical properties of the gels. Acid catalysis resulted in an increase of the maximum obtained storage modulus (G') by an order of magnitude to 50 kPa at pH 5 (**Fig. 4c**).

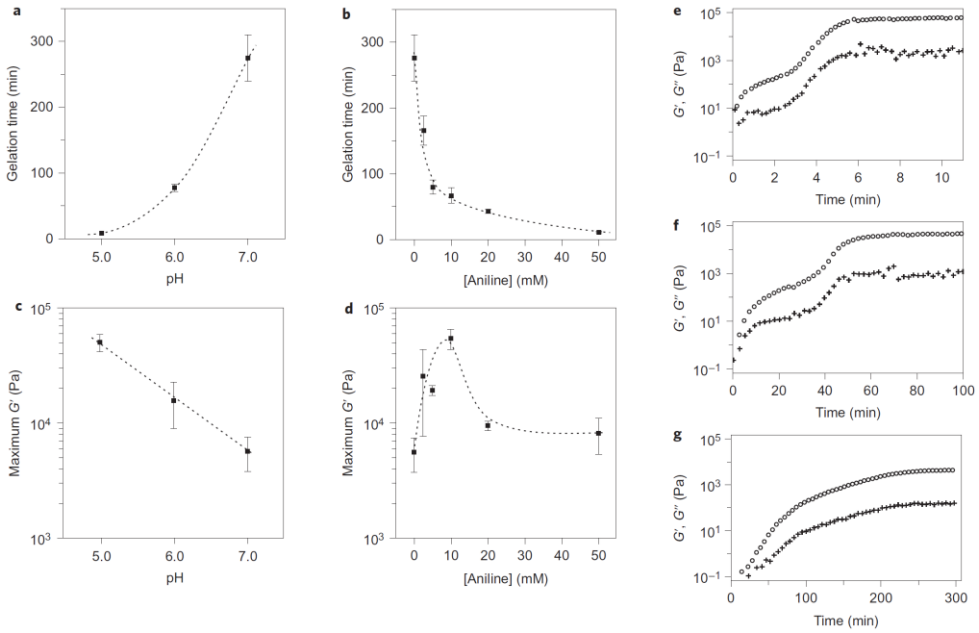

Figure 4 | Gel properties and formation dynamics depend on catalyst loading. (**a–d**) Gel formation measured by rheology: the dependence on catalyst concentration of gelation time (**a,b**) and the maximum storage modulus (G') (**c,d**). Errors are the standard deviation from duplicate experiments; the lines are to guide the eye. Both gelation time and maximum storage modulus show a strong dependence on the amount of added catalyst: in the acid-catalysed scenario (**a,c**) the gelation time is reduced and the storage modulus increased with increasing catalyst concentration. The aniline-catalysed samples (**b,d**) show a more complex behaviour: although gelation time is reduced with increasing aniline concentration, the maximum storage modulus, after an initial increase, decreases again at very high aniline concentrations, most probably because of the formation of a surface-active adduct of aniline to 2. **e–g**, The evolution of G' and G'' over time at pH 5.0 (**e**), pH 7.0 with 10 mM aniline (**f**) and pH 7.0 (**g**). All samples: **1:2** = 1:6, [**1**] = 20 mM; 0.1 M phosphate buffer.

In the case of aniline catalysis, the maximum obtained storage modulus showed a maximum using 10 mM aniline catalyst, again leading to an increase in storage modulus by an order of magnitude (55 kPa, **Fig. 4d**). However, it was observed that higher aniline concentrations led to a decrease in storage modulus. Although high aniline concentrations did not lead to unexpected rate changes, changes in conversion, network morphology or CGC, we did observe the persistent formation of the amphiphilic aniline-derived imine of aldehyde **2** at

high aniline concentrations (**Supplementary Information**), which may have a detrimental effect on the mechanical properties. Gel formation as observed by time-dependent rheology showed a two-stage process in both uncatalysed and catalysed scenarios, although less pronounced for the uncatalysed gel (**Fig. 4e-g**). In all cases the onset of percolation (when G' surpasses G'') was observed at an early stage in the process. HPLC analysis of the kinetics of formation of gelator **3** (**Supplementary Fig. S6**) showed that the majority of **3** was formed after reaching the onset of percolation, and revealed a clear relation between hydrazone formation (and thus catalytic action) and the evolution of the mechanical gel strength over time. A first plateau observed in the rheology curves (**Fig. 4e-g**) is probably associated with the addition of gelator molecules to the existing network formed at an early stage, causing it to stiffen or crosslink. At longer times, when the rate of formation of **3** increases, a further increase of the storage modulus (G') was observed until a second plateau is reached. This effect, much more pronounced in the catalysed samples, may be caused by the formation of new branched fibres interspersing with the existing network.

Additives to the gelation medium such as ions or co-solvent, can have a profound effect on gel strength and appearance. To rule out the catalysts acting as mere solvent additives that change the quality of the gelation medium, CGCs were determined of gels prepared by dissolving separately synthesized catalyst-free **3** in the appropriate catalyst-containing media (pH 5, 10 mM aniline pH 7, and pH 7), followed by controlled and relatively fast gelation (**Supplementary Information**). In all cases CGCs of 4.5 mM ± 0.5 mM were recorded, indicative of a negligible influence of the catalyst on the properties of the medium at these catalyst concentrations, thereby pointing towards a relationship between the rate of gelator formation and the gel properties.

The observation that the stronger gels, obtained under catalytic conditions, contain a dense, heavily branched fibre network whereas the weaker uncatalysed mixtures are made up of unbranched fibre bundles (**Fig. 3**), suggests that the rate of gelator formation can influence the structure of the assembled materials. Analysis of the development of turbidity over time (**Fig. 2**) in terms of the dimensionality of structure formation using the Avrami equation[41], showed a significant difference in the Avrami coefficient *n* between the uncatalysed and catalysed samples, with $n = 1.4 \pm 0.2$ (pH 7), $n = 2.3 \pm 0.2$ (pH 5) and $n = 2.4 \pm 0.2$ (10 mM aniline) (**Supplementary Fig. S10**). These results confirm a fractal-like growth in the catalysed samples, which leads to a well-connected continuous network.[42] The lower dimensionality of the growth of the uncatalysed sample indicates the formation of fibrous structures with a lower degree of branching and thereby fewer interfibre connections, which is probably responsible for the significantly lower mechanical strength of the gels. It is therefore plausible that the increase in the rate of gelator formation caused by catalysis results in faster fibre growth, which causes the incorporation of local fibre defects during assembly and hence in branching of the fibre structures, and thus leads to fortification of the resulting network structure. These results show behaviour to that of opposite from

previously reported enzyme-catalysed fibre growth[9]. Those reports showed bundling and ordering of fibres that increased with increased catalyst concentration and an associated decreased catalyst mobility, whereas in the present system highly mobile, homogeneously dispersed catalysts (acid, aniline) control fibre branching, which leads to efficient crosslinking. As these gels all have identical gelator composition, the observed differences in mechanical properties and network morphologies are manifestations of various metastable thermodynamic states of the same self-assembled system, which can be addressed by changing the rates of gelator formation using catalysis.

Conclusions

We show here how both the rate of gel formation and the resulting mechanical properties can be controlled through *in situ* catalysis of the formation of gelator molecules. Drastic enhancement of rates of formation and mechanical strength of supramolecular hydrogels were observed using either acid or nucleophilic aniline catalysis. Analysis of the kinetic data points towards a mechanism in which a higher rate of gelator formation leads to an increased formation of defects in the gel fibre, thereby resulting in branching of the gel fibres, which subsequently strengthens the resulting gel. As such, catalytic control over building-block formation provides access to alternative kinetically stable non-equilibrium self-assembled materials. In the present system, catalysis enables the rapid formation of hydrogels from simple water-soluble building blocks under ambient conditions. In particular, aniline catalysis allows the formation of tunable hydrogels at physiological pH. In the future, catalysis could provide dynamic and spatial control of material formation and properties using, for instance, switchable catalysts[43–45] or catalytically active patterned surfaces.

References

1. Stryer, L. *Biochemistry*. (W.H. Freeman, 1995).
2. Carnall, J. M. A. *et al.* Mechanosensitive Self-Replication Driven by Self-Organization. *Science* **327,** 1502–1506 (2010).
3. Capito, R. M., Azevedo, H. S., Velichko, Y. S., Mata, A. & Stupp, S. I. Self-Assembly of Large and Small Molecules into Hierarchically Ordered Sacs and Membranes. *Science* **319,** 1812–1816 (2008).
4. Korevaar, P. A. *et al.* Pathway complexity in supramolecular polymerization. *Nature* **481,** 492–496 (2012).
5. Kurihara, K. *et al.* Self-reproduction of supramolecular giant vesicles combined with the amplification of encapsulated DNA. *Nat. Chem.* **3,** 775–781 (2011).
6. Bachmann, P. A., Luisi, P. L. & Lang, J. Autocatalytic self-replicating micelles as models for prebiotic structures. *Nature* **357,** 57–59 (1992).
7. Budin, I. & Devaraj, N. K. Membrane Assembly Driven by a Biomimetic Coupling Reaction. *J. Am. Chem. Soc.* **134,** 751–753 (2012).
8. Williams, R. J. *et al.* Enzyme-assisted self-assembly under thermodynamic control. *Nat. Nanotechnol.* **4,** 19–24 (2008).
9. Hirst, A. R. *et al.* Biocatalytic induction of supramolecular order. *Nat. Chem.* **2,** 1089–1094 (2010).
10. Zhao, F. *et al.* β-Galactosidase-instructed formation of molecular nanofibers and a hydrogel. *Nanoscale* **3,** 2859 (2011).
11. Gao, Y. *et al.* Enzyme-instructed self-assembly of peptide derivatives to form nanofibers and hydrogels. *Biopolymers* **94,** 19–31 (2010).
12. Webber, M. J., Newcomb, C. J., Bitton, R. & Stupp, S. I. Switching of self-assembly in a peptide nanostructure with a specific enzyme. *Soft Matter* **7,** 9665 (2011).
13. Kühnle, H. & Börner, H. G. Biotransformation on Polymer-Peptide Conjugates: A Versatile Tool to Trigger Microstructure Formation. *Angew. Chem. Int. Ed.* **48,** 6431–6434 (2009).
14. Xing, Y., Wang, C., Han, P., Wang, Z. & Zhang, X. Acetylcholinesterase Responsive Polymeric Supra-Amphiphiles for Controlled Self-Assembly and Disassembly. *Langmuir* **28,** 6032–6036 (2012).
15. John, G., Zhu, G., Li, J. & Dordick, J. S. Enzymatically Derived Sugar-Containing Self-Assembled Organogels with Nanostructured Morphologies. *Angew. Chem. Int. Ed.* **45,** 4772–4775 (2006).
16. Gao, J. *et al.* Enzyme Promotes the Hydrogelation from a Hydrophobic Small Molecule. *J. Am. Chem. Soc.* **131,** 11286–11287 (2009).
17. Hahn, M. E. & Gianneschi, N. C. Enzyme-directed assembly and manipulation of organic nanomaterials. *Chem. Commun.* **47,** 11814 (2011).
18. Van Bommel, K. J. C., Stuart, M. C. A., Feringa, B. L. & van Esch, J. Two-stage enzyme mediated drug release from LMWG hydrogels. *Org. Biomol. Chem.* **3,** 2917 (2005).
19. Azagarsamy, M. A., Sokkalingam, P. & Thayumanavan, S. Enzyme-Triggered Disassembly of Dendrimer-Based Amphiphilic Nanocontainers. *J. Am. Chem. Soc.* **131,** 14184–14185 (2009).
20. Montarnal, D., Capelot, M., Tournilhac, F. & Leibler, L. Silica-Like Malleable Materials from Permanent Organic Networks. *Science* **334,** 965–968 (2011).
21. Boekhoven, J., Koot, M., Wezendonk, T. A., Eelkema, R. & van Esch, J. H. A Self-Assembled Delivery Platform with Post-production Tunable Release Rate. *J. Am. Chem. Soc.* **134,** 12908–12911 (2012).
22. He, X. *et al.* Synthetic homeostatic materials with chemo-mechano-chemical self-regulation. *Nature* **487,** 214–218 (2012).
23. Terech, P. & Weiss, R. G. Low Molecular Mass Gelators of Organic Liquids and the Properties of Their Gels. *Chem. Rev.* **97,** 3133–3160 (1997).
24. Steed, J. W. Supramolecular gel chemistry: developments over the last decade. *Chem. Commun.* **47,** 1379 (2011).
25. Li, J.-L., Liu, X.-Y., Wang, R.-Y. & Xiong, J.-Y. Architecture of a Biocompatible Supramolecular Material by Supersaturation-Driven Fabrication of its Fiber Network. *J. Phys. Chem. B* **109,** 24231–24235 (2005).
26. De Jong, J. J. D. Reversible Optical Transcription of Supramolecular Chirality into Molecular Chirality. *Science* **304,** 278–281 (2004).
27. Chen, L. *et al.* Self-Assembly Mechanism for a Naphthalene−Dipeptide Leading to Hydrogelation. *Langmuir* **26,** 5232–5242 (2010).

28. Suzuki, M. *et al.* Effects of Hydrogen Bonding and van der Waals Interactions on Organogelation Using Designed Low-Molecular-Weight Gelators and Gel Formation at Room Temperature. *Langmuir* **19,** 8622–8624 (2003).
29. Boekhoven, J. *et al.* Dissipative Self-Assembly of a Molecular Gelator by Using a Chemical Fuel. *Angew. Chem. Int. Ed.* **49,** 4825–4828 (2010).
30. Hunt, J. N. *et al.* Tunable, High Modulus Hydrogels Driven by Ionic Coacervation. *Adv. Mater.* **23,** 2327–2331 (2011).
31. Hirst, A. R. *et al.* Low-Molecular-Weight Gelators: Elucidating the Principles of Gelation Based on Gelator Solubility and a Cooperative Self-Assembly Model. *J. Am. Chem. Soc.* **130,** 9113–9121 (2008).
32. Hanabusa, K., Kawakami, A., Kimura, M. & Shirai, H. Small Molecular Gelling Agents to Harden Organic Liquids: Trialkyl cis-1,3,5-Cyclohexanetricarboxamides. *Chem. Lett.* 191–192 (1997). doi:10.1246/cl.1997.191
33. Van Bommel, K. J. C. *et al.* Responsive Cyclohexane-Based Low-Molecular-Weight Hydrogelators with Modular Architecture. *Angew. Chem. Int. Ed.* **43,** 1663–1667 (2004).
34. Sreenivasachary, N. & Lehn, J.-M. Gelation-driven component selection in the generation of constitutional dynamic hydrogels based on guanine-quartet formation. *Proc. Natl. Acad. Sci.* **102,** 5938–5943 (2005).
35. Deng, G., Tang, C., Li, F., Jiang, H. & Chen, Y. Covalent Cross-Linked Polymer Gels with Reversible Sol−Gel Transition and Self-Healing Properties. *Macromolecules* **43,** 1191–1194 (2010).
36. Ossipov, D. A., Yang, X., Varghese, O., Kootala, S. & Hilborn, J. Modular approach to functional hyaluronic acid hydrogels using orthogonal chemical reactions. *Chem. Commun.* **46,** 8368 (2010).
37. Corbett, P. T. *et al.* Dynamic Combinatorial Chemistry. *Chem. Rev.* **106,** 3652–3711 (2006).
38. Lehn, J.-M. Dynamic Combinatorial Chemistry and Virtual Combinatorial Libraries. *Chem. - Eur. J.* **5,** 2455–2463 (1999).
39. Dirksen, A., Dirksen, S., Hackeng, T. M. & Dawson, P. E. Nucleophilic Catalysis of Hydrazone Formation and Transimination: Implications for Dynamic Covalent Chemistry. *J. Am. Chem. Soc.* **128,** 15602–15603 (2006).
40. Bhat, V. T. *et al.* Nucleophilic catalysis of acylhydrazone equilibration for protein-directed dynamic covalent chemistry. *Nat. Chem.* **2,** 490–497 (2010).
41. Liu, X. Y. & Sawant, P. D. Formation kinetics of fractal nanofiber networks in organogels. *Appl. Phys. Lett.* **79,** 3518 (2001).
42. Liu, X. Y. & Sawant, P. D. Mechanism of the Formation of Self-Organized Microstructures in Soft Functional Materials. *Adv. Mater.* **14,** 421–426 (2002).
43. Gianneschi, N. C., Nguyen, S. T. & Mirkin, C. A. Signal Amplification and Detection via a Supramolecular Allosteric Catalyst. *J. Am. Chem. Soc.* **127,** 1644–1645 (2005).
44. Peters, M. V., Stoll, R. S., Kühn, A. & Hecht, S. Photoswitching of Basicity. *Angew. Chem. Int. Ed.* **47,** 5968–5972 (2008).
45. Piermattei, A., Karthikeyan, S. & Sijbesma, R. P. Activating catalysts with mechanical force. *Nat. Chem.* **1,** 133–137 (2009).

Supplementary information

S1 General remarks

All reagents were purchased from commercial sources and were used as provided unless otherwise stated. ^{1}H NMR spectra were recorded on a Brucker Avance-400 spectrometer, operating at 399.90 MHz for ^{1}H and 100.56 MHz for ^{13}C, or a Varian Inova-300 spectrometer, operating at 300.04 MHz for ^{1}H. All NMR spectra were recorded at 298 K. Chemical shift values are denoted in δ values (ppm) relative to residual solvent peaks ($CDCl_3$, ^{1}H δ = 7.26, ^{13}C δ = 77.00; DMSO-d_6, ^{1}H δ = 2.50, ^{13}C δ = 39.51; methanol-d_6: ^{1}H δ = 3.31, ^{13}C δ = 49.00 D_2O: ^{1}H δ = 4.79, ^{13}C NMR in D_2O was referenced to internal dioxane, δ = 67.19). HPLC-MS analysis was performed on a Shimadzu Liquid Chromatograph Mass Spectrometer, LCMS-2010, LC-8A pump with a diode array detector SPD-M20. The column used was the Xbridge Shield RP 18.5µm (4.6x150mm). UV-Vis spectroscopic measurements were performed on an Analytik Jena Specord 250 spectrophotometer. All experiments were performed using MilliQ water.

S2 Synthesis

Hydrazide **1**

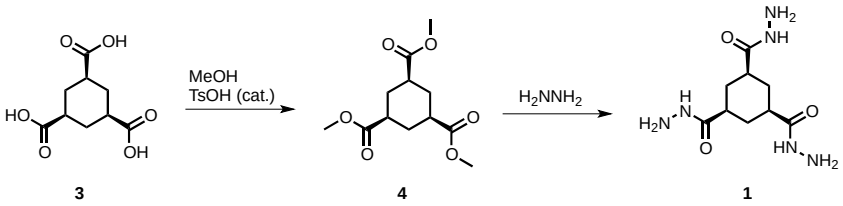

3 **4** **1**

6.0 g (28 mmol) *cis,cis*-1,3,5-triscarboxylic acid **3** was dissolved in 400 ml dry methanol. A catalytic amount of *p*-toluenesulphonic acid was added and the mixture was refluxed for 48 hours under a nitrogen atmosphere. Next, the reaction was quenched with a saturated aqueous $NaHCO_3$ solution and the resulting mixture was extracted with diethylether. The organic layer was washed with water and brine. The organic layer was dried over Na_2SO_4 and the solvents were evaporated *in vacuo*, yielding 4.9 g (19 mmol, 68%) of tri-ester **4** as a white powder. ^{1}H NMR (400 MHz, $CDCl_3$, ppm): 3.68 (s, 9H, OC*H*$_3$), 2.44-2.33 (m, 3H, C*H*), 2.31-2.23 (broad m, 3H, C*H*), 1.57-1.47 (q, 3H, C*H*); ^{13}C NMR (100 MHz, $CDCl_3$, ppm): 174.4 (*C*=O), 51.8 (O*C*H$_3$), 41.7 (*C*H), 30.4 (*C*H$_2$).

Hydrazine monohydrate (10 ml, 194 mmol) was added in portions to a solution of **4** (4.9 g, 19 mmol) in methanol. The mixture was stirred overnight at room temperature, yielding a white slurry. The solvents and hydrazine excess were evaporated *in vacuo*, yielding tris-hydrazide **1** as a white powder (4.9 g, 19 mmol, quant.). ^{1}H NMR (400 MHz, d_6-DMSO): δ 8.95 (s, 3H, N*H*), 4.13 (broad s, 6H, N*H*$_2$), 2.11 (t, J = 11, 3H, C*H*), 1.56-1.48 (m, 6H, C*H*$_2$); ^{13}C

NMR (100 MHz, D_2O): δ 176.8 (*C*=O), 41.7 (*C*H), 30.0 (*C*H_2). MS (ESI pos.) m/z 258.9 $[M+H]^+$, 280.8 $[M+Na]^+$; FT-IR (ATR, neat, cm^{-1}): ν 3305 (N-H stretch), 2941, 2923, 2865 (C-H stretch), 1652 (C=O stretch), 1533 (N-H bend).

Aldehyde **2**

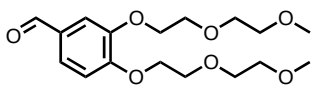

A slurry of 3,4-dihydroxybenzaldehyde (10.0 g, 72.5 mmol), tosyldiethyleneglycolmono-methylether (43.7 g, 159 mmol), potassium carbonate (41.0 g, 297 mmol) and DMF (100 mL) was stirred at 100°C overnight. After cooling to room temperature, ethyl acetate and water were added. The water layer was extracted with ethyl acetate, after which the combined organics were washed with saturated bicarbonate solution (3x), water (3x) and brine (1x). The organic layer was dried over Na_2SO_4, and removed by evaporation under reduced pressure, yielding aldehyde **2** as a colorless oil (22.3 g, 65.2 mmol, 90%). ^{1}H NMR (400 MHz, $CDCl_3$) δ 9.87 (s, 1H, C*H*O), 7.47-7.49 (m, 2H, Ar*H*), 7.05 (d, 1H, J=8.1Hz, Ar*H*), 4.26-4.30 (m, 4H, OCH_2), 3.92-3.96 (m, 4H, OCH_2), 3.76-3.80 (m, 4H, OCH_2), 3.58-3.62 (m, 4H, OCH_2), 3.42 (s, 6H, OCH_3); ^{1}H NMR (400 MHz, DMSO-d_6) δ 9.82 (s, 1H, C*H*O), 7.53 (dd, J = 8.2, 1.5, 1H, Ar*H*), 7.42 (s, 1H, Ar*H*), 7.18 (d, J = 8.3, 1H, Ar*H*), 4.20 (t, J = 4.5, 2H, OCH_2), 4.15 (t, J = 4.5, 2H, OCH_2), 3.76 (app. q, J = 4.6, 4H, OCH_2), 3.60 (app. t, J = 4.7, 4H, OCH_2), 3.44 (app. t, J = 4.6, 4H, OCH_2), 3.23 (s, 6H, OCH_3). ^{13}C NMR (100 MHz, $CDCl_3$): δ 190.1 (*C*=O), 153.8 (C_{Ar}), 148.6 (C_{Ar}), 129.7 (C_{Ar}), 125.9 (C_{Ar}), 112.0 (C_{Ar}), 111.5 (C_{Ar}), 71.9 (O*C*H_2), 71.9 (O*C*H_2), 70.2 (O*C*H_2), 70.2 (O*C*H_2), 68.9 (O*C*H_2), 68.8 (O*C*H_2), 68.2 (O*C*H_2), 68.1 (O*C*H_2), 58.3 (O*C*H_3), 1 peak missing (O*C*H_3) due to overlap; MS (ESI pos.) m/z 343.7 $[M+H]^+$, 365.3 $[M+Na]^+$. FT-IR (ATR, neat, cm^{-1}): ν 2925, 2875, 2822, 2727 (C-H stretch), 1684 (C=O stretch), 1595, 1584 (C=C stretch), 1265, 1239, 1106, 1050, 1028 (C-O-C stretch).

Fluorescein labelled aldehyde **5**

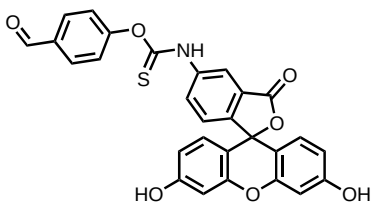

To a solution of 4-hydroxybenzaldehyde (15 mg, 0.12 mmol) and fluorescein isothiocyanate (39 mg, 0.10 mmol, mixture of isomers) in DMF (2.0 ml), K_2CO_3 (41 mg, 0.30 mmol) was added and the mixture was stirred at 80 °C overnight. After completion of the reaction, the solvent was removed under reduced pressure, and the obtained residue was washed several times with CH_2Cl_2 to remove excess 4-hydroxybenzaldehyde. The red residue was dissolved in MeOH and filtered. Concentration under reduced pressure provided the desired compound as a red colored solid (47 mg, 92 %). ^{1}H NMR (300 MHz, CD_3OD, ppm): δ 9.42 (s, 1H, C*H*O), 8.01 (s, 1H, Ar*H*), 7.90 (m, 1H, Ar*H*), 7.57 (d, *J* = 8.5 Hz, 2H, Ar*H*), 7.18 (m, 3H, Ar*H*), 6.56 (m, 6H, Ar*H*). ^{13}C NMR (100 MHz, CD_3OD): δ (ppm) = 191.9 (*C*HO), 182.6 (*C*=S), 172.3 (O-*C*=O), 160.2 (C_{Ar}), 159.2 (C_{Ar}), 143.7 (C_{Ar}), 138.4 (C_{Ar}), 134.2 (C_{Ar}), 133.7 (C_{Ar}), 132.5 (C_{Ar}), 132.1 (C_{Ar}), 127.7(C_{Ar}), 126.9 (C_{Ar}), 124.2 (C_{Ar}), 123.8 (C_{Ar}), 120.1 (C_{Ar}), 113.1 (C_{Ar}), 109.7 (C_{Ar}), 104.5 (C_{Ar}), 1 peak missing (C_{Spiro}) due

to poor quaternary carbon signal strength resulting from poor solubility. FT-IR (ATR, neat, cm^{-1}): □ 3341 (broad), 1634, 1570, 1504, 1461, 1391, 1304, 1213, 1170, 1150, 1109, 1080, 850, 913. HPLC (gradient 5→20 % MeOH/H_2O): 3.18 min. MS (ESI neg.): *m/z* = 254.8 $(M-2H)^{2-}$, 263.9 $(M-2H+H_2O)^{2-}$, 272.9 $(M-2H+2H_2O)^{2-}$, 280.9 $(M-2H+3H_2O)^{2-}$.

Spectra

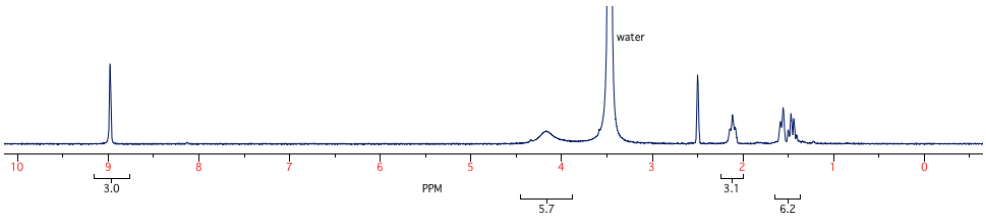

Figure S1a | ^{1}H NMR (DMSO-D_6) of hydrazide **1**.

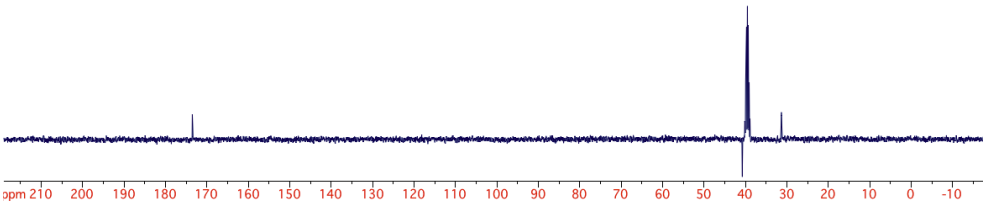

Figure S1b | ^{13}C NMR, APT (DMSO-D_6) of hydrazide **1**.

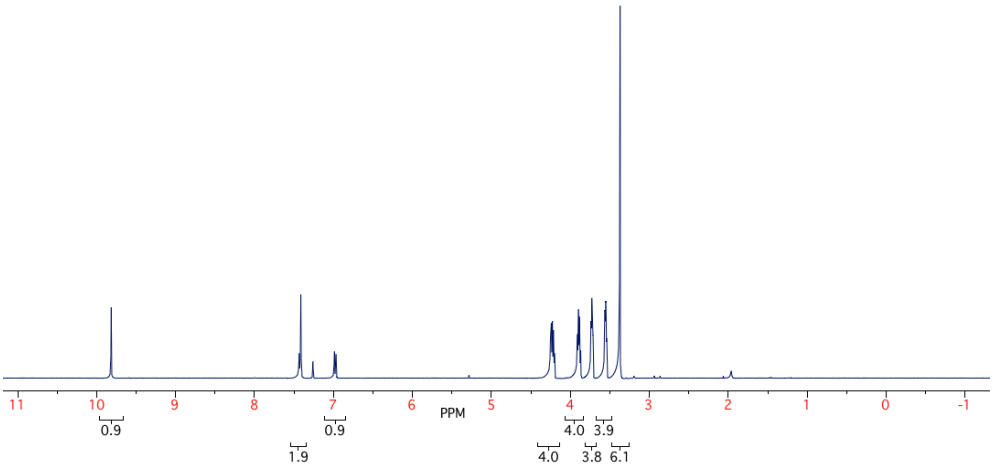

Figure S1c | ^{1}H NMR ($CDCl_3$) of aldehyde **2**.

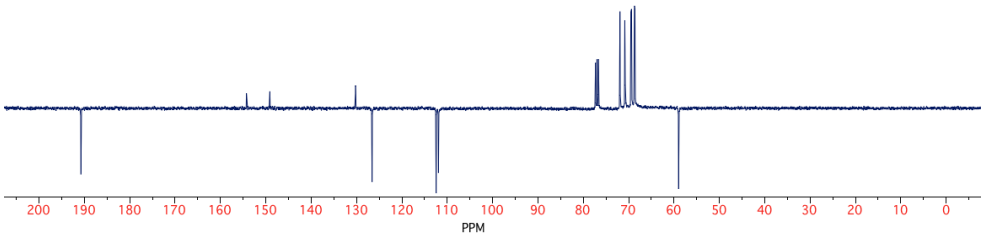

Figure S1d | ^{13}C NMR, APT ($CDCl_3$) of aldehyde **2**.

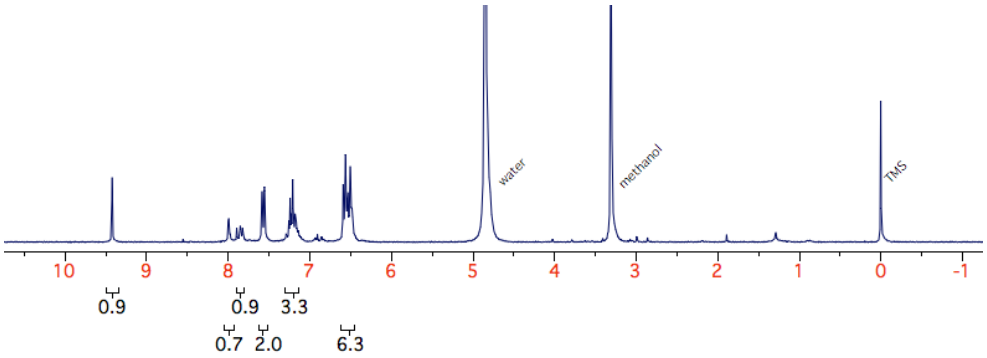

Figure S1e | ^{1}H NMR (CD_3OD) of fluorescein labeled aldehyde **5**.

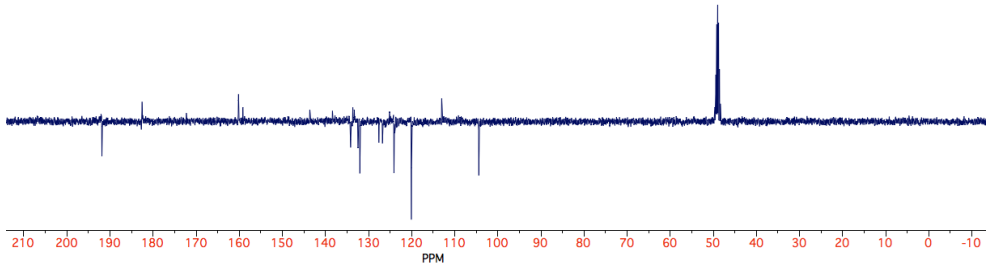

Figure S1f | ^{13}C NMR, APT (CD_3OD) of fluorescein labeled aldehyde **5**.

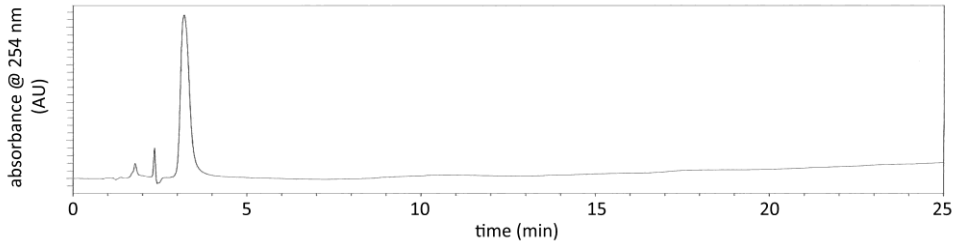

Figure S1g | HPLC trace of fluorescein labeled aldehyde **5**, monitored at 254 nm.

S3 Other experimental techniques and remarks

Most experiments were performed at an initial ratio of **1**:**2**=1:6, i.e. 2 aldehyde groups per 1 hydrazide group. Increasing or decreasing this ratio (either to 3:1 aldehyde:hydrazide or to 1:1 aldehyde:hydrazide) had no significant effect on the final product distribution. It did affect the overall kinetics of conversion, showing the expected faster reactions at higher ratios.

Typical stock solutions

Hydrazide: [**1**] = 40 mM in phosphate buffer. Aldehyde: [**2**] = 240 mM in phosphate buffer.

Critical gelation concentration (CGC) test procedure

All solutions were prepared from aqueous 100 mM sodium phosphate buffer at the appropriate pH. A sample vial (2 ml) was filled with the appropriate volumes of stock solution and made up to 1 ml total volume by addition of buffer. The vial was closed, shaken vigorously and allowed to stand overnight. The test tube was inverted to see whether a gel network had formed. The CGC is the point in between the last concentration where a gel was formed and the concentration where the solvent could no longer be supported.

Cryo-TEM

A few microliters of suspension were deposited on a Quantifoil 3.5/1 holey carbon coated grid. After blotting away the excess of liquid the grids were plunged quickly in liquid ethane. Frozen-hydrated specimens were mounted in a cryo-holder (Gatan, model 626) and observed in a Philips CM 120 electron microscope, operating at 120 kV. Micrographs were recorded under low-dose conditions on a slow-scan CCD camera (Gatan, model 794).

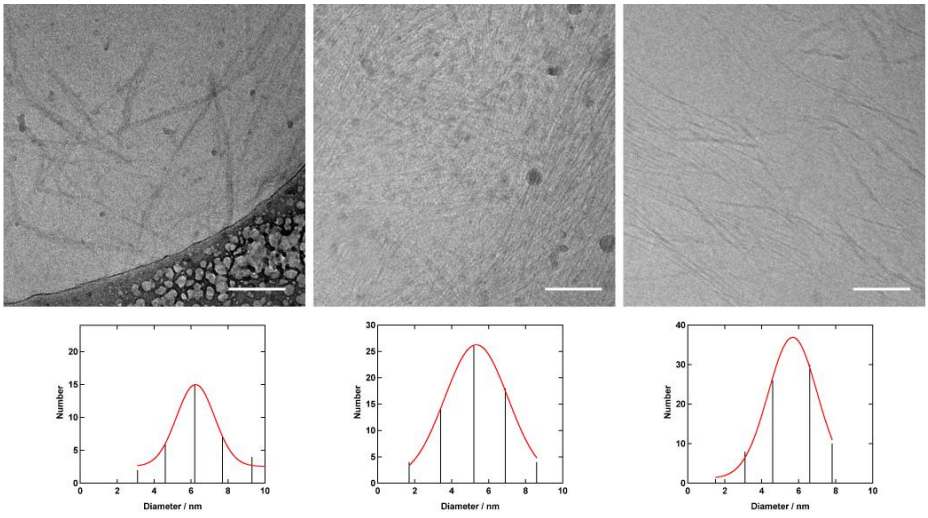

Figure S2 | Cryo-TEM pictures of pH 7.0 (left), pH 7.0 + 10 mM aniline (middle), pH 5.0 (right); all samples where prepared by mixing solution of **1** and **2** ([**1**]=20 mM, **1**:**2**=1:6, 0.1 M phosphate buffer) at room temperature. Below are the statistical distributions of single fibre diameters (obvious fibre bundles were omitted) and their Gaussian fits. All scale bars are 150 nm.

Confocal Laser Scanning Microscopy (CLSM)

Confocal Laser Scanning Microscopy (CLSM) pictures were obtained in the fluorescence mode on a Zeiss LSM 700 confocal laser scanning microscope. To a stock solution of hydrazide **1** at pH 5, pH 7 or with 10 mM aniline at pH 7 was added a fluorescein-derived-aldehyde **5** solution so that the final concentration of fluorescent probe **5** was 30 μM. To form gels, 0.5 mL of this fluorescently labeled hydrazide solution was added to 0.5 mL aldehyde **2** solution. The mixture was immediately deposited into a PDMS cuvette closed off with a glass wafer and was allowed to stand overnight. The laser beam was focused on a 40X oil immersion objective and the sensitivity of detectors and filters were adjusted accordingly in order to obtain maximum signal to noise ratio.

Scanning Electron Microscopy (SEM)

SEM samples were prepared by gently transferring small amounts of gel (±50 μL) to a glass cover slip. The samples were then dehydrated by exchange with ethanol by submerging them in a solution with increasing concentration ethanol over the course of an hour (starting at 10% to finally 100% with increments of 10%). Finally, by means of critical point drying (CPD) the ethanol was removed. The coverslips were glued to SEM stubs and coated with 4 nm of osmium using an osmium plasma coater in order to minimize charging during imaging. Finally, SEM micrographs were obtained on a Hitachi SU8030, operating at 2 kV with a typical current of 5 μA. If charging took place the current was decreased to 2 μA.

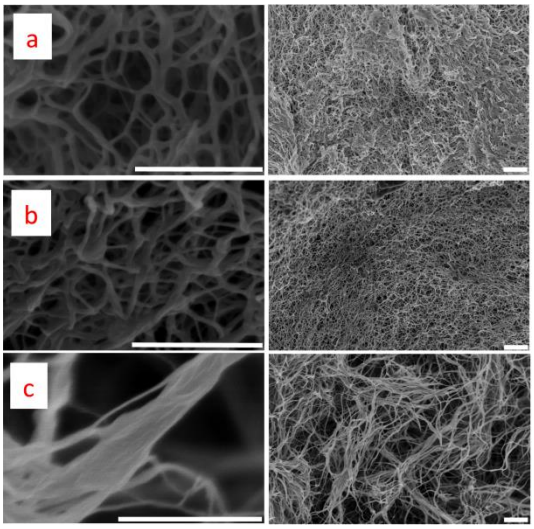

Figure S3 | Influence of catalysis on material morphology, as observed by scanning electron microscopy. a) pH 5.0, b) pH 7.0 with 10 mM aniline, c) pH 7.0; all samples where prepared by mixing solutions of 1 and 2 ([**1**]=4 mM, **1**:**2**=1:6, 0.1 M phosphate buffer). All scale bars are 500 nm.

Wide angle x-ray diffraction

Wide angle X-ray diffraction experiments were performed on a Bruker D8 Discover X-ray diffractometer equipped with a 2-dimensional Hi-Star Area Detector and Cross Coupled Göbel Mirrors. The measurements were performed in transmission mode at room temperature using monochromatic Cu Kα radiation with a wavelength of 0.154 nm and a sample to detector distance of 6 cm. The diffraction data was recorded for 2θ values between 2.5° and 39° using a 10 minutes exposure time and correction for the background.

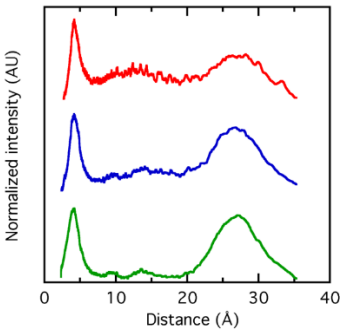

Figure S4 | wide angle x-ray diffraction patterns of freezedried gels. Green: pH 5.0, blue: pH 7.0 with 10 mM aniline, red: pH 7.0.

S4 Gelator characterization

Gelator **3** was prepared and isolated by adding a 60 mL of a 16 mM hydrazide **1** solution in MQ water to 60 mL of a 96 mM aldehyde **2** solution in MQ water so that the final ratio is 1:6 hydrazide to aldehyde, as all previous described experiments. This solution was allowed to stand overnight upon which a gel was formed. This gel was freeze dried to yield a mixture of gelator **3** and aldehyde **2** in a final 1:3 ratio as a white powder.

A similar procedure was applied for the synthesis of gelator **3** without excess aldehyde, using an initial **1**:**2**=1:3 ratio.

Characterization

The composition of gelator mixtures was analyzed by HPLC, using a water:MeOH+0.5% triethylamine (TEA) gradient (**Fig. S5**). Hydrazone formation and exchange was quenched by adding a 50 μL aliquot of reaction mixture to a 200 μL THF + 200 μL water (saturated with triethylamine) mixture.

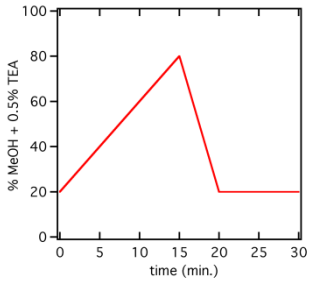

Figure S5 | HPLC solvent gradient.

HPLC-MS: aldehyde **2**: retention time 3.4 min., MS (ESI pos.) m/z 343.7 $[M+H]^+$, 365.3 $[M+Na]^+$; mono-hydrazone: retention time 8.4 min., MS (ESI pos.) m/z 605.3 $[M+Na]^+$, calcd 605.3; di-hydrazone: retention time 10.4 min., MS (ESI pos.) m/z 907.6 $[M+H]^+$, calcd 907.5; 929.5 $[M+Na]^+$, calcd 929.5; tri-hydrazone: retention time 12.0 min., MS (ESI pos.) m/z 638.1 $[M+2Na]^{2+}$, calcd 638.3; 1253.8 $[M+Na]^+$, calcd 1253.6.

Gelator **3**, initial ratio **1**:**2**=1:3: Composition (HPLC-MS): >95% tri-hydrazone, <5% di-hydrazone, <0.5% mono-hydrazone (not observed); ^{1}H NMR (DMSO-d_6): δ 11.28 (s, 1.7H, N-H), 11.15 (s, 1.3H, N-H), 8.10 (s, 1.7H, HC=N), 7.90 (s, 1.3H, HC=N), 7.31-7.01 (m, 9H, Ar-H), 4.11 (br s, 12H), 3.74 (br s, 12H), 3.60 (br s, 12H), 3.47 (peak partly obscured by DMSO peak), 3.23 (s, 18H), 2.05 (br, 1.3H), 1.91 (br, 1.7H), 1.63 (br, 6H); FT-IR (ATR, neat, cm^{-1}): ν 2923, 2872, 2815 (C-H Stretch), 1652 (C=O stretch),1601 (C=N stretch), 1576 (C=C stretch), 1560, 1512 (N-H bend).

Gelator **3**, initial ratio **1**:**2**=1:6: Composition (HPLC-MS): >95% tri-hydrazone, <5% di-hydrazone, <0.5% mono-hydrazone (not observed); FT-IR (ATR, neat, cm^{-1}): ν 2923, 2876, 2820 (C-H stretch), 1684 (C=O stretch of **2**), 1656 (C=O stretch), 1597, 1584, (C=C stretch), 1560, 1512 (N-H bend).

S5 Media effects on gelation

The influence of the catalysts on the gelation media was investigated by measuring critical gelation concentrations of separately prepared (catalyst-free) gelator **3** in the appropriate catalyst-buffer solutions. Attempts were made to prepare such gels by either heating-induced dissolution, or solvent injection. Neither method proved viable. At the appropriate concentrations, no complete dissolution of **3** in water was observed even after prolonged heating at > 100 °C, and heating might displace the equilibrium between gelator **3**, the hydrazone and aldehyde. For solvent injection, no organic, water-miscible solvent was found that allowed dissolution of **3** at a high enough concentration to keep the concentration of cosolvent to a minimum, and for the solvent systems tested only inhomogeneous gels were obtained, if any. Therefore an alternative method was developed. To dissolve gelator **3** in buffer THF was used as a cosolvent. After dissolution of

3 the THF was slowly evaporated to allow the formation of gels, using the following protocol: A mixture of gelator **3** and aldehyde **2**, at a final 1:3 ratio, was suspended in 400 µl of the appropriate buffer (0.1M phosphate: pH5; pH7; pH7 with 10 mM aniline). 200 µl THF was added and the system was heated by less than 15 °C, leading to the formation of an isotropic solution. The isotropic solutions were stored at room temperature at a slightly reduced pressure (100 mbar) to remove the THF over the course of 2 hours. During these 2 hours the samples became more turbid indicative of the formation of gels. The turbidity increased at visually equal rates for all samples, and at the end of the process visually indistinguishable gels were obtained. Once the THF was fully removed the critical gelation concentration was determined by means of an inverted tube test. This resulted in a cgc of 4.5 mM ± 0.5 mM for all three media, indicating that, after formation of the gelator molecules, the employed catalysts do not influence the gelation process to any significant extent.

S6 Gelator conversion and rheology

Oscillatory experiments were performed using a rheometer (AR G2, TA instruments) in a strain-controlled mode, equipped with a steel plate-and-plate geometry of 40 mm in diameter, equipped with a water-trap. The temperature of the plates was controlled at 25 ± 0.2°C. All solutions were prepared from aqueous 100 mM sodium phosphate buffer at pH 5, 6 or 7. A sample vial (glass, 4 ml) was filled with 0.2 ml aldehyde stock solution. First, 0.1 ml of an appropriate aniline stock solution or plain buffer was added and shaken vigorously. Subsequently, 0.1 ml of hydrazide stock solution was added, and after vigorous shaking the sample was immediately positioned onto the rheometer plate. The most reproducible results were observed when the gel was poured directly onto the plate. Due to the fast nature of gelation of the gels at pH 5, these samples were prepared by directly pipetting the two solutions on the rheometer and mixing quickly with a spatula. Both methods of preparation imply that the start of the measurement (t=0 in **Fig S6a-c**) occurs with a slight delay with respect to the start of the formation of **3**. All gels showed a linear viscoelastic regime up to 0.5% strain. Therefore, all time sweeps were performed under 0.05% stain with a frequency of 1 Hz until no increase in G' was observed.

The formation of potential gelators over time was followed by HPLC, using a water (MQ):MeOH+0.5% triethylamine (TEA) gradient (**Fig. S5**). Hydrazone formation was quenched by adding a 50 µL aliquot of reaction mixture to a 200 µL THF + 200 µL water (saturated TEA) mixture.

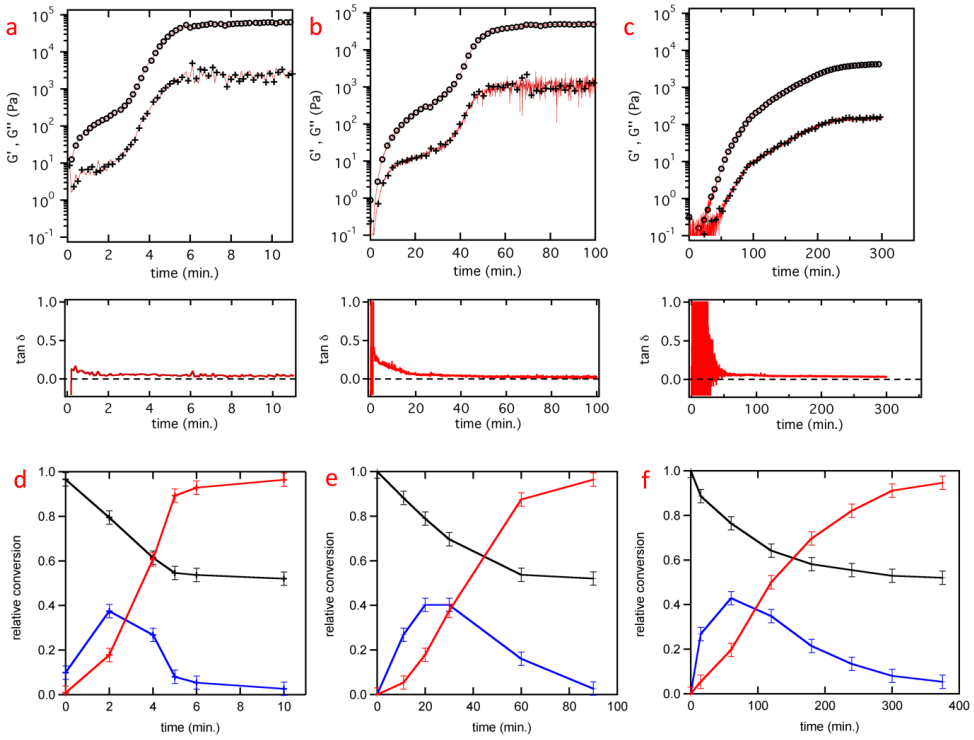

Figure S6 | Time-dependent rheology gel formation, and gelator formation over time: pH 5 (left), pH7+10mM aniline (middle), pH 7 (right). a-c: rheology (G' and G''); tan δ is plotted below each graph. d-f: HPLC data shows formation of di-hydrazone (blue), tri-hydrazone (red), and the consumption of aldehyde (black). HPLC conversion was calculated at 274 nm (isosbestic point), compensating for an assumed linear dependence of the extinction coefficient on the number of aromatic hydrazones per molecule; conversion 1.0 = 100% theoretical conversion. All samples: **1**:**2**=1:6, [**1**]=20 mM; 0.1 M phosphate buffer.

S7 Aniline dependence

To investigate the origin of the non-linear dependence of the mechanical strength of aniline-catalyzed gels (**Fig. 3d**), on the aniline concentration, a series of experiments was conducted. All experiments were performed under the conditions of the rheology experiment in **Fig. 3** ([**1**] = 20 mM, **1**:**2**=1:6, pH 7.0, 0.1 M phosphate buffer, [aniline] = 0-50 mM). First, the influence of the aniline concentration on final conversion and rate of structure formation was investigated (**Fig. S7**). The final conversion to gelator after equilibration was found to be independent of aniline concentration (**Fig. S7b**). Structure formation as followed by turbidity measurements using a UV-VIS spectrometer showed a typical dependence of the rate on the aniline concentration, with higher rates observed for higher concentrations (**Fig. S7a**). Confocal laser scanning microscopy (**Fig. S8**) and scanning electron microscopy (**Fig. S9**) showed the formation of fibrous structures, with dense networks made up of thin, branched fibres in the presence of catalyst, and much less dense

networks made up of thick bundles of fibres at very low or zero catalyst concentrations (**Figs. S8a-b, S9a-b**). CGC tests using evaporation of THF as a cosolvent to test the influence of the presence of aniline on the media quality (see section S5) revealed no changes in CGC with changing aniline concentration. However, HPLC-MS analysis did reveal the formation of the aniline-derived imine (MS (ESI pos.) m/z 418.4 $[M+H]^+$, 440.4 $[M+Na]^+$) of aldehyde **2** at high aniline concentrations (20 and 50 mM). This amphiphilic imine may interact with the gel fibres, thus weakening the structures.

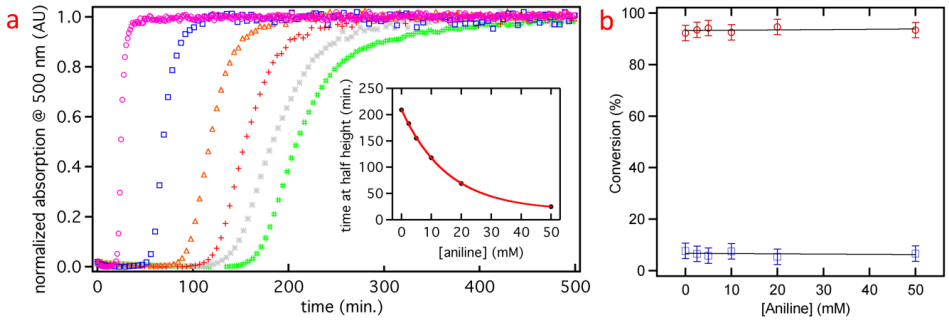

Figure S7 | a) Turbidity measurements, showing normalized time-dependent absorbance of 500 nm light during structure formation, with varying concentrations of aniline ([aniline]: 0 mM (green), 2.5 mM (grey), 5 mM (red), 10 mM (orange), 20 mM (blue), 50 mM (violet). The inset shows the relation between the rate of turbidity development (plotted as the time at half-height) and aniline concentration. The red curve is a fitted exponential function. All samples were prepared by mixing solutions of **1** and **2** ([**1**]=20 mM, **1**:**2**=1:6, pH 7.0; 0.1 M phosphate buffer). b) HPLC data shows formation of di-hydrazone (blue), tri-hydrazone (red), depending on aniline concentration. Samples were measured after equilibration (24 hours, room temperature). HPLC conversion was calculated at 274 nm (isosbestic point), compensating for an assumed linear dependence of the extinction coefficient on the number of aromatic hydrazones per molecule; conversion 1.0 = 100% theoretical conversion. All samples: **1**:**2**=1:6, [**1**]=20 mM; pH 7.0; 0.1 M phosphate buffer. The grey lines are fitted linear functions.

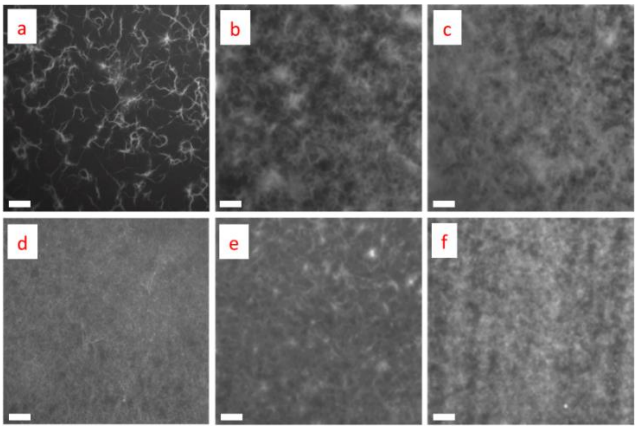

Figure S8 | Influence of aniline catalysis on material morphology, measured by confocal laser scanning fluorescence microscopy. a) [aniline]=0 mM; b) [aniline]=2.5 mM; c) [aniline]=5 mM; d) [aniline]=10 mM; e) [aniline]=20 mM; f) [aniline]=50 mM. All samples were prepared by mixing solutions of **1** and **2** ([**1**]=20 mM, **1**:**2**=1:6, pH 7.0; 0.1 M phosphate buffer) and 30 μM fluorescent probe at room temperature. Scale bar = 10 μm.

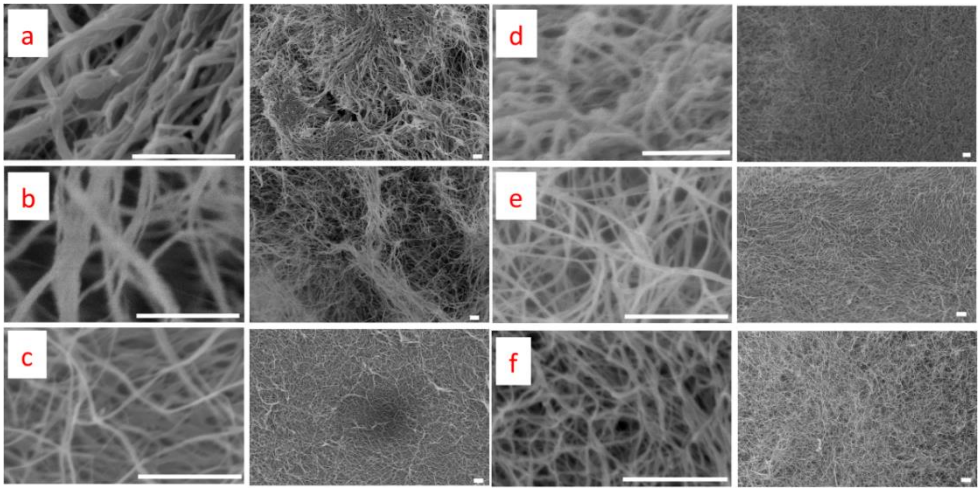

Figure S9 | Influence of aniline catalysis on material morphology, as observed by scanning electron microscopy. a) [aniline]=0 mM; b) [aniline]=2.5 mM; c) [aniline]=5 mM; d) [aniline]=10 mM; e) [aniline]=20 mM; f) [aniline]=50 mM. All samples were prepared by mixing solutions of **1** and **2** ([**1**]=20 mM, **1**:**2**=1:6, pH 7.0; 0.1 M phosphate buffer). All scale bars are 500 nm.

S8 Avrami analysis

To determine the Avrami coefficient *n*, ln(-ln(1-X)) was plotted against ln(t-t_0), with X = (Abs_t-Abs_0)/(Abs_∞-Abs_0) as a measure of conversion. The Avrami coefficient is then the slope of the first part of the curve, as this is where the primary nucleation-growth process takes place.

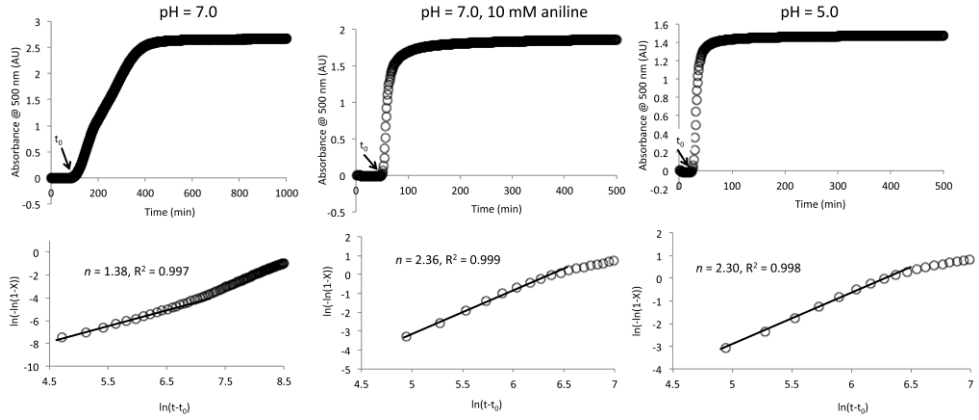

Figure S10 | time-dependent absorbance of samples during gelation (upper), and the derived Avrami plots (lower).

A toolbox for controlling the properties and functionalisation of hydrazone-based supramolecular hydrogels

4

Abstract

In recent years, we have developed a low molecular weight hydrogelator system that is formed in situ at ambient conditions through catalysed hydrazone formation between two individually non-gelating components. In this contribution, we describe a molecular toolbox based on this system which allows us to 1) investigate the limits of gel formation and fine tuning of their bulk properties, 2) introduce multicolour fluorescent probes in an easy fashion to enable high-resolution imaging, and 3) chemically modify the supramolecular gel fibres through click and non-covalent chemistry, to expand the functionality of the resultant materials. In this paper we show preliminary applications of this toolbox, enabling covalent and non-covalent functionalisation of the gel network with proteins and multicolour imaging of hydrogel networks with embedded mammalian cells and their substructures. Overall, the results show that the toolbox allows for on demand gel network visualisation and functionalisation, enabling a wealth of applications in the areas of chemical biology and smart materials.

Published as:

A toolbox for controlling the properties and functionalisation of hydrazone-based supramolecular hydrogels

Jos M. Poolman, Chandan Maity, Job Boekhoven, Lars van der Mee, Vincent A.A. le Sage, G.J. Mirjam Groenewold, Sander I. van Kasteren, Frank Versluis, Jan H. van Esch and Rienk Eelkema

Journal of materials chemistry B **4,** 852–858 (2016)

Introduction

Supramolecular systems consist of self-assembled structures that are held together by non-covalent interactions. By carefully balancing the strength of the individually weak interactions, relatively robust architectures can be devised, retaining the ability to respond to environmental changes such as temperature[1], light[2] and pH[3]. In recent years, a wealth of systems capable of forming supramolecular fibres and hydrogels has been reported.[4,5] Due to the reversible nature of the bonds that hold the network together, supramolecular hydrogels find applications as biomaterials[6], sensors[7] and host-guest systems[8]. The gelators are often derived from biological materials such as peptides[9–12], nucleobases,[13–15] saccharides[16–18] and hybrids thereof.[19–21] Alternatively, small synthetic organic compounds have been used extensively to form hydrogels based on non-covalent interactions.[22–28] Nevertheless, it remains difficult and laborious to modulate the properties of the obtained hydrogels, as it requires complete synthesis of a new hydrogelator. Furthermore, introduction of functional groups on the fibrillar networks typically requires multi-step syntheses of functionalised monomers[29–31], rendering gel functionalisation an inefficient process. To overcome these challenges, we present a modular hydrogelator system that spontaneously forms in situ by chemical bond formation between non-gelating precursors. The chemical structure and properties of the resulting materials can be easily tuned by slight modifications of the precursor molecules. These precursor molecules are synthesised in a few, straightforward steps from readily available starting materials. Moreover, by mixing in small amounts of functionalised precursors with the standard precursors, hydrogel networks are obtained that are molecularly designed to display specific functions. In all, this strategy allows for easy tuning of hydrogel properties and further modification of the fibre network.

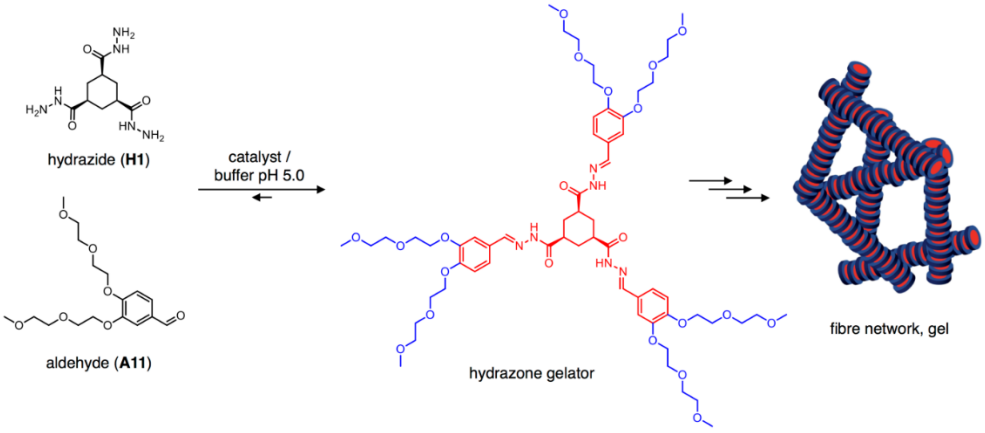

Figure 1 | Schematic representation of catalysed gel formation. Soluble, non-gelating starting components **H1** and **A11**, react to give a self-assembling hydrogelator molecule, which assembles into fibres and finally a network, gelling the solvent.

Recently, we have developed a supramolecular hydrogelator that is formed in situ through hydrazone formation between water-soluble hydrazide **H1** and aldehyde **A11** under ambient conditions **(Fig. 1)**.[32–34] Gels will form spontaneously at room temperature after mixing of the precursors, without the need for a heating step to aid dissolution of the gelator. The rate of hydrazone formation can be increased through the use of catalysts such as aniline or acid, reducing gelation times from hours to minutes. Upon reaching a critical minimum concentration, the hydrazone gelator self-assembles into fibres, which in due course form a network capable of retaining water. The use of catalysis supplies us with a handle through which the rate of formation and mechanical properties of the gel network can be controlled.[33,34] Additionally, we have shown that through the catalyst the spatial distribution of gel formation can be controlled, using micro-patterned catalytic surfaces[35] or a light triggered catalyst[36]. In this contribution we present a molecular toolbox which is aimed at: 1) investigating the molecular constraints of gel formation, 2) covalently functionalising the network with a variety of fluorescent probes and 3) the integration of reactive groups in the hydrogel network, allowing for further modification of the gel fibres **(Fig. 2)**. Our approach enables easy tuning of the physical properties of the gel network and its further functionalisation. We accomplish this either using derivatives of the aldehyde and hydrazide precursors as the majority components in the gelation mixture, or by mixing in small amounts of functionalised derivatives of the benzaldehyde precursor with the standard aldehyde precursor **A11**. This makes our gel system highly versatile, enabling the incorporation of a wide variety of benzaldehyde-derived functional compounds into the gel network. Additionally, the synthesis of these derivatives is generally straightforward and can be achieved in a few steps from commonly available precursors.

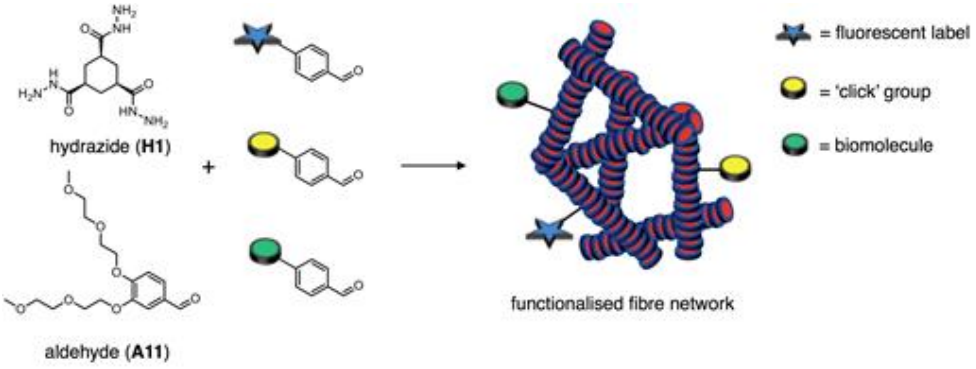

Figure 2 | Concept of functionalised gel fibre network formation via partial replacement of the original aldehyde (**A11**) by a functionalised aldehyde creating a gel with tailored functionalities.

Experimental section

Synthesis

Detailed synthetic procedures and characterisations are found in the supporting information.

Critical gelation concentration experiments

Gels were formed by preparing stock solutions of the aldehyde (240 mM) and hydrazide (40 mM) in 100 mM sodium phosphate buffer (Na_2HPO_4/NaH_2PO_4, pH 5.0). Appropriate amounts of the stock solutions were mixed and vortexed vigorously for three seconds. The mixed samples were left to gel overnight and gelation was checked using the inverted vial test. The critical gel concentration (CGC) is expressed as the initial concentration (in mM) of the hydrazide precursor in the mixture and defined as the point between the lowest concentration at which gels were formed and the highest concentration at which the solvent cannot be supported.

Confocal Laser Scanning Microscopy

Stock solution of **H1**, **A11**, functionalised aldehydes (**A14** - **A23**, **A25**) and reactive compounds (azide-fluor 545, FITC-SH, Fluor 488-alkyne, Cy5-labelled azide-Ovalbumin and fluorescein labelled Concanavalin A were prepared in phosphate buffer of pH 5.0 **(see supplementary information for details)**. Gel samples were prepared by mixing an appropriate amount of stock solutions of **H1**, **A11** and the functionalised aldehyde. The mixture was immediately deposited into a polydimethylsiloxane cuvette or imaging chamber (diameter×thickness = 20 mm×0.6 mm), closed off with a glass cover slide and was allowed to stand overnight. Confocal laser scanning micrographs were obtained in fluorescence mode on a Zeiss LSM 700. The laser beam was focused on a 40× oil immersion objective and the sensitivity of detectors and filters were adjusted accordingly to obtain the maximum signal to noise ratio. CLSM micrographs **(Fig. 7 and supplementary information)** were recorded using the same settings (apart from excitation wavelength) to allow comparison of fluorescence intensity for analysis purposes.

Results and discussion

In a first study, we examined the influence of the molecular design of the precursors on gelation behaviour. To do so, we synthesised a small library of aldehyde and hydrazide derivatives, and tested all possible combinations for their gelation behaviour in a simple mixing + reaction experiment (**Fig. 3, Table 1**). The benzaldehyde derivatives were functionalised with one or two ethylene glycol (EG) chains of varying length (**Fig. 3**), which increases the water solubility of the compounds due to the hydrophilic nature of EG and possibly prevents precipitation of the corresponding hydrazone through favourable

interactions between the supramolecular fibres and the solvent.[37] These functions of the EG chains are assumed to be of paramount importance for the self-assembly of the hydrazone materials into fibres and subsequent gelation. The hydrazide series contained a trishydrazide (**H1**) and six bishydrazide (**H2-H7**) compounds, with a varying spacer length between the two hydrazide moieties, ranging 2-7 carbon atoms. The hydrazides (**H1-H7**) were either commercially available or easily synthesised in one step from their corresponding methyl esters in quantitative yield without any purification steps. The aldehyde derivatives (**A2-A4**, **A7-A9**, and **A11-A13**) were synthesised in good yield (78-99 %) from the corresponding hydroxybenzaldehydes (**A1**, **A6** or **A10**) by reaction with the relevant tosylated ethylene glycol monomethyl ether. Compound A5 was synthesised in a single step by reacting A1 and 2-[2-(2-chloroethoxy)ethoxy]ethanol.

Critical gel concentration (CGC) tests were performed to investigate the influence of the molecular design of the starting aldehydes and hydrazides on the gelation behaviour of the resulting hydrazone products. In a typical experiment, the aldehyde and hydrazide derivatives were dissolved separately in a phosphate buffer of pH 5. Whereas the starting materials did not self-assemble under these conditions, mixing the two solutions resulted in conversion to the expected gelating hydrazone products.[32] To promote the full conversion of hydrazides into hydrazones, two equivalents of aldehyde were added for each hydrazide group. Evaluation of the CGC tests was performed by the inverted vial test after the solution had been left to stand overnight at room temperature.

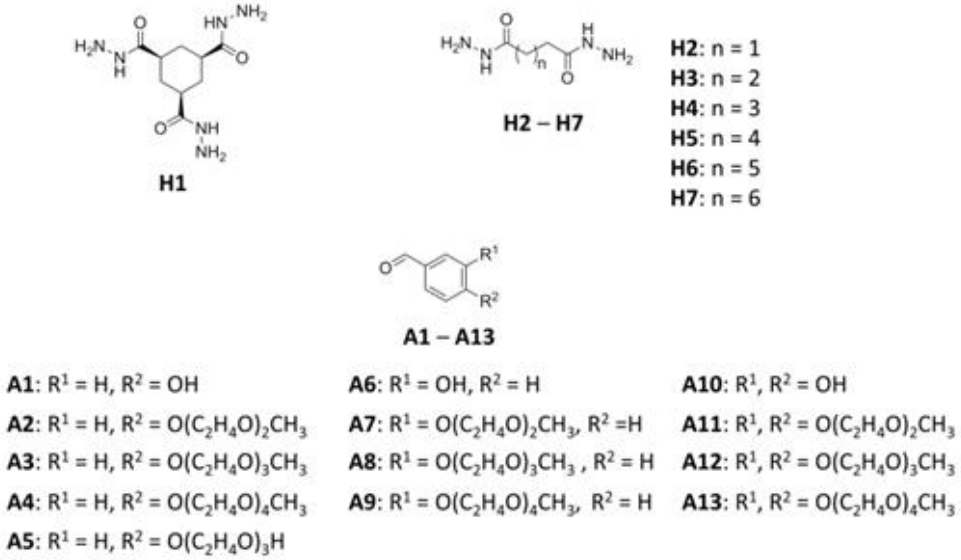

Figure 3 | Molecular structures of the hydrazide and aldehyde derivatives.

Mixing hydrazide H1 with non EG-modified benzaldehyde derivatives (**A1**, **A6**, **A10**) yielded precipitated hydrazone materials instead of gelation. In contrast, benzaldehyde derivatives

bearing more than four EG monomers (**A12**, **A13**) yielded too water-soluble hydrazone materials, maintaining clear solutions after reaction (**Table 1**). In between these two extremes however, opaque gels with a water content of up to 99.5 % (w/w), were obtained from benzaldehyde derivatives modified with 2 to 4 EG, pointing towards a balance between the crystallisation and solubilisation processes. Para-functionalised benzaldehyde derivatives (**A2-A5**) provided stable hydrogels. The optimum gelation efficiency (i.e. lowest CGC, 3.5 mM) was obtained using three EG units (**A3**), whereas benzaldehyde derivatives with shorter (**A2**) and longer EG (**A4**, **A5**) needed higher gelator concentrations (8, 11 and 13 mM respectively). In contrast, meta-functionalised benzaldehyde derivatives (**A7-A9**) showed poor solubility in water compared to their para-functionalised counterparts. This effect is presumably due to higher aromatic surface exposure towards the aqueous environment. Reacting **H1** with either **A7** or **A9** (containing 2 and 4 EG, resp.) yielded gels at the respective concentrations of 5.5 mM and 16 mM, whereas **A8** with 3 EG provided a hydrazone material that precipitated in the form of oil droplets on the bottom of the vial. The meta- and para-functionalised aldehyde (**A11**) with four EG provided a hydrogel with a CGC of 4.5 mM. Furthermore, a benzaldehyde derivative with a terminal hydroxy group on the EG (**A5**) gelated less efficiently than the corresponding derivative with a methyl terminated chain (**A3**).

		benzaldehydes												
		para-substitution					meta				meta, para			
		A1	A2	A3	A4	A5	A6	A7	A8	A9	A10	A11	A12	A13
hydrazides: tris	H1	P	G 8	G 3.5	G 11	G 13	P	G 5.5	P	G 16	P	G 4.5	S	S
hydrazides: bis-hydrazides	H2	P	G 25	WG >25	G 25	WG >25	P	P	P	P	P	S	S	S
	H3	P	P	P	P	P	P	P	P	P	P	S	S	S
	H4	P	G 17.5	G 25	G 20	WG >25	P	P	P	P	P	S	S	S
	H5	P	P	P	P	P	P	P	P	P	P	S	S	S
	H6	P	G 14.5	P	WG >25	P	P	P	P	P	P	P	S	S
	H7	P	P	P	P	P	P	P	P	P	P	P	S	S

Table 1 | Critical gel concentration (CGC) tests with hydrazide and aldehyde derivatives in a pH 5 sodium phosphate buffer under ambient conditions. The tests were performed by mixing the appropriate amount of hydrazide and aldehyde precursors in a sample vial and allowing the samples to stand overnight. Results after inverting the vial were classified into precipitation (P), homogeneous solution (S), opaque gel (G) and weak gel (WG), which is a gel which is not capable of supporting its own weight for >30 seconds. The given numbers are CGC values in mM, where CGC is defined as the minimum concentration of the hydrazide precursor to form a gel that withstands gravity when turned upside down.

Mixing benzaldehyde derivatives with dihydrazide compounds (**H2-H7**) generally afforded gels at higher minimum gelation concentrations (14.5-25 mM) than for **H1** (3.5-16 mM). Also, the range of benzaldehyde derivatives that would yield a gel was narrower (**Table 1**). Remarkably, dihydrazides with a spacer composed of an even number of carbon atoms (**H2**, **H4**, and **H6**) yielded hydrogels, whereas precipitation was observed for the dihydrazides with an odd numbered carbon spacer (**H3**, **H5**, and **H7**). Upon reaction with meta-functionalised benzaldehydes (**A7-A9**), dihydrazides with an even carbon atom spacer yielded crystalline precipitates whereas hydrazone materials with odd carbon atom spacer phase separated in the form of oil droplets. Increasing the length of the carbon atom spacer and thereby decreasing hydrophobicity has a favourable effect on the gelation of the formed hydrazones as lower gelator concentrations are observed with increasing chain length, eventually limited by the solubility of the hydrazide derivative.

For selected samples, we determined the stiffness of the obtained gels using oscillatory rheology (**Fig. 4a**). The elastic modulus G' varied over three orders of magnitude, between 45 Pa (**H2+H3**) and 1.2*105 Pa (**H1+A11**). In general, an inverse relation between the observed elastic modulus and the CGC can be observed (**Fig. 4b**), showing that a lower CGC in general predicts a higher elastic modulus of the obtained material. As all samples were measured at a fixed 20 mM concentration, this general trend partly originates from the higher fibre density for lower-CGC samples, leading to higher G'. **Fig. 4b** also shows a bifurcation in the CGC-G' dependence, with a steeper dependence for **H1** derived gels compared to those derived from **H2-6**. Such a difference in behaviour may point to a different mode of gelation. To get some insight into the morphology of these gels, we collected TEM micrographs for the **H1+A2**, **H1+A7**, **H1+A11** and **H6+A2** gels. All **H1** derived gels gave dense fibre networks consisting of fibres with diameters <10 nm. The **H6+A2** gel however, showed plate-type structures with dimensions in the micrometre range (see the supporting information). This change in morphology may account for the marked difference in both CGC and relation between CGC and G', when compared to **H1** derived gels.

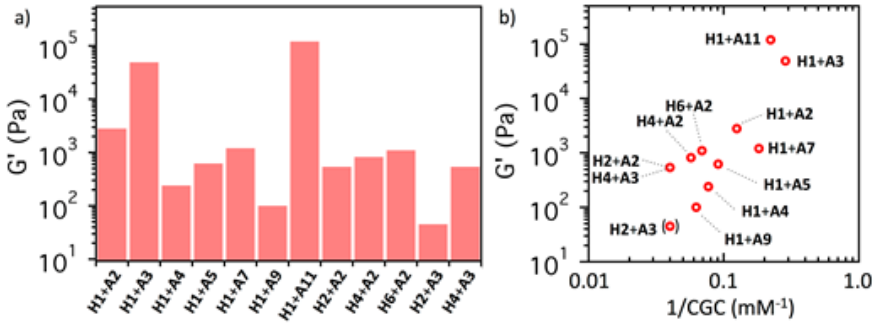

Figure 4 | Rheological data of selected hydrogels. a) shows elastic moduli (G'), measured for 20 mM gels (20 mM of any hydrazide derivative, 120 mM of aldehyde derivative (for **H1**) or 80 mM of aldehyde derivative (for **H2-6**). b) a plot of G' versus the inverse of the CGC. For each point, the corresponding gel mixture is indicated. The **H2+A3** data point is indicated in parentheses, as its CGC was determined at >25 mM (see **Table 1**).

As shown above, our supramolecular gel system enables the tuning of gelation properties such as CGC, elastic modulus or network morphology by changing the aldehyde or hydrazide structure. Next, we made use of this modularity to incorporate chemical labels in the structure. For these experiments, we used the well-characterised **H1-A11** system[32–34] as a common gelator. In a first example, we replaced small fractions of the reacting aldehyde derivatives with aldehyde-derived fluorophores (**Fig. 4**). As we observed earlier that the trishydrazide (**H1**) showed gelation after reaction with a wide range of aldehyde derivatives (**Table 1**), we anticipated that small percentages of other aldehyde derivatives can be incorporated into the supramolecular gel network without hindering gel formation. Using fluorescently labelled aldehyde derivatives allows for imaging of the structure of the supramolecular network using confocal laser scanning microscopy (CLSM). We used various fluorescent probes, with different excitation wavelengths. This strategy increases our flexibility with respect to future applications of our hydrogel system, for instance as scaffolds for 3D cell culturing. There, typically, imaging of cell membranes or nuclei will be performed with the aid of a fluorescent probe, illustrating the need for flexibility in the choice of probe to simultaneously image the hydrogel network structure. Therefore, we synthesised fluorescent styryl, coumarin, fluorescein, rhodamine and cyanine derivatives that contain an aldehyde functionality (**Fig. 5**).

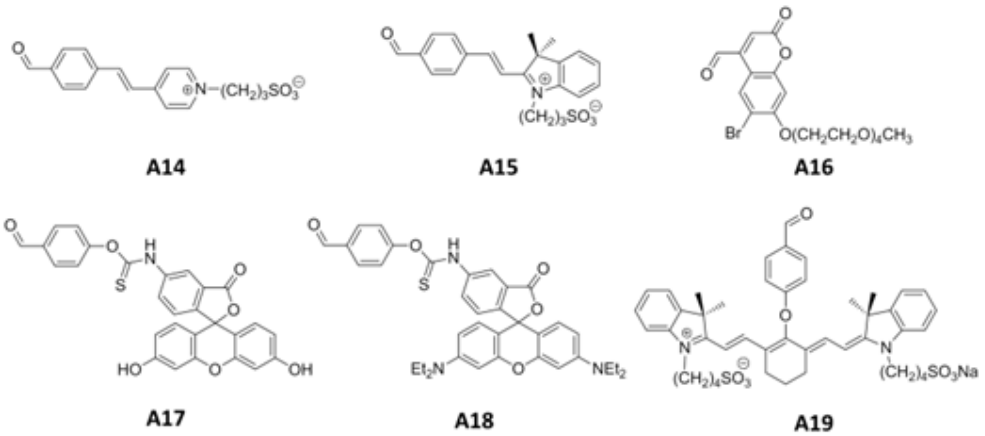

Figure 5 | Molecular structures of fluorophore labelled aldehydes.

Styryl labelled aldehydes (**A14**, **A15**) were synthesised from terephthalaldehyde via a condensation reaction with the corresponding pyridinium (yielding **A14**) and indolium (yielding **A15**) sulfonate salts. Coumarin labelled aldehyde (**A16**) was synthesised via allylic oxidation of the corresponding methyl derivative. Fluorescein (**A17**), rhodamine (**A18**) and cyanine (**A19**) labelled aldehydes were acquired via reaction of 4-hydroxybenzaldehyde with fluorescein isothiocyanate, rhodamine B isothiocyanate and IR-783, respectively. After obtaining compounds **A14-A19**, gels were formed using hydrazide **H1** and aldehyde **A11**,

incorporating 0.1 mol% (with respect to aldehyde **A11**) of the fluorescently labelled aldehyde. Subsequently, the structure of the resulting gel networks were analysed using CLSM (**Fig. 6**). In all cases, a branched network of fibre bundles is observed, showing that the fluorescently labelled aldehydes are incorporated into the gel network, without observably disturbing fibre formation. Furthermore, exciting the various probes was achieved using lasers with different wavelengths, depending on their absorption characteristics. The styryl (**A14**, **A15**) and coumarin (**A16**) derivatives were excited at 405 nm, whereas the fluorescein (**A17**), rhodamine (**A18**), and cyanine derivatives (**A19**) required 488, 543 and 633 nm lasers, respectively. Therefore, this toolbox of fluorescently labelled aldehydes should allow for the introduction of other species with orthogonal fluorescent labels into our gel system (e.g. cells).

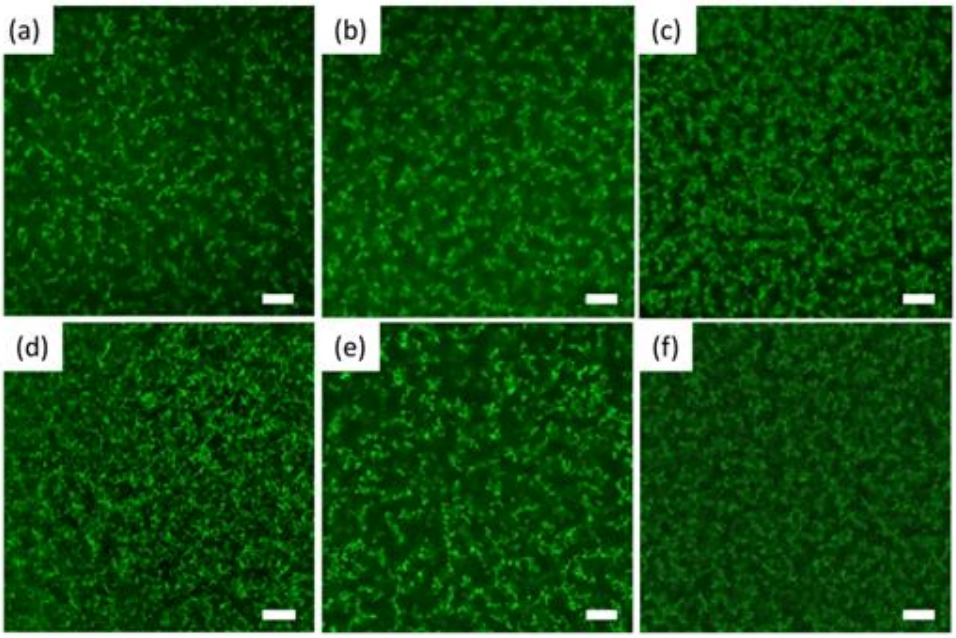

Figure 6 | Confocal laser scanning fluorescence micrographs (CLSM) of gel networks made using various aldehyde-derived fluorescent probes (scale bar = 20 μm): (a) styryl-pyridinium derivative (**A14**), (b) styryl-indolium derivative (**A15**), (c) coumarin derivative (**A16**), (d) fluorescein derivative (**A17**), (e) rhodamine derivative (**A18**), and (f) cyanine derivative (**A19**). General conditions: [H1]:[A11]=5:30 mM, a 1:2 ratio of hydrazide to aldehyde functional groups at pH 5, fluorophore labelled aldehyde (30 μM, 0.1 mol% with respect to **A11**).

Encouraged by the above results, we set out to demonstrate the use of our fluorescent gel network in combination with fluorescently tagged mammalian cells (mouse brain derived astrocytes). In a preliminary set of experiments, we first fluorescently labelled these cells with calcein-AM, a green marker for viable cells. These cells were combined with our gel network that was functionalized with the red fluorescent **A18** dye. Using fluorescence

microscopy, we imaged the cells in the green channel and the fibres in the red channel and found the cells embedded in the gel network (**Fig. 7a**). Secondly, we used the same astrocytes, but in this case the cells were fixed and permeabilised. Subsequently, their actin filaments were labelled with a fluorescein-conjugated phalloidin (green) and their nuclei with DAPI (blue). Finally, the gel network with the red fluorescent **A18** dye was added to demonstrate the orthogonality of the fluorescent dyes. Using confocal microscopy, we imaged the system and found the nucleus, actin filaments and gel network individually marked blue, green and red, respectively (**Fig. 7b**).

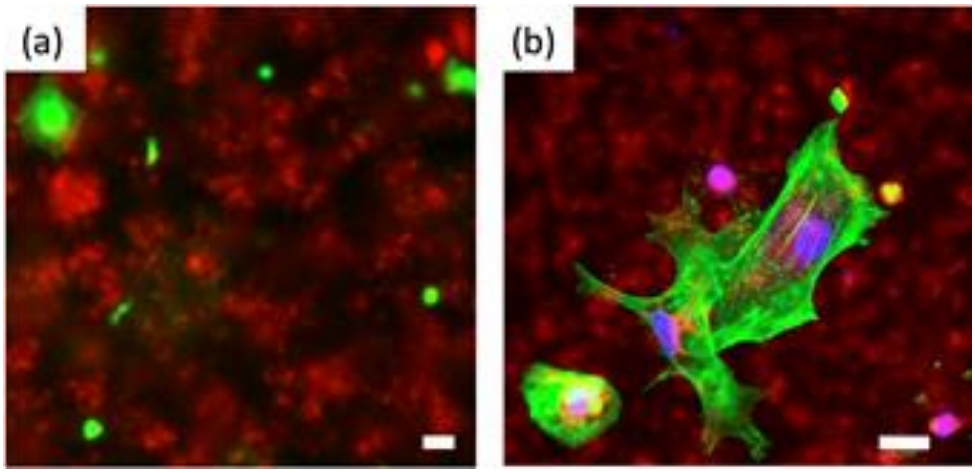

Figure 7 | Merged confocal laser scanning micrographs (CLSM) of astrocytes embedded in a gel network made of **H1**, **A11** and **A18** (scale bar = 20 μm). (a) The green channel shows calcein-AM-stained cells (λexc. = 488 nm) and the red channel gel fibres (λexc. = 543 nm), (b) nuclei are shown in blue (λexc. = 404 nm), the green channel are actin filaments (λexc. = 488 nm) and the red channel represents gel fibres (λexc.=543 nm). Concentrations: [H1]:[A11]=10:60 mM, [A18]=30 μM.

We further expanded the toolbox of functional precursors by synthesising aldehyde derivatives with reactive groups, allowing for modification of the fibre network, either through the formation of permanent covalent bonds via click chemistry[38,39], or by non-covalent interactions with biomolecules. Three aldehyde derivatives were synthesised containing functionalities for either Michael addition or alkyne-azide click chemistry, and an D-mannose derived aldehyde was synthesised to decorate the fibres with sugar groups, and to show non-covalent binding of the lectin Concanavalin A (ConA) to the gel fibres.[40] The aldehydes with reactive groups were synthesised from 4-(2-(2-(2-hydroxyethoxy)ethoxy)ethoxy)benzaldehyde (**A5**) (**Fig. 8**). Alkyne (**A20**) and enone (**A21**) labelled aldehyde derivatives were synthesised via nucleophilic substitution of **A5** to propagyl bromide and acryloyl chloride respectively. Alternatively, the hydroxy group of **A5** was converted to a tosylate group (**A22**) via the treatment with tosyl chloride. An azide derivative (**A23**) was obtained from **A22** via nucleophilic substitution with azide ion. A Cu-

catalysed cycloaddition of **A22** with the alkyne-functionalised 2,3,4,6-tetraacetylpropargyl-α-mannoside provided the acetate-protected mannose-benzaldehyde conjugate **A24**, which afforded the mannose derivative **A25** via removal of the acetate groups.

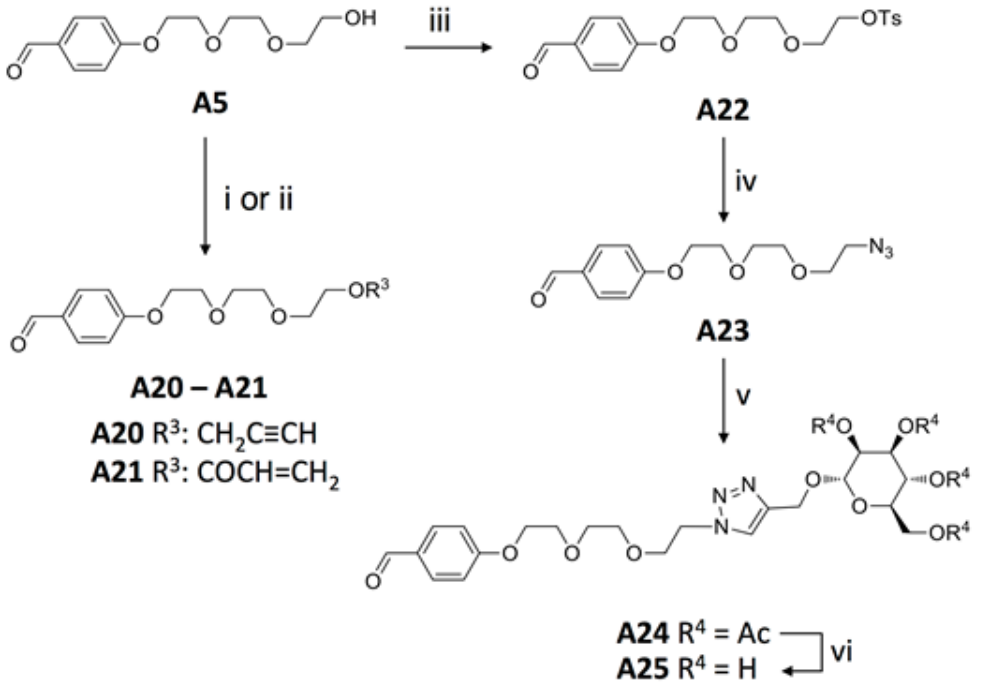

Figure 8 | Synthesis of aldehyde derivatives with functional groups for fibre-modification. Reagents and conditions: i) Br-$CH_2C{\equiv}CH$, NaH, THF, rt; ii) $ClCOCH{=}CH_2$, Et_3N, CH_2Cl_2, 0 °C→rt; iii) TsCl, Et_3N, CH_2Cl_2, rt; iv) NaN_3, DMF, Δ; v) 2,3,4,6-tetraacetylpropargyl-α-mannoside, CuI, Et_3N, CH_2Cl_2, rt; vi) NaOMe, MeOH, rt.

Incorporation of alkyne bearing aldehyde **A20** into the network allows for covalent addition of azide compounds, whereas azide containing compound **A23** enables the Cu mediated azide alkyne Huisgen cycloaddition with any alkyne derivative. Incorporation of alkene **A21** allows for Michael addition of thiols. Gel network functionalisation with **A20** and **A23** was attempted by forming gels with **H1** and **A11**, mixed with **A20** or **A23** (0.3 mol%, with respect to **A11**). Styryl labelled aldehyde **A15** (0.05 mol%) was used for imaging the gel network (**Fig. 9**). During gel formation, azide functionalised rhodamine (azide-fluor 545) was added to the gelation mixture containing acetylene derivatised aldehyde **A20**, whereas acetylene functionalised rhodamine (fluor 488-alkyne) was added to the gelation mixture containing azido-aldehyde **A23**. CuI was added to catalyse the click reaction. After gelation, confocal imaging showed colocalisation of the rhodamine fluorescence with the styryl fluorescence of the gel network (**Fig. 9**). These findings clearly demonstrate successful functionalisation of styryl stained fibres with a rhodamine dye using click chemistry. Similar to the Cu-catalysed click reaction to functionalise azide or alkyne derived gelators, a thia-Michael click

reaction was performed during gelation to generate functionalised gel fibres. During gelation, 0.5 mol% enone-derived **A21** (with respect to **A11**) and fluorescein labelled thiol (FITC-SH) were added to the mixture. The gel network was visualised using incorporated **A15** and again, the fluorescence colocalisation of fluorescein and **A15** indicated functionalisation of the fibres using the click reaction (**Fig. 9**).

To determine the scope of the approach, we also applied this methodology to functionalise the gel network with various biomolecules. We first attempted the direct attachment of a protein to the gel by performing a click-reaction of a model antigenic protein (Ovalbumin[41], Ova), with the gel matrix. Ova is the most commonly used model antigen in immune assays. In future, ovalbumin-conjugation to the gel matrix would allow the study of any immunogenicity of these gel matrices using standard T-cell assays.[42] The protein was functionalised with azides by expression in a methionine auxotrophic strain of E. coli to replace all methionines with azidohomoalanines[43–45] without affecting structure and function of the protein.[46] The protein was further functionalised with Cy5 dyes through lysine modification, to allow facile visualisation using confocal microscopy. By adding the azide-Ova to a gelation mixture containing Cu(I) and the acetylene-aldehyde **A20**, as well as the styryl-aldehyde probe **A15** for visualisation of the fibre network, an Ova-functionalised gel was obtained. CLSM showed extensive colocalisation of the styryl and Cy5 dyes indicating binding of Ova to the fibres (**Fig. 9 d, i, n**). Controls with wild-type Ova (without azide tag) or by leaving out the acetylene-aldehyde from the gelation mixture showed a severely weakened intensity of the fluorescence intensity of the Cy5 probe, as well as a diminished colocalisation with the styryl probe, indicating a lack of binding to the fibres (**Supplementary information, Fig. S7**). As a second class of biomolecules, we functionalised the fibres with sugar groups. To demonstrate that aldehyde **A25** allows for the functionalisation of the gel network with mannose moieties, gels were formed using trishydrazide **H1** and aldehyde **A11**, mixed with 1 mol% (with respect to aldehyde **A11**) mannose derivative **A25**. Furthermore, rhodamine labelled aldehyde **A18** was incorporated (0.02 mol%) to enable imaging of the gel network using CLSM (**Fig. 9**). During gel formation, a fluorescein derivative of the lectin Concanavalin A (ConA) was added, which was expected to bind specifically to the mannose present in the gel fibres.[30] Confocal imaging showed that the ConA fluorescence (**Fig. 9**) displayed extensive colocalisation with the rhodamine fluorescence of the gel network, indicating functionalisation of the fibre network with mannose and selective binding to the lectin. Control experiments, in which the gel sample was prepared without addition of the functional aldehydes, did not show fluorescence colocalization by CLSM from two different fluorophores used in the sample (**Supplementary information, Fig. S6**), thus ruling out the possibility of non-specific binding of the added functional groups to the gel fibres. Using TEM, we investigated the impact of the incorporation of a fluorophore (**A18**), or the **A25**-ConA pair on the morphology of **H1+A11** fibres. In both cases, no significant changes in morphology or fibre diameter were observed

(see the supporting information). These experiments show that it is possible to functionalise the fibres with aldehyde-derived sugar groups, and that such functional groups can subsequently be used for non-covalent binding to other (protein) biomolecules. Overall, these examples clearly illustrate that modification of the gel network can be achieved using these functional aldehydes and shows the utility of the various fluorescently labelled aldehydes that we developed.

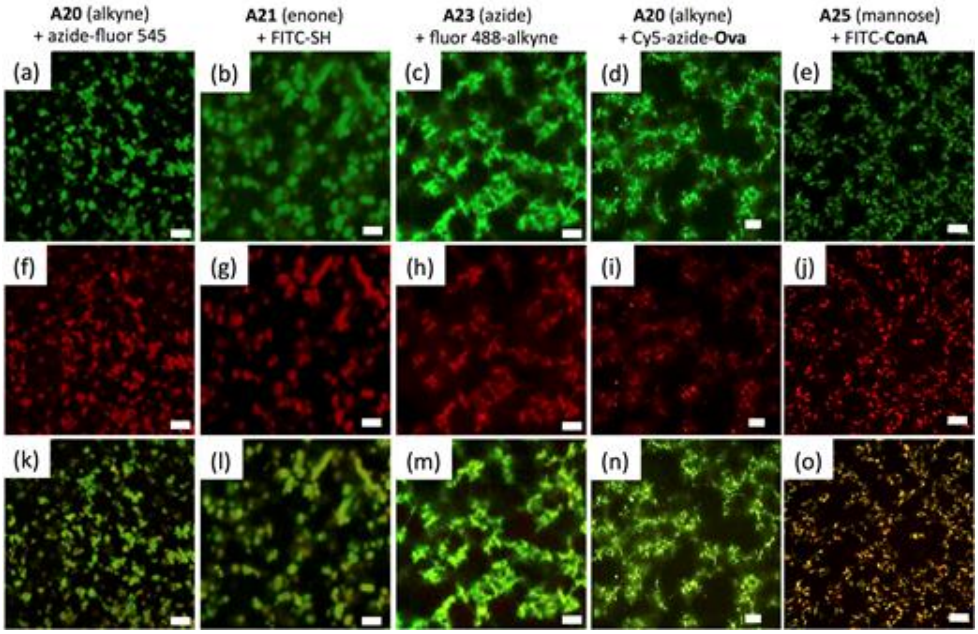

Figure 9 | Confocal laser scanning fluorescence micrographs of functionalised gel networks (scale bar = 20 μm) in presence of **A20** and azide-fluor 545 (**a, f, k**), A21 and FITC-SH (**b, g, l**), A23 and fluor 488-alkyne (**c, h, m**), A20 and Cy5-azide-Ova (**d, i, n**), and **A25** with FITC-ConA (**e, j, o**): (**a, b, c, d**) λexc. = 405 nm (exciting the **A15** styryl dye), (**e, g**) λexc. = 488 nm (exciting FITC), (**f**) λexc. = 543 nm (exciting fluor-545), (**h**) λexc. = 488 nm (exciting fluor-488), (**i**) λexc. = 633 nm (exciting Cy5), (**j**) λexc. = 543 nm (exciting **A18** rhodamine), (**k**) λexc. = 405 & 543 nm, (**l**) λexc. = 405 & 488 nm, (**m**) λexc. = 405 & 488 nm, (**n**) λexc. = 405 & 633 nm and (**o**) λexc. = 488 & 543 nm. For general conditions, see the **supplementary information**.

Conclusions

In this paper, we present a molecular toolbox for controlling the gelation properties and functionalisation of hydrazone-derived supramolecular gels. These gels are made in the gelation medium at ambient conditions by hydrazone formation between simple, non-gelating building blocks. First we show that by varying the chemical structure and hydrophilicity of the individually non-gelating starting components the gelation behaviour of the resulting hydrazone compounds can be controlled. Next, we show how replacing a small part of the regular aldehyde by an aldehyde carrying a functional tag can be used to

introduce functional groups in the supramolecular gels. Introduction of various fluorescent probes in the gel network was performed using fluorescently labelled aldehydes. Confocal imaging showed that these fluorescent probes can be used for imaging of the gel network at a wide range of excitation wavelengths. This enables multicolour imaging which allows for the visualisation of hydrogel networks in conjunction with cells and cellular substructures. Next, aldehyde derivatives with various functional groups were synthesised, allowing for facile covalent and non-covalent modification of the supramolecular fibres. In particular, various labels for click-chemistry were introduced, as well as a sugar-derived functional group capable of non-covalent binding to a lectin protein. The click groups were used for in situ connection to fluorescent labels or protein tags. The results show that the gel system can be modified on demand without hindering gel formation, enabling applications in the area of smart materials and chemical biology. Moreover, the modular nature of the gel formation and the facile synthesis of the various building blocks make this a straightforward method to construct complex functional materials from simple building blocks, eliminating the need for long and difficult synthetic procedures.

References

1. Cordier, P., Tournilhac, F., Soulié-Ziakovic, C. & Leibler, L. Self-healing and thermoreversible rubber from supramolecular assembly. *Nature* **451,** 977–980 (2008).
2. Zhao, Y. Light-Responsive Block Copolymer Micelles. *Macromolecules* **45,** 3647–3657 (2012).
3. Frisch, H. & Besenius, P. pH-Switchable Self-Assembled Materials. *Macromolecular Rapid Communications* **36,** 346–363 (2015).
4. Buerkle, L. E. & Rowan, S. J. Supramolecular gels formed from multi-component low molecular weight species. *Chemical Society Reviews* **41,** 6089 (2012).
5. Du, X., Zhou, J. & Xu, B. Supramolecular Hydrogels Made of Basic Biological Building Blocks. *Chemistry - An Asian Journal* **9,** 1446–1472 (2014).
6. Stupp, S. I. Self-Assembly and Biomaterials. *Nano Letters* **10,** 4783–4786 (2010).
7. Bardelang, D. *et al.* Interfacing Supramolecular Gels and Quantum Dots with Ultrasound: Smart Photoluminescent Dipeptide Gels. *Advanced Materials* **20,** 4517–4520 (2008).
8. Dong, S., Zheng, B., Wang, F. & Huang, F. Supramolecular Polymers Constructed from Macrocycle-Based Host–Guest Molecular Recognition Motifs. *Accounts of Chemical Research* **47,** 1982–1994 (2014).
9. Korevaar, P. A., Newcomb, C. J., Meijer, E. W. & Stupp, S. I. Pathway Selection in Peptide Amphiphile Assembly. *Journal of the American Chemical Society* **136,** 8540–8543 (2014).
10. Li, J. *et al.* Dephosphorylation of D -Peptide Derivatives to Form Biofunctional, Supramolecular Nanofibers/Hydrogels and Their Potential Applications for Intracellular Imaging and Intratumoral Chemotherapy. *Journal of the American Chemical Society* **135,** 9907–9914 (2013).
11. Li, J. *et al.* D -Amino Acids Boost the Selectivity and Confer Supramolecular Hydrogels of a Nonsteroidal Anti-Inflammatory Drug (NSAID). *Journal of the American Chemical Society* **135,** 542–545 (2013).
12. Frederix, P. W. J. M. *et al.* Exploring the sequence space for (tri-)peptide self-assembly to design and discover new hydrogels. *Nature Chemistry* **7,** 30–37 (2014).
13. Arigon, J., Prata, C. A. H., Grinstaff, M. W. & Barthélémy, P. Nucleic Acid Complexing Glycosyl Nucleoside-Based Amphiphile. *Bioconjugate Chemistry* **16,** 864–872 (2005).
14. Sreenivasachary, N. & Lehn, J.-M. Gelation-driven component selection in the generation of constitutional dynamic hydrogels based on guanine-quartet formation. *Proceedings of the National Academy of Sciences* **102,** 5938–5943 (2005).
15. Park, S. M. & Kim, B. H. Ultrasound-triggered water gelation with a modified nucleoside. *Soft Matter* **4,** 1995 (2008).
16. Matsumoto, S. *et al.* Photo Gel-Sol/Sol-Gel Transition and Its Patterning of a Supramolecular Hydrogel as Stimuli-Responsive Biomaterials. *Chemistry - A European Journal* **14,** 3977–3986 (2008).
17. Vemula, P. K., Li, J. & John, G. Enzyme Catalysis: Tool to Make and Break Amygdalin Hydrogelators from Renewable Resources: A Delivery Model for Hydrophobic Drugs. *Journal of the American Chemical Society* **128,** 8932–8938 (2006).
18. Wang, G. *et al.* Synthesis and Characterization of Monosaccharide-Derived Carbamates as Low-Molecular-Weight Gelators †. *Langmuir* **25,** 8696–8705 (2009).
19. Du, X., Li, J., Gao, Y., Kuang, Y. & Xu, B. Catalytic dephosphorylation of adenosine monophosphate (AMP) to form supramolecular nanofibers/hydrogels. *Chemical Communications* **48,** 2098 (2012).
20. Li, X. *et al.* Supramolecular Nanofibers and Hydrogels of Nucleopeptides. *Angewandte Chemie International Edition* **50,** 9365–9369 (2011).
21. Yang, Z. *et al.* Supramolecular hydrogel of kanamycin selectively sequesters 16S rRNA. *Chemical Communications* **48,** 9257 (2012).
22. Zhou, J., Du, X., Gao, Y., Shi, J. & Xu, B. Aromatic–Aromatic Interactions Enhance Interfiber Contacts for Enzymatic Formation of a Spontaneously Aligned Supramolecular Hydrogel. *Journal of the American Chemical Society* **136,** 2970–2973 (2014).
23. Bastings, M. M. C. *et al.* A Fast pH-Switchable and Self-Healing Supramolecular Hydrogel Carrier for Guided, Local Catheter Injection in the Infarcted Myocardium. *Advanced Healthcare Materials* **3,** 70–78 (2014).
24. Leckie, J. *et al.* Nanopropulsion by Biocatalytic Self-Assembly. *ACS Nano* **8,** 9580–9589 (2014).
25. Kuang, Y. *et al.* Pericellular Hydrogel/Nanonets Inhibit Cancer Cells. *Angewandte Chemie International Edition* **53,** 8104–8107 (2014).
26. Albertazzi, L. *et al.* Probing Exchange Pathways in One-Dimensional Aggregates with Super-Resolution Microscopy. *Science* **344,** 491–495 (2014).

27. van Bommel, K. J. C. *et al.* Responsive Cyclohexane-Based Low-Molecular-Weight Hydrogelators with Modular Architecture. *Angewandte Chemie International Edition* **43,** 1663–1667 (2004).
28. Guo, M. *et al.* Tough Stimuli-Responsive Supramolecular Hydrogels with Hydrogen-Bonding Network Junctions. *Journal of the American Chemical Society* **136,** 6969–6977 (2014).
29. Hartgerink, J. D., Beniash, E. & Stupp, S. I. Peptide-amphiphile nanofibers: A versatile scaffold for the preparation of self-assembling materials. *Proceedings of the National Academy of Sciences* **99,** 5133–5138 (2002).
30. Müller, M. K. & Brunsveld, L. A Supramolecular Polymer as a Self-Assembling Polyvalent Scaffold. *Angewandte Chemie International Edition* **48,** 2921–2924 (2009).
31. Kim, B.-S., Hong, D.-J., Bae, J. & Lee, M. Controlled Self-Assembly of Carbohydrate Conjugate Rod−Coil Amphiphiles for Supramolecular Multivalent Ligands. *Journal of the American Chemical Society* **127,** 16333–16337 (2005).
32. Boekhoven, J. *et al.* Catalytic control over supramolecular gel formation. *Nature Chemistry* **5,** 433–437 (2013).
33. Poolman, J. M. *et al.* Variable gelation time and stiffness of low-molecular-weight hydrogels through catalytic control over self-assembly. *Nature Protocols* **9,** 977–988 (2014).
34. Eelkema, R. & van Esch, J. H. Catalytic control over the formation of supramolecular materials. *Organic & Biomolecular Chemistry* **12,** 6292 (2014).
35. Olive, A. G. L. *et al.* Spatial and Directional Control over Self-Assembly Using Catalytic Micropatterned Surfaces. *Angewandte Chemie International Edition* **53,** 4132–4136 (2014).
36. Maity, C., Hendriksen, W. E., van Esch, J. H. & Eelkema, R. Spatial Structuring of a Supramolecular Hydrogel by using a Visible-Light Triggered Catalyst. *Angewandte Chemie International Edition* **54,** 998–1001 (2015).
37. van Esch, J. H. We Can Design Molecular Gelators, But Do We Understand Them? †. *Langmuir* **25,** 8392–8394 (2009).
38. Xi, W., Scott, T. F., Kloxin, C. J. & Bowman, C. N. Click Chemistry in Materials Science. *Advanced Functional Materials* **24,** 2572–2590 (2014).
39. Tang, W. & Becker, M. L. 'Click' reactions: a versatile toolbox for the synthesis of peptide-conjugates. *Chem. Soc. Rev.* **43,** 7013–7039 (2014).
40. Voskuhl, J., Stuart, M. C. A. & Ravoo, B. J. Sugar-Decorated Sugar Vesicles: Lectin-Carbohydrate Recognition at the Surface of Cyclodextrin Vesicles. *Chemistry - A European Journal* **16,** 2790–2796 (2010).
41. Shimonkevitz, R., Colon, S., Kappler, J. W., Marrack, P. & Grey, H. M. Antigen recognition by H-2-restricted T cells. II. A tryptic ovalbumin peptide that substitutes for processed antigen. *J Immunol* **133,** 2067–2074 (1984).
42. Karttunen, J. & Shastri, N. Measurement of ligand-induced activation in single viable T cells using the lacZ reporter gene. *Proceedings of the National Academy of Sciences* **88,** 3972–3976 (1991).
43. Kiick, K. L., Saxon, E., Tirrell, D. A. & Bertozzi, C. R. Incorporation of azides into recombinant proteins for chemoselective modification by the Staudinger ligation. *Proceedings of the National Academy of Sciences* **99,** 19–24 (2002).
44. Kiick, K. L. & Tirrell, D. A. Protein Engineering by In Vivo Incorporation of Non-Natural Amino Acids: Control of Incorporation of Methionine Analogues by Methionyl-tRNA Synthetase. *Tetrahedron* **56,** 9487–9493 (2000).
45. van Kasteren, S. I., Kramer, H. B., Gamblin, D. P. & Davis, B. G. Site-selective glycosylation of proteins: creating synthetic glycoproteins. *Nature Protocols* **2,** 3185–3194 (2007).
46. van Kasteren, S. I. *et al.* Expanding the diversity of chemical protein modification allows post-translational mimicry. *Nature* **446,** 1105–1109 (2007).

Supplementary information

General remarks

All reagents were purchased from commercial sources and were used as provided unless stated otherwise. 4-(2-(2-(2-Hydroxyethoxy)ethoxy)ethoxy)benzaldehyde (**A5**),[1] *cis,cis*-cyclohexane-1,3,5-tricarbohydrazide(**H1**),[2] 3,4-bis(2-(2-methoxyethoxy)ethoxy)benzaldehyde (**A11**), fluorescein labelled aldehyde (**A17**),[3] 2,3,4,6-tetraacetylpropargylmannoside,[4] 3-(4-methylpyridiniumyl)propane-1-sulfonate,[5] 2,3,3-trimethyl-1-(3-sulfonatepropyl)-3H-indolium[6] and 6-bromo-4-methyl-7-hydroxycoumarin[7] were synthesised according to literature procedures. NMR spectra were recorded on a Bruker Avance-400 spectrometer (399.90 MHz for ^{1}H and 100.56 MHz for ^{13}C) or a Varian Inova-300 spectrometer (operating at 300.04 MHz for ^{1}H) at 298 K using residual protonated solvent signals as internal standard (^{1}H: $\delta(CHCl_3)$ = 7.26 ppm, $\delta((CH_3)_2SO)$ = 2.50 ppm, $\delta(CH_3OH)$ = 3.31 ppm, $\delta(D_2O)$ = 4.79 ppm, and ^{13}C: $\delta(CHCl_3)$ = 77.16 ppm, $\delta(CH_2Cl_2)$ = 53.80 ppm, $\delta((CH_3)_2SO)$ = 39.52 ppm, $\delta(CH_3OH)$ = 49.00 ppm, D_2O was referenced to internal dioxane, 67.19 ppm. TLC was performed on Merck Silica Gel 60 F254 TLC plates with a fluorescent indicator with a 254 nm excitation wavelength and compounds were visualized under UV light of 254 nm wavelength. HPLC-MS analysis was performed on a Shimadzu Liquid Chromatograph Mass Spectrometer, LCMS-2010, LC-8A pump with a diode array detector SPD-M20. The column used was the Xbridge Shield RP 18.5µm (4.6x150mm). UV-Vis spectroscopic measurements were performed on an Analytik Jena Specord 250 spectrophotometer. Fluorescence spectroscopy was performed on a Jasco 815 spectrophotometer. All experiments were performed using MilliQ water.

Compounds used in this study

Hydrazide derivatives

Succinohydrazide (**H2**), adipohydrazide (**H4**), nonanedihydrazide (**H7**) were purchased from commercial sources. Glutarohydrazide (**H3**), heptanedihydrazide (**H5**), octanedihydrazide (**H6**) were synthesised in one step from their corresponding methyl esters derivatives.

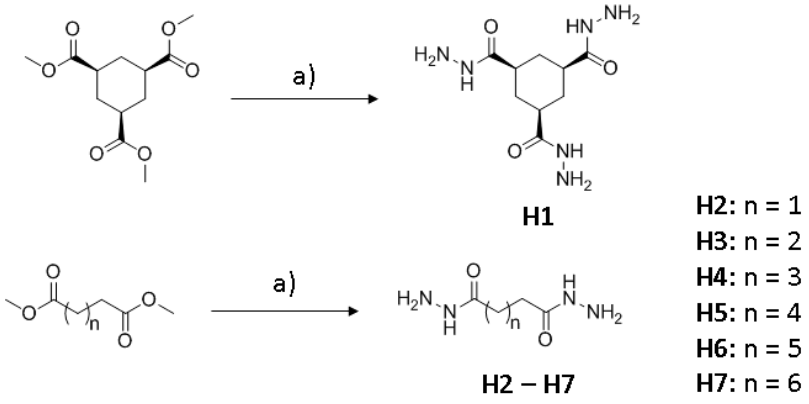

Scheme S1 | Synthesis of hydrazide derivatives. Reagent and conditions: a) $N_2H_4.H_2O$, MeOH, rt, 16 h (for **H1, H3, H5, H6**).

General procedure for hydrazide synthesis

Hydrazine monohydrate (194.0 mmol) was added in portions to a solution of the methyl ester derivative (19.0 mmol) in methanol. The mixture was stirred overnight at room temperature, yielding a white slurry. The solvent and excess hydrazine were evaporated *in vacuo*, yielding the desired compound (quantitative).

Benzaldehyde derivatives

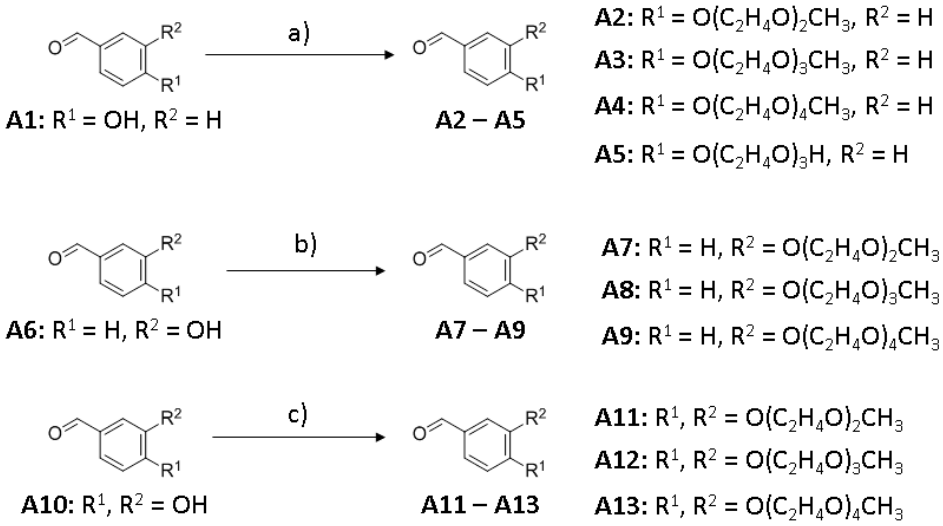

Scheme S2 | Synthesis of benzaldehyde derivatives. Reagents and conditions: a) R^1Ts, K_2CO_3, DMF, 90 °C, 16 h (for **A2 – A4**); or $Cl(C_2H_4O)_3H$, K_2CO_3, DMF, 90 °C, 16 h (for **A5**); b) R^2Ts, K_2CO_3, DMF, 90 °C, 16 h (for **A7 – A9**), and c) RTs (R = R^1, R^2), K_2CO_3, DMF, 90 °C, 16 h (for **A11 – A13)**.

General procedure for benzaldehyde derivative synthesis

A slurry of a benzaldehyde derivative (1 eq.), the required tosyl derivative (or chloride in case of **A5**; 1.1 for monohydroxy benzaldehyde and 2.2 eq. for dihydroxy benzaldehyde), potassium carbonate (2 or 4 eq.) and DMF was stirred at 90 °C for overnight. After cooling to room temperature, ethyl acetate and water were added. The water layer was extracted with ethyl acetate, after which the combined organic layers were washed with saturated bicarbonate solution (3x), water (3x) and brine (1x). The organic layer was dried over $MgSO_4$, and removed by evaporation under reduced pressure, yielding the desired compound.

Fluorophore Labelled Aldehydes

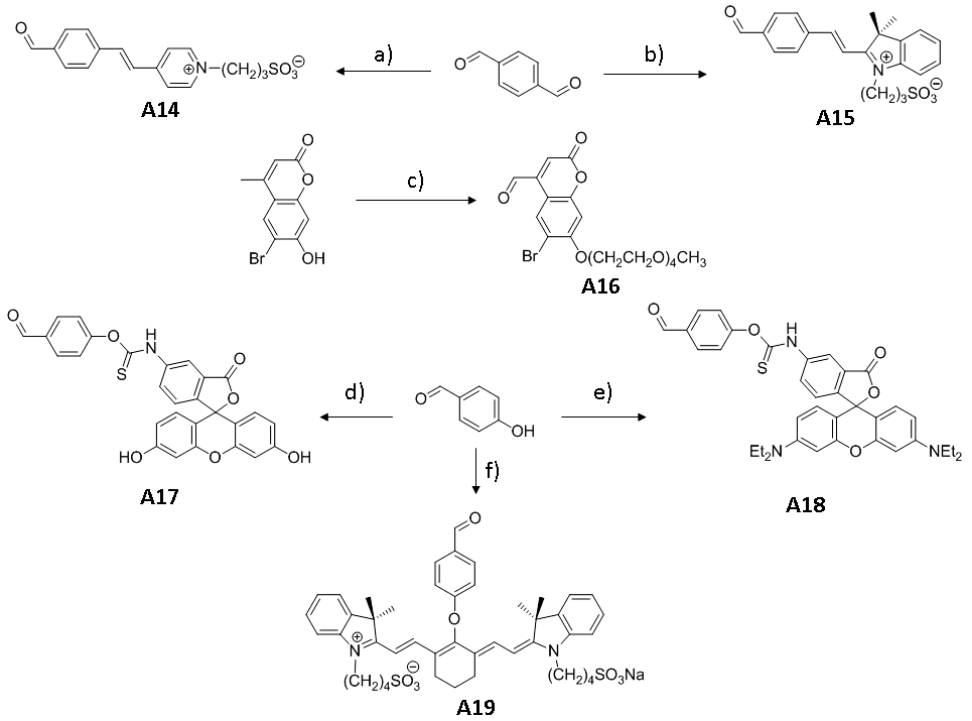

Scheme S3 | Synthetic route for fluorophore labelled aldehydes. Reagents and Conditions: a) 3-(4-methylpyridiniumyl)propane-1-sulfonate, piperidine, EtOH, Δ; b) 2,3,3-trimethyl-1-(3-sulfonatepropyl)-3H-indolium, AcOH, Δ; c) i) 2-(2-(2-(4-formylphenoxy)ethoxy)ethoxy)ethyl 4-methylbenzenesulfonate, K_2CO_3, DMF, Δ; ii) SeO_2, Xylene, Δ; d) Fluorescein isothiocyanate, K_2CO_3, DMF, Δ; e) Rhodamine B isothiocyanate, NaH, DMF, Δ; f) IR-783, NaH, DMF, Δ.

Synthetic procedure for Fluorophore Labelled Aldehydes

Styryl labelled aldehydes (**A14**, **A15**) were synthesised from terephthalaldehyde via condensation with the corresponding pyridinium and indolium sulfonate salts which were obtained from 1,3-propane sulfonate via condensation with 4-methylpyridine and 2,3,3-trimethyl-3*H*-indole respectively. Fluorescein (**A17**), rhodamine (**A18**) and cyanine dye (**A19**) labelled aldehydes were synthesised by deprotonation of 4-hydroxybenzaldehyde and subsequent reaction with fluorescein isothiocyanate, rhodamine B isothiocyanate and IR-783 respectively. Coumarine labelled aldehyde (**A16**) was obtained via SeO_2 oxidation reaction from 6-bromo-4-methyl-7-*O*-(2-(2-(2-(2-methoxyethoxy)ethoxy)ethoxy)ethoxy)coumarin, which was synthesised via alkylation reaction of tetraethylene glycol monomethyl ether tosylate and 6-bromo-4-methyl-7-hydroxycoumarin.

Functional aldehyde derivatives

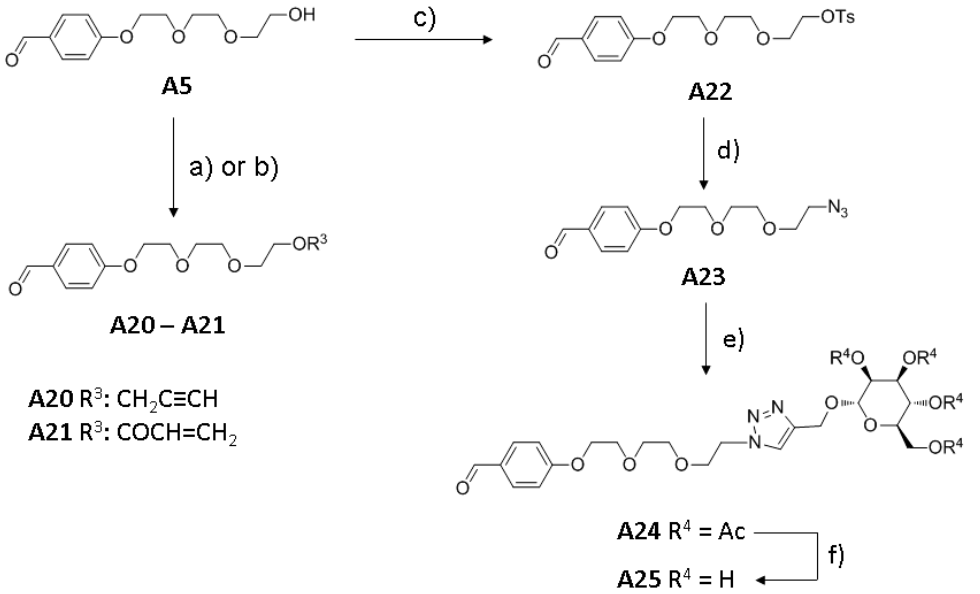

Scheme S4 | Synthesis route for functional aldehyde derivatives. Reagents and Conditions: a) Br-$CH_2C{\equiv}CH$, NaH, THF, rt; b) $ClCOCH{=}CH_2$, Et_3N, CH_2Cl_2, 0 °C→rt; c) TsCl, Et_3N, CH_2Cl_2, rt; d) NaN_3, DMF, Δ; e) 2,3,4,6-tetraacetylpropargyl-α-mannoside, CuI, Et_3N, CH_2Cl_2, rt; f) NaOMe, MeOH, rt.

Synthetic procedure for functional aldehyde derivatives

Functional aldehyde derivatives were synthesised from 4-(2-(2-(2-hydroxyethoxy)ethoxy)ethoxy)benzaldehyde (**A5**). Alkyne and alkene labelled aldehyde derivatives (**A20** and **A21**) were synthesised via nucleophilic substitution of **A5** to propargyl bromide and acrylyl chloride respectively, in the presence of base (NaH and Et_3N respectively). The hydroxy group of **A5** was converted to a tosylate group (**A22**) via treatment with tosyl chloride. The azide derivative (**A23**) was obtained from **A22** via nucleophilic substitution with azide ions. Copper catalysed click reaction of **A23** and 2,3,4,6-tetraacetylpropargyl-(α)-mannoside provided acetate derivative **A24**, which, via subsequent deprotection by NaOMe, provided the mannose derivative **A25**.

Click-group functionalised fluorophores

Rhodamine labelled azide and acetylene derivative (azide-fluor 545 and fluor 488-alkyne respectively), fluorescein labelled concanavalin A (Concanavalin A, FITC conjugate, Type IV) were purchased from commercial sources. Thiol labelled fluorescein derivative (**FITC-SH**) was synthesised following a literature procedure.[8]

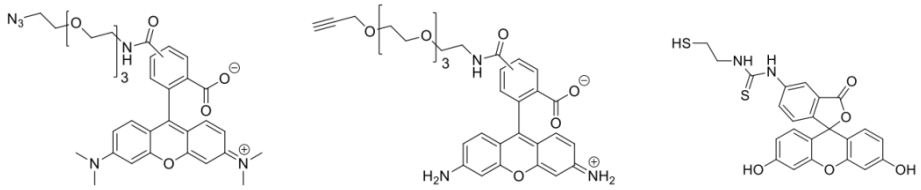

Figure S1 | Chemical structure of click group functionalised fluorophores.

Cy5-Azide-Ovalbumin

Production of azide-derived Ovalbumin (azide-Ova)

Ovalbumin carrying a *C*-terminal 6His-tag was expressed from the previously reported plasmid pMCSG7-OVA[9] (a kind gift from N. Del Cid) in *E. coli* B834(DE3) using methods previously described [10-12]. Briefly, *E. coli* B834(DE3) was transformed with the above plasmid and grown to an OD_{600} of 0.9-1.0 in LB-medium (1L over 2 x 2L flasks). Cells were harvested by centrifugation at 3000 *g* for 10 minutes at 4°C and then resuspended in 2 x 100 mL PBS. After recentrifugation (same conditions), the cells were taken up in SelenoMet-medium (Molecular Dimensions), augmented with either 4 mM methionine or 4 mM azidohomoalanine. Cells were incubated at 30 degrees for 1h prior to induction of expression by the addition of isopropylthiogalactoside (IPTG, 1 mM final concentration). Expression was continued at 30 degrees for 18 hours. Cells were harvested by centrifugation and resuspended in 25 mL of equilibration buffer (50 mM NaH_2PO_4, 500 mM NaCl, pH 8.1) augmented with 250U benzonase + one EDTA-free protease inhibitor tablet (Roche) and lysed by sonic disruption at 4 degrees. The soluble fraction was isolated by centrifugation (40,000 *g*, 45 minutes) and the supernatant was passed over a Ni-NTA-agarose resin (2mL resin slurry per litre of culture) that had been equilibrated with equilibration buffer. The resin-bound protein was washed with 20 column volumes of wash buffer (equilibration buffer containing 10 mM imidazole) prior to elution with 2 x 2 column volumes of elution buffer (equilibration buffer augmented with 500 mM imidazole). SDS-PAGE analysis showed that elution fraction 2 contained the desired proteins in >75% purity. Both OVA expressed with methione and OVA expressed with azidohomoalanine were used without further purification.

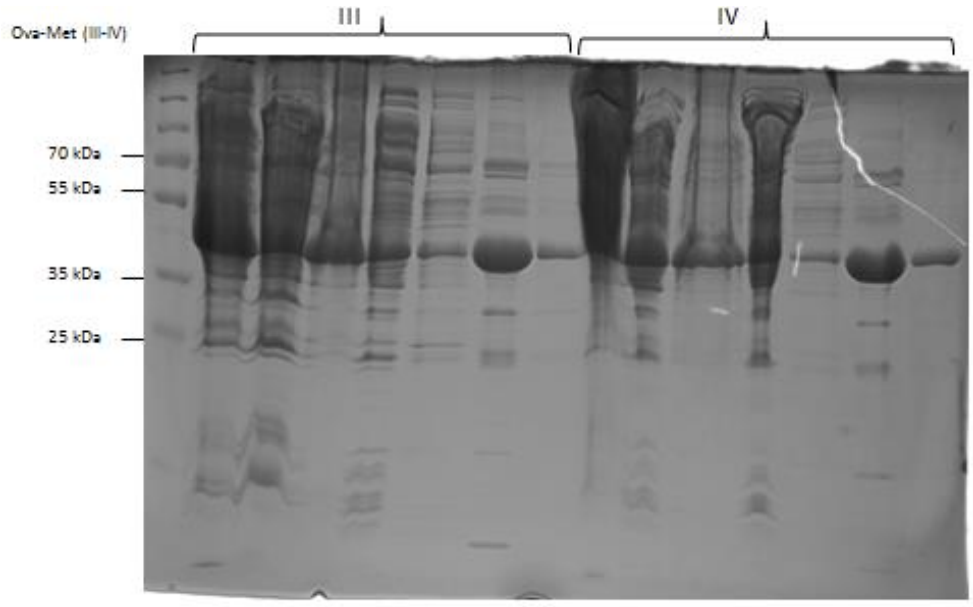

Figure S2 | SDS-PAGE gel.

Fluorophore modification of azide-Ova and wild type-Ova

1 mg of protein (as determined by Bradford Assay[13]) was volume adjusted to 2.3 mL in elution buffer. 0.7 mg of Cy5-HOSu-ester (Lumiprobe, cat. No: 23020) was added to each of the protein samples (as a freshly prepared solution in DMSO; 200 uL). The tubes containing the mixtures were inverted 4 times and left unagitated at room temperature for 1 hour. After this time, the modified proteins were purified over sephadex G-25 resin (PD-10 column), that was pre-equilibrated with PBS according to the manufacturer's protocol. Purified proteins were used *as is* in further reactions.

General procedure of gel preparation[2,3]

The procedure is explained for the **H1** and **A11** compounds but holds for any combination of hydrazides and aldehydes. Also, the functionalised gel samples were prepared using this procedure, including the desired functional aldehyde by replacing that amount of aldehyde **A11**.

The trishydrazide (**H1**) (40 mM) and aldehyde (**A11**) (240 mM) derivatives were dissolved in aqueous 100 mM sodium phosphate buffer at pH 5. After mixing appropriate amounts of the two stock solutions, the resulting mixture was allowed to react overnight. All experiments were performed at room temperature. To ensure the complete conversion of all hydrazide groups, gels were always prepared in a 1:2 functional group molar ratio of the hydrazide and aldehyde, which means that there is an initial 1:6 molar ratio between **H1** and **A11**. For example, starting with 16 mM of **H1** and 96 mM of **A11** would yield close to 16 mM of hydrogelator in the final mixture accompanied by 48 mM free aldehyde in solution, which was not removed.

Critical gelation concentration (CGC) test procedure

A sample vial (2 ml) was filled with the appropriate volumes of aldehyde and hydrazide stock solution and made up to 1 ml total volume by addition of buffer. The vial was closed, shaken vigorously and allowed to stand overnight. The vial was inverted to see whether a gel network had formed. The CGC is the minimal amount of gelator needed to trap the solvent and form a stable gel. The CGC is defined as the average value of the lowest concentration where a gel was formed and the highest concentration where the solvent could no longer be supported. The CGC is expressed as the initial concentration of hydrazide, in mM.

General procedure for fibre network functionalization

Stock solutions of various compounds [**H1** (40.0 mM), **A11** (240.0 mM), fluorophore labelled aldehyde: **A15**, **A18** (1.0 mM), functional aldehydes: **A20**, **A21**, **A23**, **A25** (1.0 mM) and functional compounds: azide-fluor 545 (1.6 mM), thiol labelled fluorescein derivative (**FITC-SH**,1.0 mM), Fluor 488-alkyne (1.6 mM), fluorescein labelled Concanavalin A (0.1 mM)] were prepared by dissolving compounds in phosphate buffer (pH 5.0). Functionalised gel samples were prepared as described in the general procedure above but now including a functional aldehyde (0.3-1.0 mol%, with respect to **A11**) and a corresponding functional compound (0.02–0.03 mol%, with respect to **A11**), both listed directly above. After vigorous shaking, the mixture was transferred to an imaging chamber (for confocal laser scanning microscopy) and was covered with a glass slide. Next, the sample was allowed to stand overnight in order to ensure complete conversion and gelation before imaging. For control experiment samples were prepared in similar way as functionalised gel sample, replacing the functional aldehyde derivative with equal volume of buffer solution.

Confocal laser scanning microscopy

Confocal laser scanning micrographs were obtained with a Zeiss LSM 700 confocal laser scanning microscope equipped with a Zeiss Axio Observer inverted microscope and a 40x PlanFluor oil immersion objective lens (NA 1.3) using an incident laser. The confocal pinhole was set to 1.0 airy unit and the data files were processed using ZEN 2011 software. Image dimensions were 95.35 μm x 95.35 μm with a resolution of 1024 x 1024 pixels. Exposition time per pixel was 1.58 μs. The gel networks were imaged using confocal laser scanning microscopy via incorporating an aldehyde functionalised fluorophore derivative (**A14**-**A19**) into the fibre formation process. The gel samples were prepared as before, but now including 30 μM (0.02-0.1 mol%, replacing that amount of aldehyde **A11**) of the aldehyde functionalised fluorescent probe. After vigorous shaking, the sample mixture was transferred to the imaging chamber (diameter × thickness = 20 mm × 0.6 mm), which was subsequently closed off with a glass cover slide. Next, the sample was allowed to stand overnight in order to ensure complete conversion and gelation before imaging.

Microscopy on astrocytes in gels

For the microscopy experiments on astrocytes in combination with gels, a gel was first prepared in a glass vial (pH 5.0 buffer, 10 mM **H1**, 60 mM **A11**, 30 μM **A18**). This gel was allowed to equilibrate for at least 12 hours. The mouse brain-derived astrocytes were trypsinised, and washed with incubation media (10% foetal bovine serum (FBS) in Dulbecco's modified Eagle medium (DMEM)), before plating 10^5 cells on a 24 well plate and 10^5 cells on a PDL coated coverslip. After incubation for 5 hours in incubation media at 37°C

and 5% CO_2, the cells plated on the tissue culture plastic plate were washed and stained with calcein-AM following the vendor's protocol. After incubation for 30 minutes, the calcein-AM containing media was removed and 100 µL of PBS was added. Then, 100 µL of the previously prepared gel containing **A18** was added. After addition of the gel, the cells were immediately imaged using a Nikon Eclipse inverted microscope through a 10X objective. Similarly, the astrocytes plated on the PDL coverslips were incubated in incubation media for 5 hours at 37°C and 5% CO_2. After incubation, the cells were fixed using glutaraldehyde, their membranes were permeabilised using Triton-X and they were stained with DAPI and FITC phalloidin, all following a literature procedure.[14] After staining, the cells were washed and 5 µL of the previously prepared gel containing **A18** was added. The excess gel was wicked away and the coverslips were mounted prior to imaging with a confocal microscope (Zeiss LSM 510 equipped with a 40X oil immersion objective).

Fibre network functionalization with A20

A11 was added to the mixture of CuI, azide-fluor 545, **H1**, **A15** and **A20** in pH 5 buffer (final concentrations of 10 mM **H1**, 59 mM **A11**, 30 µM **A15**, 0.2 mM **A20**, 20 µM azide-fluor 545 and 20 µM CuI). After a vigorous shake, the mixture was transferred to a reaction chamber and was allowed to stand overnight to form a gel. Control experiments were performed in a similar way as above replacing **A20** with an equal volume of buffer solution.

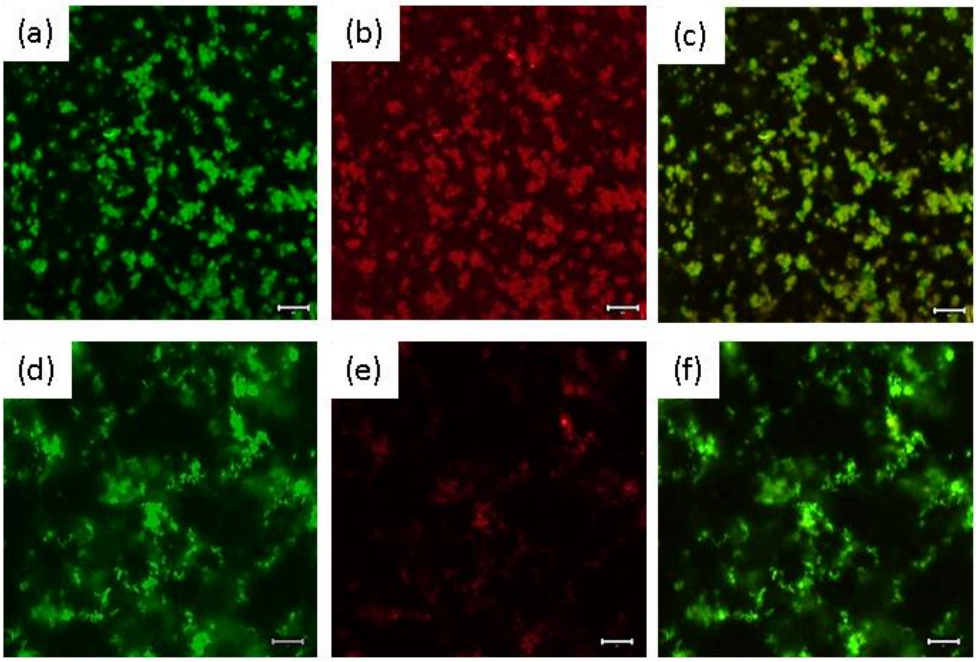

Figure S3 | Confocal laser scanning micrographs of gel fibres (scale bar - 20 µm) in presence (top) or absence (bottom) of **A20**: (**a,d**) exciting styryl-indolium ($\lambda_{exc.}$ = 405 nm), emitted light collection: 410-471 nm range; master gain 703 V, digital gain 1.0 (for **a**) and master gain 817 V, digital gain 1.0, (for **d**), (**b,e**) exciting fluor 545 ($\lambda_{exc.}$ = 546 nm), emitted light collection: 646-797 nm range; master gain 1028 V, digital gain 1.0 (for **b**), and master gain 1141 V, digital gain 1.0 (for **e**), and (**c,f**) merged: $\lambda_{exc.}$ = 405 nm and 546 nm.

Fibre network functionalization with A21

H1 was added to a mixture of **A15**, **A21** and **FITC-SH**. After gentle mixing, **A11** was added to it and the mixture was *vortexed* (final concentration of 10 mM **H1**, 59 mM **A11**, 30 μM **A15**, 0.3 mM **A21**, and 10 μM **FITC-SH)**. Then, it was transferred to a reaction chamber to stand overnight for complete gelation before imaging. A control experiment was performed similar as above replacing equal volume of **A21** with buffer solution.

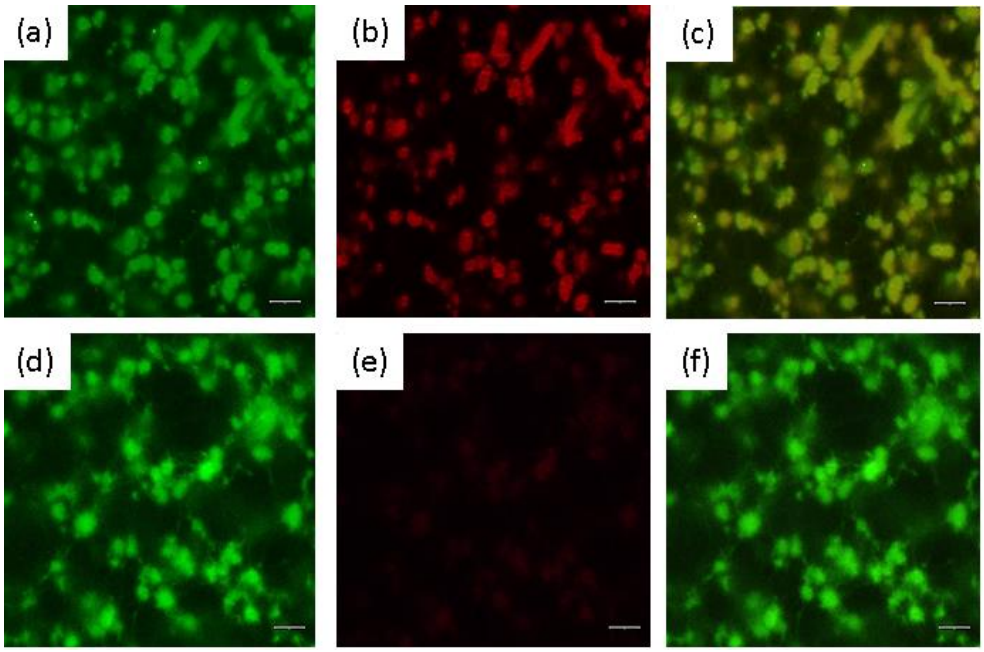

Figure S4 | Confocal laser scanning micrographs of gel fibres (scale bar - 20 μM) in presence (top) or absence (bottom) of **A21**: (**a,d**) exciting styryl-indolium ($\lambda_{exc.}$ = 405 nm), emitted light collection: 410-460 nm range; master gain 830 V, digital gain 1.0 (for a) and master gain 957 V, digital gain 1.0 (for d), (b, e) exciting fluorescein ($\lambda_{exc.}$ = 488 nm), emitted light collection: 610-797 nm range; master gain 1000 V, digital gain 1.2 (for b) and master gain 1200 V, digital gain 1.0 (for e), and (c, f) merged: $\lambda_{exc.}$ = 405 nm and 488 nm.

Fibre network functionalization with A23

Similar experiment was performed as fibre network functionalization with **A20**, except **A20** and azide-fluor 545 were replaced by **A23** and Fluor 488-alkyne respectively. The gel contained the final concentration of 10 mM **H1**, 59 mM **A11**, 30 μM **A15**, 0.2 mM **A23**, 20 μM Fluor 488-alkyne and 20 μM CuI. A control experiment was performed similar way as above replacing **A23** with equal volume of buffer solution.

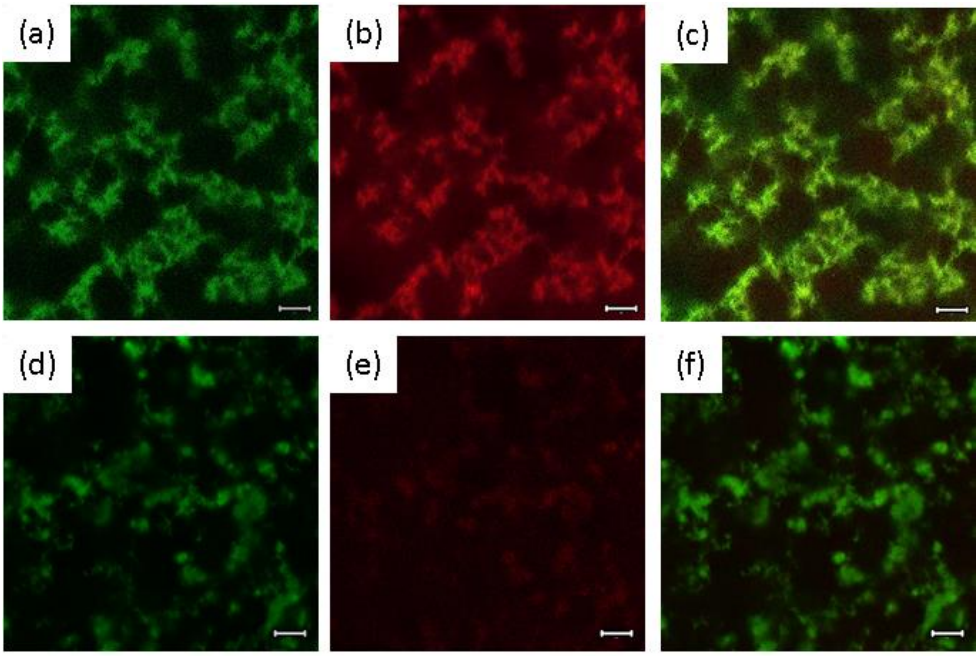

Figure S5 | Confocal laser scanning micrograph of gel fibre (scale bar - 20 μM) in presence (top) or absence (bottom, blank experiment) of **A23**: (**a,d**) exciting styryl-indolium ($\lambda_{exc.}$ = 405 nm), emitted light collection: 410-458 nm range; master gain 904 V, digital gain 1.0 (for **a**) and master gain 747 V, digital gain 1.0 (for **d**), (**b,e**) exciting Fluor 488 ($\lambda_{exc.}$ = 488 nm), emitted light collection: 605-797 nm range; master gain 798 V, digital gain 1.2 (for **b**) and master gain 923 V, digital gain 1.2 (for **e**), and (**c,f**) merged: $\lambda_{exc.}$ = 405 nm and 488 nm.

Fibre network functionalization with A25

H1 was added to a mixture of **A18**, **A25** and fluorescein labelled concanavalin A. After gentle mixing, **A11** was added to the mixture and the solution was mixed vigorously. Then, it was transferred to a reaction chamber to stand overnight for complete gelation before imaging. The gel contained a final concentration of 15 mM **H1**, 89 mM **A11**, 20 μM **A18**, 0.9 mM **A25**, and 20 μM fluorescein labelled concanavalin A. A control experiment was performed similar as above replacing equal volume of **A25** with buffer solution.

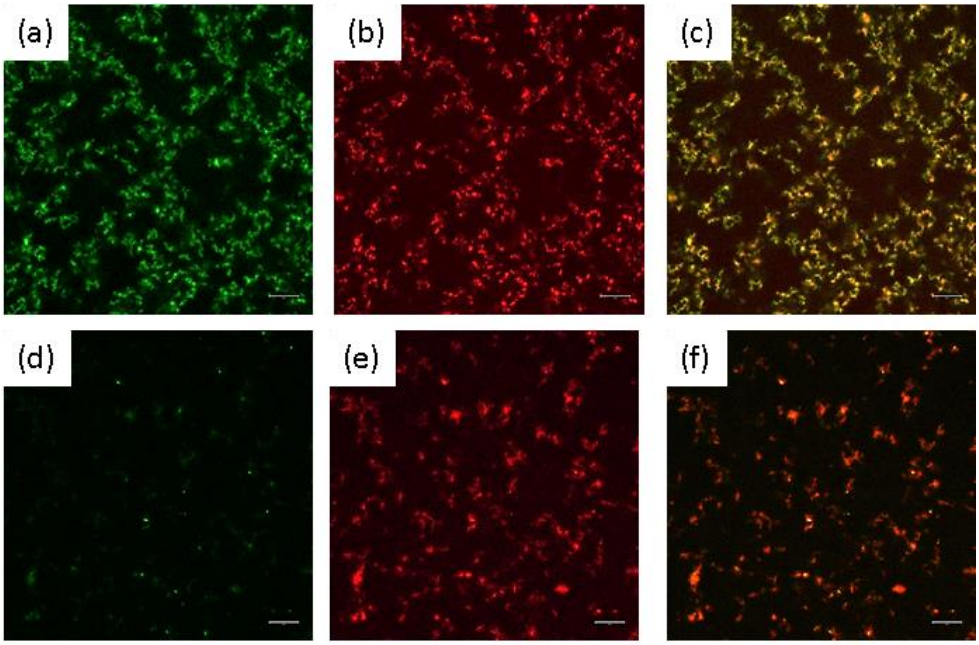

Figure S6 | Confocal laser scanning micrograph of gel fibre (scale bar - 20 μM) in presence (top) or absence (bottom, blank experiment) of **A25**: (**a,d**) exciting fluorescein ($\lambda_{exc.}$ = 488 nm), emitted light collection: 486-534 nm range; master gain 1051 V, digital gain 1.2 (for **a**) and master gain 961 V, digital gain 1.2 (for **d**), (**b,e**) exciting rhodamine ($\lambda_{exc.}$ = 545 nm), emitted light collection: 581-797 nm range; master gain 946 V, digital gain 1.2 (for **b**) and master gain 871 V, digital gain 1.2 (for **e**), (**c,f**) merged: $\lambda_{exc.}$ = 488 nm and 545 nm.

Fibre network functionalization with A20 and click reaction with azide functionalised Ovalbumin protein

H1 was added to a mixture of **A15**, **A20, CuI** and azide-functionalised Cy5-labelled *Ovalbumin (azide-**Ova**)*. After gentle mixing, **A11** was added to it and the solution was mixed vigorously. Then, it was transferred to a reaction chamber to stand overnight for complete gelation before imaging. The gel contained a final concentration of 10 mM **H1**, 59 mM **A11**, 30 μM **A15**, 0.2 mM **A20**, 20 μM CuI and 1 μM azide-**Ova**. Control experiments were performed similar as above replacing either an equal volume of **A20** with buffer solution (thus leaving out the alkyne) or an equal volume of azide-**Ova** solution with wild type-**Ova** solution.

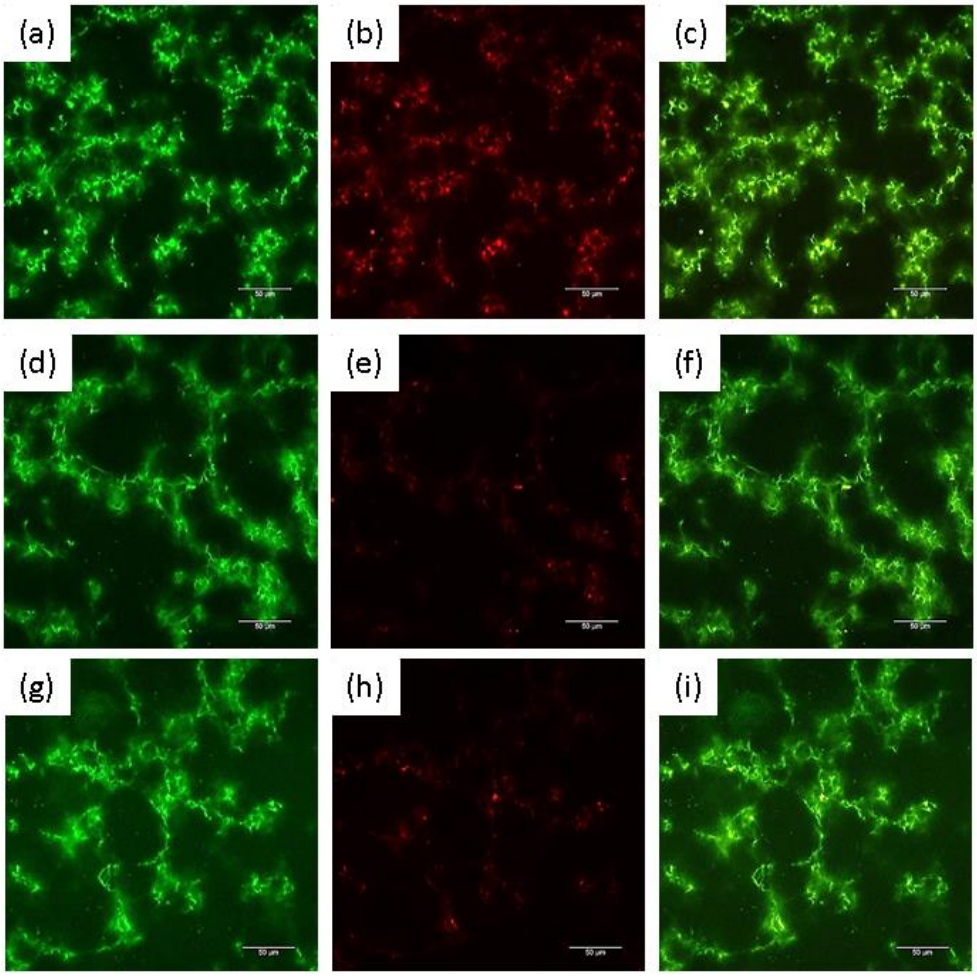

Figure S7 | Confocal laser scanning micrograph of gel fibre (scale bar - 50 μM) with **A20** and azide-**Ova** (top row), only with azide-**Ova** (middle row), and with **A20** and wild type-**Ova** (bottom row): (**a,d,g**) exciting styryl-indolium ($\lambda_{exc.}$ = 405 nm), emitted light collection: 401-463 nm range; master gain 933 V, digital gain 1.2 (for **a**), master gain 970 V, digital gain 1.2 (for **d**), and master gain 950 V, digital gain 1.2 (for **g**), (**b,e,h**) exciting cyanine ($\lambda_{exc.}$ = 633 nm), emitted light collection: 644-797 nm range; master gain 1108 V, digital gain 1.2 (for **b**) and master gain 1138 V, digital gain 1.2 (for **e**), and master gain 1098 V, digital gain 1.2 (for **h**), and (**c,f,i**) merged: $\lambda_{exc.}$ = 405 nm and 633 nm.

Transmission Electron Microscopy

A few microliters of suspension were deposited on a Quantifoil R 1.2/1.3 Holey Carbon coated grid. After blotting away the excess of liquid the grids were stained with phosphotungstic acid (2 wt% in water) and dried. Samples were observed in a JEOL JEM-1400Plus electron microscope, operating at 120 kV. Micrographs were recorded under low-dose conditions on a slow-scan CCD camera (Gatan, 830)

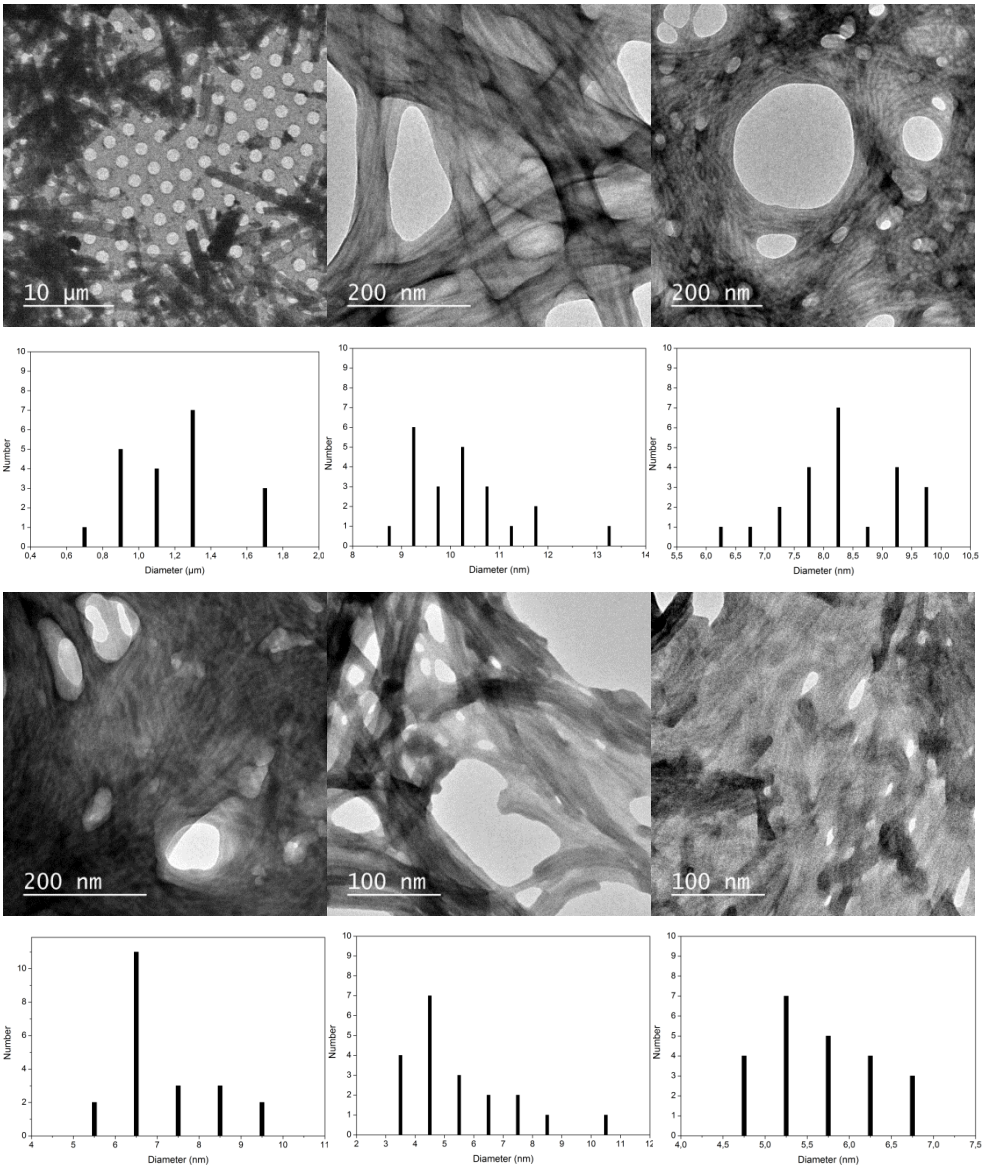

Figure S8 | TEM images of fibres of hydrogelators prepared from (top, left to right) **H6** (15.5 mM) and **A2** (62 mM); **H1** (9 mM) and **A2** (54 mM); **H1** (6.5 mM) and **A7** (39 mM); (bottom, left to right) **H1** (5.5 mM) and **A11** (33 mM); **H1** (5.5 mM) and **A11** (33 mM) with **A18** (330 µM); and Concanavalin A (7 µM), **H1** (5.5mM) and **A11** (33 mM) with **A25** (330 µM). Below are the statistical distributions of single fibre diameters (obvious fibre bundles were omitted). A control with only **A11** showed no discernable structures.

Rheology

Oscillatory experiments were performed using a AR G2 rheometer from TA Instruments in a strain-controlled mode; the rheometer was equipped with a steel plate-and- plate geometry of diameter 40 mm and a water trap. The temperature of the plates was controlled at 25 ± 0.2 °C. Measurements were performed at a frequency of 1 Hz while applying 0.05% strain. During measurement, the storage and loss moduli *G*' and *G*'' were followed as a function of the time. Total volume = 1mL and gelator concentration = 20 mM (20 mM of hydrazide derivative, 120 mM of aldehyde derivative (for **H1**) or 80 mM of aldehyde derivative (for **H2**-**H6**). The reported G´ value is where G' reaches a plateau value.

Characterisation data

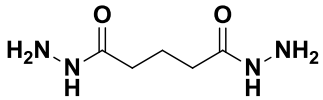

Glutarohydrazide (H3)

Although the compound is described in the literature,[15] some characterisation data were not reported. **Yield**: quantitative. **^{1}H NMR** (400 MHz, DMSO-D_6) $\delta = 8.92$ (s, 2H, CON*H*), 4.13 (s, 4H, NHN*H*$_2$), 1.98 (bs, 4H, C*H*$_2$), 1.70 (d, 2H, C*H*$_2$). **^{13}C NMR** (100 MHz, DMSO-D_6): $\delta = 171.6$ (*C*O), 33.3 (CO*C*H$_2$-), 21.9 (-*C*H$_2$-). **MS** (ESI$^+$) m/z: 161.0 $[M+H]^+$, 183.1 $[M+Na]^+$.

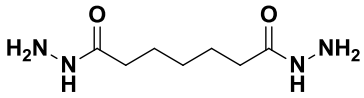

Heptanedihydrazide (H5)

Yield: quantitative. **^{1}H NMR** (400 MHz, DMSO-D_6) $\delta =$ 8.89 (s, 2H, CON*H*), 4.13 (s, 4H, NHN*H*$_2$), 1.97 (bs, 4H, C*H*$_2$), 1.46 (bs, 4H, C*H*$_2$), 1.19 (d, 2H, C*H*$_2$). **^{13}C NMR** (100 MHz, DMSO-D_6): $\delta = 172.0$ (*C*O), 33.7 (CO*C*H$_2$-), 28.7 (*C*H$_2$), 25.4 (-*C*H$_2$-). **MS** (ESI$^+$) m/z: 189.1 $[M+H]^+$, 211.1 $[M+Na]^+$.

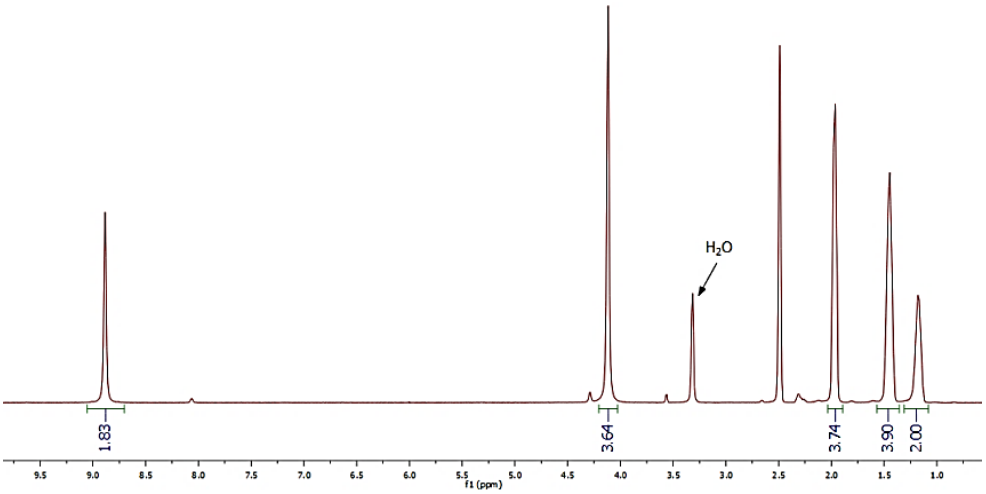

Figure S9 | ^{1}H NMR spectrum of heptanedihydrazide (**H5**) in DMSO-D_6 at 25 °C.

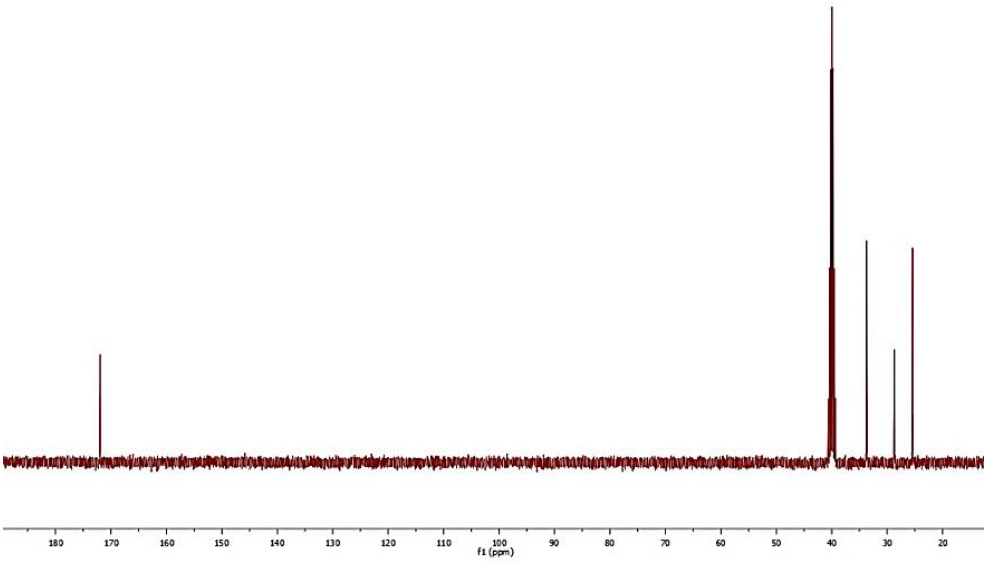

Figure S10 | ^{13}C NMR spectrum of heptanedihydrazide (**H5**) in DMSO-D_6 at 25 °C.

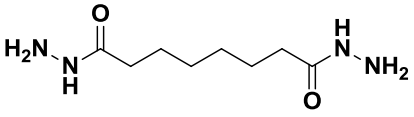

Octanedihydrazide (H6)

Yield: quantitative. The spectroscopic data matched with the corresponding reported data in the literature.[16]

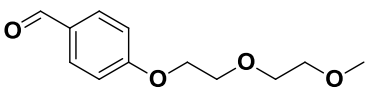

4-(2-(2-Methoxyethoxy)ethoxy)benzaldehyde (A_2)

Yield: 78 %. The spectroscopic data matched with the corresponding reported data in the literature.[17]

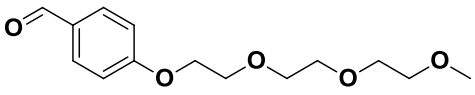

4-(2-(2-(2-Methoxyethoxy)ethoxy) ethoxy)benzaldehyde (A3)

Yield: 88 %. The spectroscopic data matched with the corresponding reported data in the literature.[18]

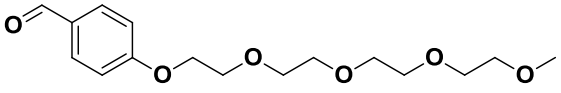

4-(2-(2-(2-(2-Methoxyethoxy) ethoxy)ethoxy)ethoxy)benzaldehyde (A4)

Yield: 91 %. The spectroscopic data matched with the corresponding reported data in the literature.[19]

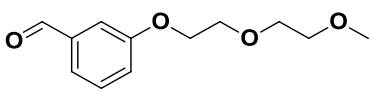

3-(2-(2-Methoxyethoxy)ethoxy)benzaldehyde (A7)

Although the compound is described in the literature, some characterisation data were not reported.[20] **Yield**: 89 %. **^{1}H NMR** (400 MHz, $CDCl_3$): δ = 9.96 (s, 1H, C*H*O), 7.45 – 7.39 (m, 3H, Ar*H*), 7.02 (dt, 1H, *J* = 2.1 Hz, *J* = 7.3 Hz, Ar*H*), 4.20 (t, 2H, CH_2), 3.88 (t, 2H, CH_2), 3.72 (t, 2H, CH_2), 3.57 (t, 2H, CH_2), 3.38 (s, 3H, CH_3). **^{13}C NMR** (100 MHz, $CDCl_3$): δ = 192.3 (*C*HO), 159.6 (C_{Ar}), 138.0 (C_{Ar}), 130.2 (C_{Ar}), 123.8 (C_{Ar}), 122.2 (C_{Ar}), 113.3 (C_{Ar}), 72.2 (*C*H_2), 71.0 (*C*H_2), 69.9 (*C*H_2), 67.9 (*C*H_2), 59.3 (*C*H_3). **MS** (ESI^+) m/z: 225.3 $[M+H]^+$.

3-(2-(2-(2-Methoxyethoxy)ethoxy)ethoxy)benzaldehyde (A8)

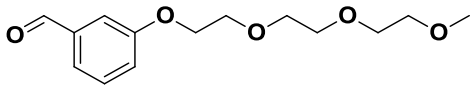

Yield: 91 %. The spectroscopic data matched with the corresponding reported data in the literature.[18]

3-(2-(2-(2-(2-Methoxyethoxy)ethoxy)ethoxy)ethoxy)benzaldehyde (A9)

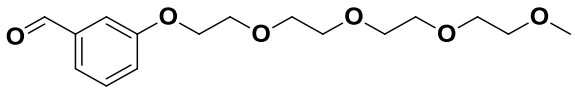

Yield: 87 %. The spectroscopic data matched with the corresponding reported data in the literature.[21]

3,4-Bis(2-(2-(2-methoxyethoxy)ethoxy)ethoxy)benzaldehyde(A12)

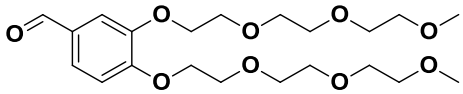

Yield: 99 %. The spectroscopic data matched with the corresponding reported data in the literature.[22]

3,4-Bis(2-(2-(2-(2-methoxyethoxy)ethoxy)ethoxy)ethoxy)benzaldehyde (A13)

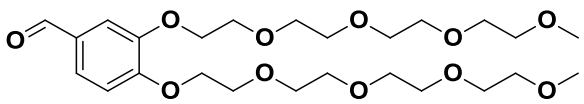

Yield: 79 %. ^{1}H NMR (400 MHz, $CDCl_3$): δ = 9.76 (s, 1H, C*H*O), 7.43 (bs, 2H, Ar*H*), 6.94 (d, *J* = 6.3 Hz, 1H, Ar*H*), 4.17-4.14 (m, 4H, CH_2), 3.83 (s, 4H, CH_2), 3.67 (s, 4H, CH_2), 3.59 (bs, 14H, CH_2), 3.47 (s, 4H, CH_2), 3.29 (s, 6H, CH_3). ^{13}C NMR (100 MHz, $CDCl_3$): δ = 190.7 (*C*HO), 154.3 (C_{Ar}), 149.1 (C_{Ar}), 130.2 (C_{Ar}), 126.5 (C_{Ar}), 112.5 (C_{Ar}), 111.9 (C_{Ar}), 71.8 (2x*C*H_2), 70.9 (*C*H_2), 70.8 (*C*H_2), 70.6 (2x*C*H_2), 70.5 (4x*C*H_2), 70.4 (2x*C*H_2), 69.5 (*C*H_2), 69.3 (*C*H_2), 68.7 (*C*H_2), 68.3 (*C*H_2), 58.9 (2x*C*H_3). MS (ESI^+) m/z: 520.0 $[M+H]^+$.

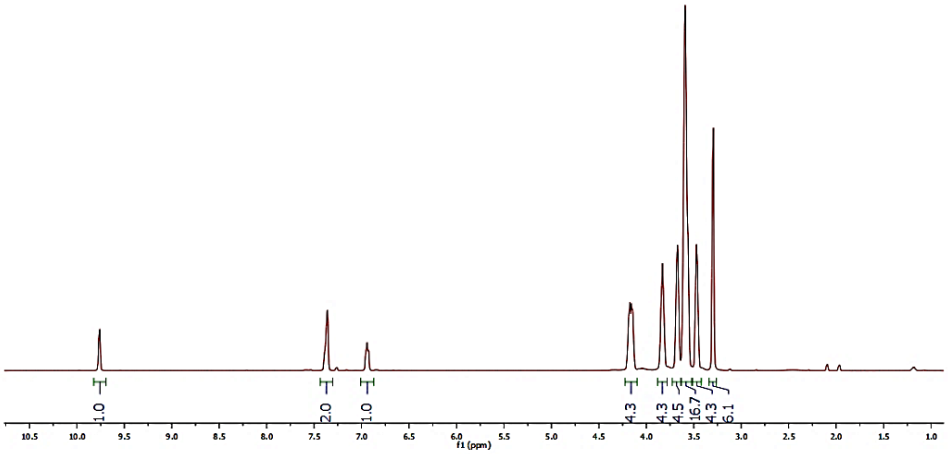

Figure S11 | ^{1}H NMR spectrum of 3,4-bis(2-(2-(2-methoxyethoxy)ethoxy)ethoxy)-benzaldehyde (**A13**) in $CDCl_3$ at 25 °C.

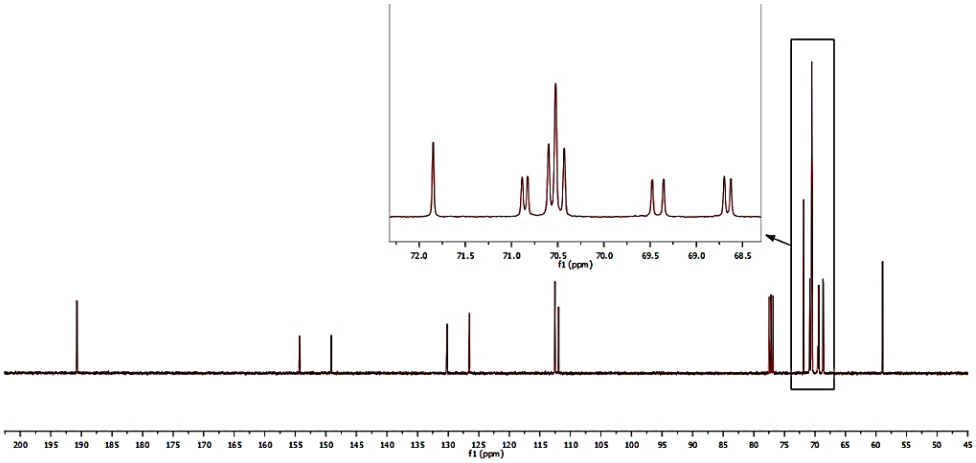

Figure S12 | ^{13}C NMR spectrum of 3,4-bis(2-(2-(2-methoxyethoxy)ethoxy)ethoxy)benzaldehyde (**A13**) in $CDCl_3$ at 25 °C.

3-(4-(4-Formylstyryl)pyridiniumyl)propane-1-sulfonate (A14)

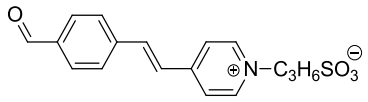

3-(4-Methylpyridiniumyl)propane-1-sulfonate (0.97 g, 4.5 mmol) and terephthalaldehyde (1.81 g, 13.5 mmol) were dissolved in EtOH (5.0 mL). Piperidine (0.45 mL, 4.5 mmol) was added to the mixture and it was refluxed for overnight. After cooling at ambient temperature, a greenish solid was obtained by filtration, which was washed with ethanol, acetone and dried under reduced pressure to obtain the desired compound as pale greenish solid (0.70 g, 47 %). ^{1}H NMR (400 MHz, DMSO-D_6): δ = 10.06 (s, 1H, C*H*O), 8.99 (d, *J* = 6.7 Hz, 2H, Ar*H*), 8.27 (d, *J* = 6. 8 Hz, 2H, Ar*H*), 8.03 (m, 3H, Ar*H*), 7.84 (s, 2H, Ar*H*), 7.66 (d, *J* = 16.3 Hz, 1H, Ar*H*), 4.67 (q, 2H, CH_2), 2.45 (t,

2H, CH_2), 2.24 (m, 2H, CH_2). MS (ESI Pos.): *m/z* = 284.1 ([MH-O_3]$^+$), 209 [(MH-$C_3H_7SO_3$)$^+$], 180, 152.

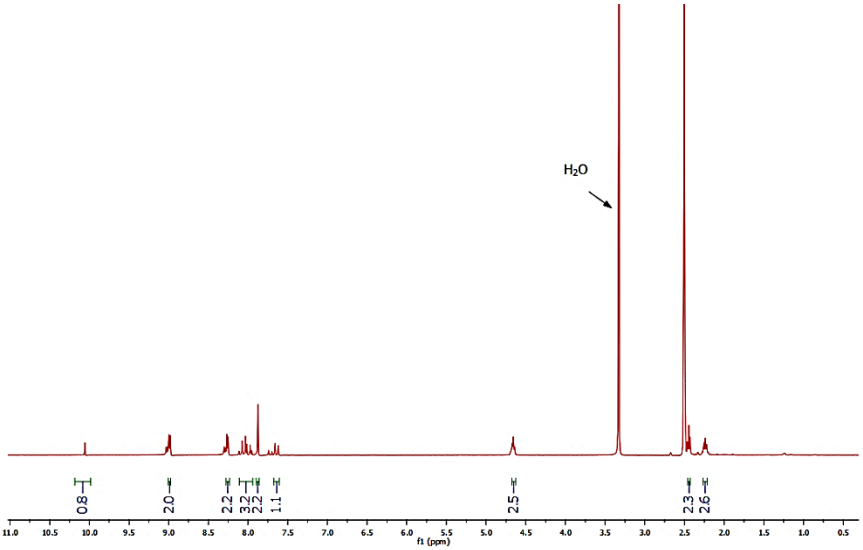

Figure S13 | ^{1}H NMR spectrum of 3-(4-(4-formylstyryl)pyridiniumyl)propane-1-sulfonate (**A14**) in DMSO-D_6 at 25 °C.

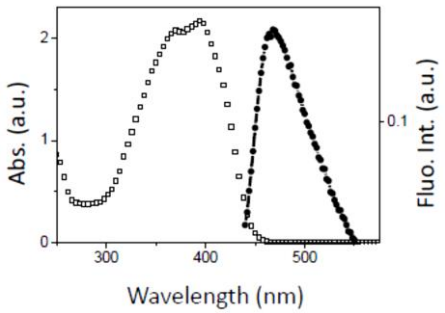

Figure S14 | UV-Vis and fluorescence spectra of styryl derivative (**A14**) in water (C = 10^{-4} M, $\lambda_{exc.}$ = 430 nm).

<u>3-(2-(4-Formylstyryl)-3,3-dimethyl-3*H*-indoliumyl)propane-1-sulfonate (A15)</u>

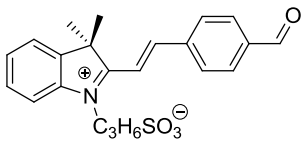

2,3,3-Trimethyl-1-(3-sulfonatepropyl)-3*H*-indolium (0.28 g, 1.0 mmol) and terephthalaldehyde (0.67 g, 5.0 mmol) were dissolved in acetic acid (5.0 mL) and the mixture was refluxed for overnight. After completion of the reaction, it was concentrated under reduced pressure and the obtained residue was washed with $CHCl_3$, followed by acetone to obtain the desired compound as an orange solid (0.35 g, 88 %). ^{1}H NMR (400 MHz, DMSO-D_6): δ = 10.11 (s, 1H, C*H*O), 8.53 (m, 3H, Ar*H*), 8.10 (m, 4H, Ar*H*), 7.92 (d, *J* = 3.1 Hz, 1H, Ar*H*), 7.69 (d, *J* = 3.1 Hz, 2H, Ar*H*), 4.96 (d, 2H, CH_2), 2.70 (t, 2H, CH_2), 2.23 (bs, 2H, CH_2), 1.83 (s, 6H, C(CH_3)$_2$). MS (ESI Pos.): *m/z* =284[M+Na-$C_3H_4SO_4$]$^+$), 142.

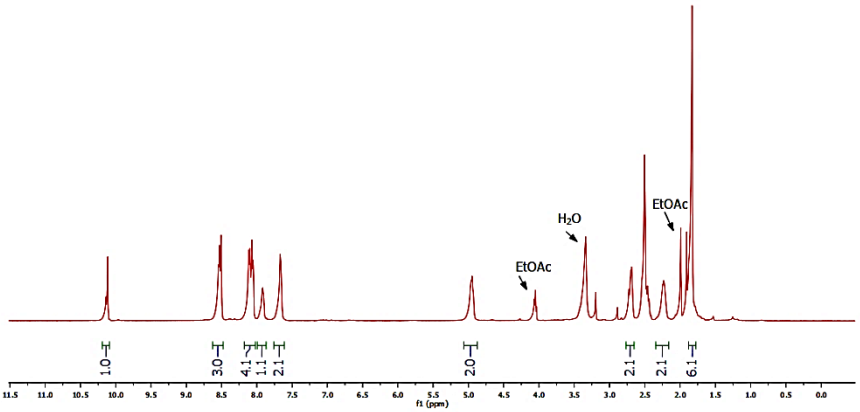

Figure S15 | ^{1}H NMR spectrum of indolium derivative (**A15**) in DMSO-D_6 at 25 °C.

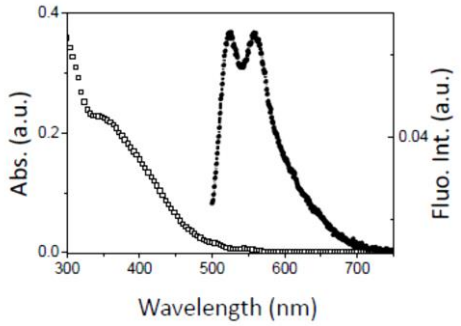

Figure S16 | UV-Vis and fluorescence spectra of indolium derivative (**A15**) in water (C = 10^{-4} M, $\lambda_{exc.}$ = 420 nm).

<u>6-Bromo-4-methyl-7-*O*-(2-(2-(2-(2-methoxyethoxy)ethoxy)ethoxy)ethoxy)coumarin</u>

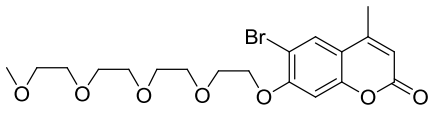

K_2CO_3 (2.76 g, 20.0 mmol) was added to a solution of 6-bromo-4-methyl-7-hydroxycoumarin (2.55 g, 10.0 mmol) in DMF (20.0 mL). The mixture was heated at 80 °C for 30 minutes. After that, tetraethylene glycol monomethyl ether tosylate (5.44 g, 15.0 mmol) was added to the mixture and heating was continued for overnight. After completion of the reaction, it was concentrated under reduced pressure and diluted with EtOAc. The organic layer was washed with water, brine and dried over MgSO4. After removal of the solvent, the crude substance was purified by column chromatography (silica gel, $CHCl_3$/EtOAc) to obtain the desired compound as a brownish liquid (2.70 g, 61 %). ^{1}H NMR (400 MHz, CD_3OD): δ = 7.81 (s, 1H, Ar*H*), 6.92 (s, 1H, Ar*H*), 6.16 (s, 1H, Ar*H*), 4.28 (t, 2H, $OCH_2CH_2O_4C_7H_{15}$), 3.96 (t, 2H, $OCH_2CH_2O_4C_7H_{15}$), 3.81 (t, 2H, $OC_2H_4OCH_2CH_2O_3C_5H_{11}$), 3.70 – 3.63 (m, 10H, $OC_2H_4OCH_2CH_2O_2C_4H_8OCH_3$), 3.56 (s, 3H, $O_4C_8H_{16}OCH_3$), 2.40 (s, 3H, Ar-CH_3). MS (ESI Pos.): *m/z* =445.7 $[(M+H)]^+$.

6-Bromo-4-formyl-7-*O*-(2-(2-(2-(2-methoxyethoxy)ethoxy)ethoxy)ethoxy)coumarin (A16)

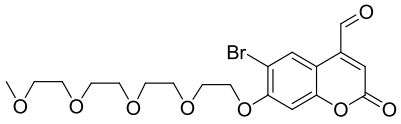

A mixture of 6-bromo-4-methyl-7-O-(2-(2-(2-(2-methoxyethoxy)ethoxy)ethoxy)ethoxy)coumarin (4.45g, 10.0 mmol) and SeO_2 (1.44 g, 13.0 mmol) in xylene (15.0 mL) was stirred at reflux temperature for 2 days. After completion of the reaction, it was filtered through celite and concentrated under reduced pressure. The obtained crude substance was purified by column chromatography (silica gel, $CHCl_3$/EtOAc) to afford the desired compound as oil (2.60 g, 57 %). ^{1}H NMR (400 MHz, $CDCl_3$): δ = 9.95 (s, 1H, C*H*O), 8.66 (s, 1H, Ar-*H*), 6.79 (s, 1H, Ar-*H*), 6.69 (s, 1H, Ar-*H*), 4.17 (t, 2H, $OCH_2CH_2O_4C_7H_{15}$), 3.89 (t, 2H, $OCH_2CH_2O_4C_7H_{15}$), 3.72 (t, 2H, $OC_2H_4OCH_2CH_2O_3C_5H_{11}$), 3.63 – 3.55 (m, 8H, $O_2C_3H_6CH_2OC_2H_4OCH_2CH_2OCH_3$), 3.47 (t, 2H, $O_3C_6H_{12}OCH_2CH_2OCH_3$), 3.29 (s, 3H, $O_4C_8H_{16}OCH_3$). ^{13}C NMR (100 MHz, $CDCl_3$): δ = 191.5 (*C*HO), 160.0 (*C*O), 158.4 (C_{Ar}), 155.2 (C_{Ar}), 142.5 (C_{Ar}), 130.0 (C_{Ar}), 123.3 (C_{Ar}), 109.1 (C_{Ar}), 108.8 (C_{Ar}), 101.0 (C_{Ar}), 71.9 (CH_2), 71.2 (CH_2), 70.6 (CH_2), 70.5 (2 x CH_2), 70.4 (CH_2), 69.5 (CH_2), 69.1 (CH_2), 59.0 (CH_3). MS (ESI Pos.): *m/z* =481.7 $[(M+Na)]^+$, 459.6 $[(M+H)]^+$.

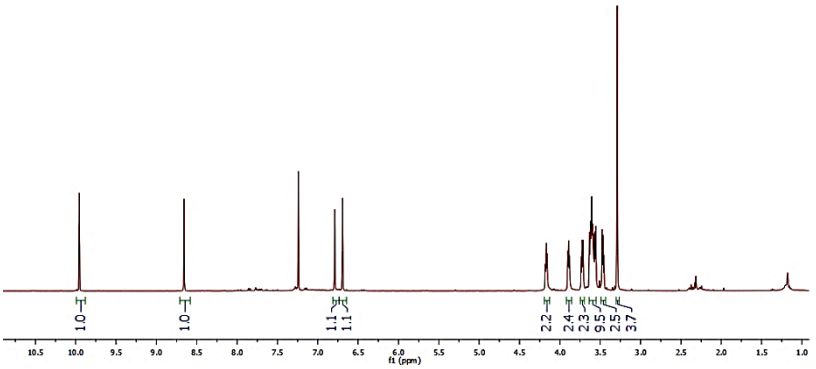

Figure S17 | ^{1}H NMR spectrum of coumarin derivative (**A16**) in $CDCl_3$ at 25 °C.

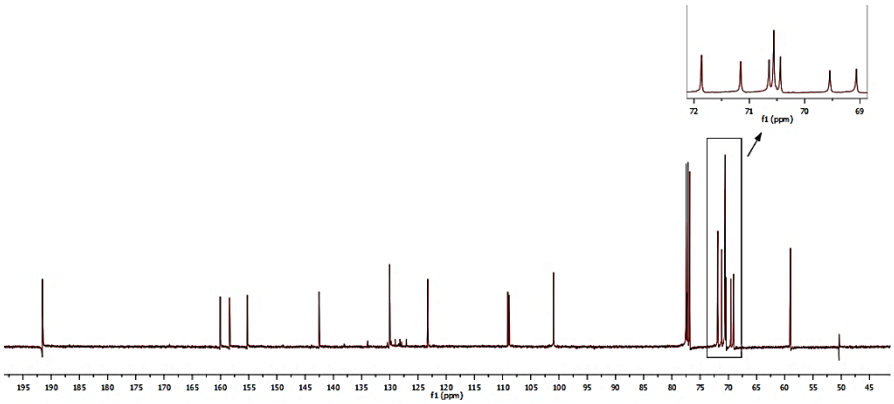

Figure S18 | ^{13}C NMR spectrum of coumarin derivative (**A16**) in $CDCl_3$ at 25 °C.

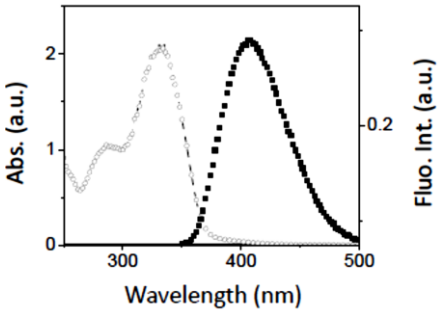

Figure S19 | UV-Vis and fluorescence spectra of coumarin derivative (**A16**) in water (C = 10^{-5} M, $\lambda_{exc.}$ = 350 nm).

Fluorescein Labelled Aldehyde (A17)

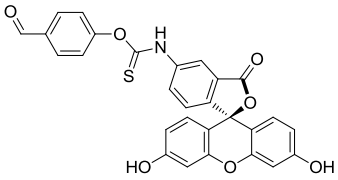

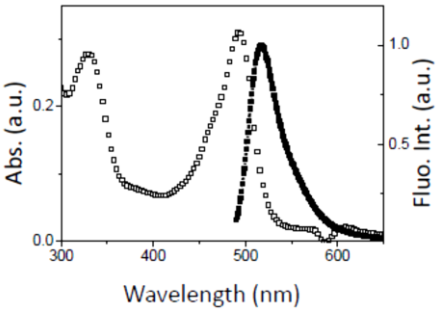

Figure S20 | UV-Vis spectrum of fluorescein derivative (**A17**) in water (C = 10^{-6} M, $\lambda_{exc.}$ = 490 nm).

Rhodamine Labelled Aldehyde (A18)

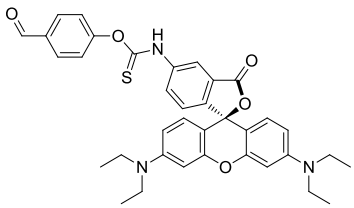

NaH (0.01 g, 0.40 mmol) was added to a solution of 4-hydroxybenzaldehyde (0.02 g, 0.20 mmol) in DMF (2.0 mL) at 0 °C. A solution of rhodamine B isothiocyanate (0.05 g, 0.10 mmol, Sigma Aldrich) in DMF (1.0 mL) was added afterwards to the mixture and it was stirred for overnight at 80 °C. After that, the solvent was evaporated under reduced pressure and the obtained residue was taken in minimum amount of water and aqueous layer was washed with CH_2Cl_2 to remove the excess of benzaldehyde derivative. The aqueous layer was then concentrated under reduced pressure and dried to obtain desired compound as red solid (0.04 g, 64 %). MS (ESI Neg.): *m/z* =620.1 ($[M-H]^+$).

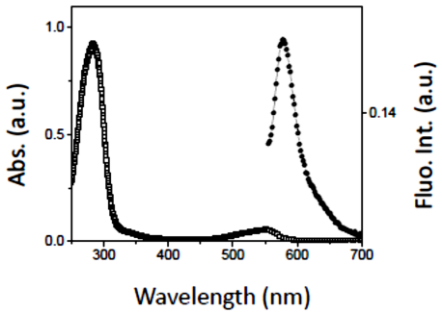

Figure S21 | UV-Vis and fluorescence spectra of rhodamine derivative (**A18**) in water (C = 10^{-5} M, $\lambda_{exc.}$ = 550 nm).

Cyanine Dye Labelled Aldehyde (A19)

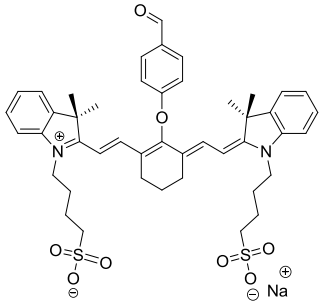

4-Hydroxybenzaldehyde (15.0 mg, 0.12 mmol) and NaH (3.0 mg, 0.12 mmol) were dissolved in anhydrous DMF (5.0 mL) and the mixture was stirred at room temperature for 10 min. Then a solution of IR-783 (2-[2-[2-Chloro-3-[2-[1,3-dihydro-3,3-dimethyl-1-(4-sulfobutyl)-2H-indol-2-ylidene]-ethylidene]-1-cyclohexen-1-yl]-ethenyl]-3,3-dimethyl-1-(4-sulfobutyl)-3H-indolium hydroxide; Sigma Aldrich) (37.0 mg, 0.05 mmol, Sigma Aldrich) in DMF (5.0 mL) was added to the mixture and it was further stirred for overnight. After that, the solvent was removed under reduced pressure and the obtained residue was washed with $CHCl_3$ to obtain the desired compound as a dark green solid (3.0 mg, 72 %). ^{1}H NMR (400 MHz, CD_3OD): δ = 9.48 (bs, 3H, -C*H*O & Ar*H*), 7.95 (bs, 3H, Ar*H*), 7.59 (bs, 5H, Ar*H*), 7.26 (bs, 1H, Ar*H*), 6.62 (bs, 5H, Ar*H*), 3.28 (bs, 2H, -C*H*$_2$-), 2.96 (bs, 4H, -C*H*$_2$-), 2.83 (bs, 12H, -C*H*$_2$-), 1.89 (bs, 4H, -C*H*$_2$-), 1.28 (bs, 6H, C(C*H*$_3$)$_2$), 0.86 (bs, 6H, C(C*H*$_3$)$_2$). MS (ESI Neg.): *m/z* = 811.3 ([M-Na]$^+$).

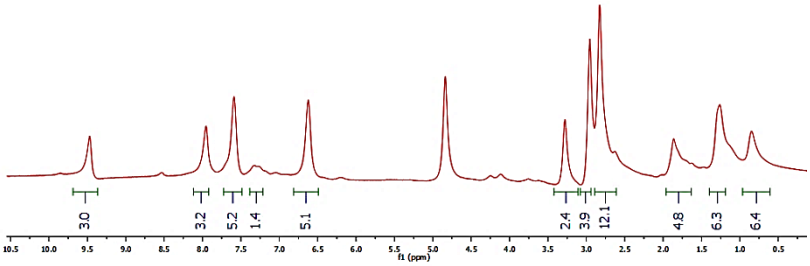

Figure S22 | ^{1}H NMR spectrum of cyanine derivative (**A19**) in CD_3OD at 25 °C.

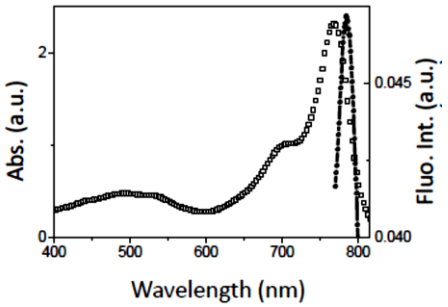

Figure S23 | UV-Vis and fluorescence spectra of cyanine derivative (**A19**) in water (C = 10^{-5} M, $\lambda_{exc.}$ = 765 nm).

4-(2-(2-(2-(Prop-2-yn-1-yloxy)ethoxy)ethoxy)ethoxy)benzaldehyde (A20)

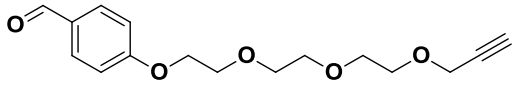

4-(2-(2-(2-Hydroxyethoxy)ethoxy)ethoxy)benzaldehyde (5.00 g, 19.7 mmol) was dissolved in dry THF (200.0 mL) and the solution was cooled to 0 °C using an ice bath. NaH (0.94 g, 60 wt% in mineral oil, 23.60 mmol) was added to the solution and it was stirred for 1h. Propargyl bromide (2.22 mL, 80 wt% in toluene, 21.63 mmol) was added to the mixture and it was allowed to obtain ambient temperature. The reaction mixture was stirred overnight. After completion of the reaction, it was concentrated under reduced pressure and diluted with water (200 mL). The aqueous layer was extracted with CH_2Cl_2 (3 x 200 mL). The organic layers were combined and washed with brine (600 mL). The organic layer was dried over $MgSO_4$, then filtered off and concentrated under reduced pressure. The obtained residue was purified by column chromatography (Silica gel, EtOAc/PE 1/1) yielding the desired product as a light-yellow oil (2.52 g, 44 %). ^{1}H NMR (400 MHz, $CDCl_3$): δ = 9.82 (s, 1H), 7.78 (d, *J* = 8.6 Hz, 2H, Ar-*H*), 6.98 (d, *J* = 8.6 Hz, 2H, Ar-*H*), 4.19-4.13 (m, 4H, C*H*$_2$), 3.87-3.82 (m, 2H, C*H*$_2$), 3.77-3.71 (m, 2H, C*H*$_2$), 3.66-3.61 (m, 6H, C*H*$_2$), 2.41 (t, J = 2.2 Hz, 1H, C*H*). ^{13}C NMR (100 MHz, $CDCl_3$): δ = 190.8 (*C*HO), 163.9 (*C*$_{Ar}$), 132.0 (2x*C*$_{Ar}$), 130.1 (*C*$_{Ar}$), 114.9 (2x*C*$_{Ar}$), 79.7 (*C*≡CH), 74.7 (C≡*C*H), 70.9 (*C*H$_2$), 70.7 (*C*H$_2$), 70.5 (*C*H$_2$), 69.5 (*C*H$_2$), 69.1 (*C*H$_2$), 67.8 (*C*H$_2$), 58.4 (*C*H$_2$). MS (ESI Pos.): *m/z* = 293.5 ([M+H]$^+$).

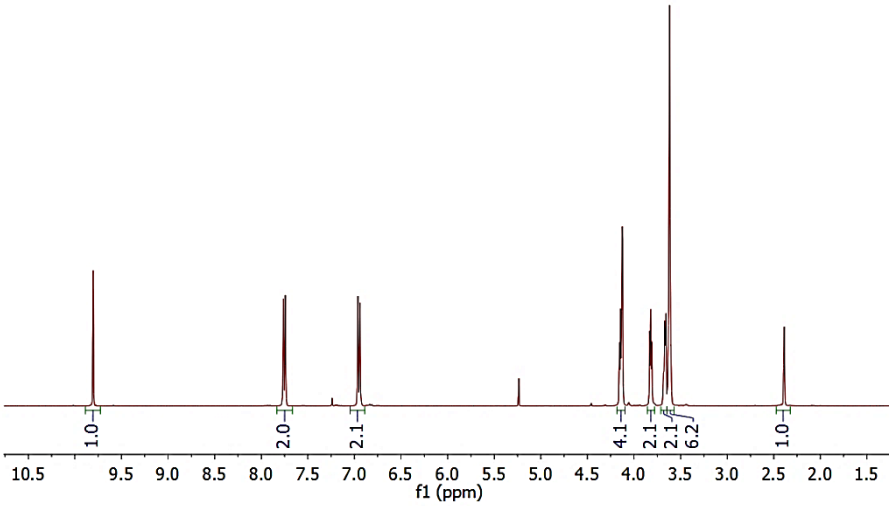

Figure S24 | ^{1}H NMR spectrum of 4-(2-(2-(2-(prop-2-yn-1-yloxy)ethoxy)ethoxy)ethoxy)-benzaldehyde (**A20**) in $CDCl_3$ at 25 °C.

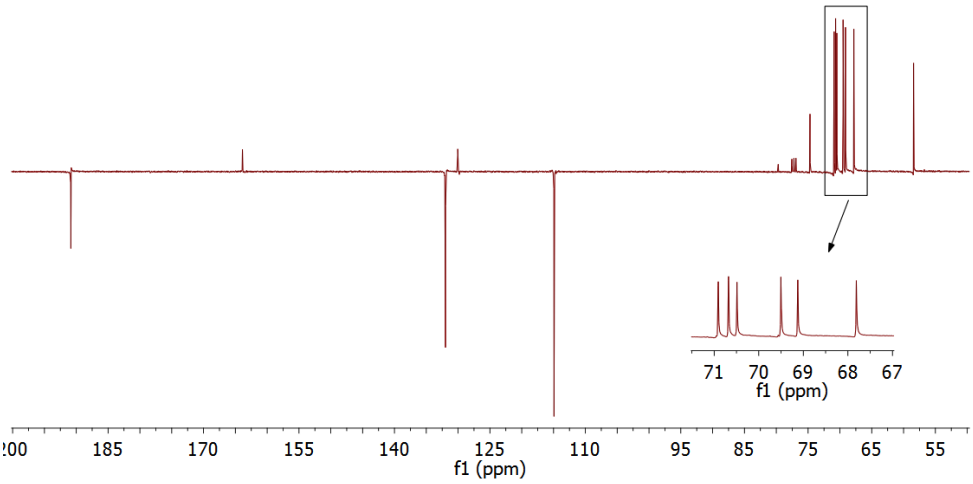

Figure S25 | ^{13}C NMR spectrum of 4-(2-(2-(2-(prop-2-yn-1-yloxy)ethoxy)ethoxy)ethoxy)-benzaldehyde (**A20**) in $CDCl_3$ at 25 °C.

2-(2-(2-(4-Formylphenoxy)ethoxy)ethoxy)ethyl acrylate (A21)

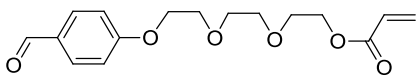

Acryloyl chloride (1.45 mL, 18.0 mmol) was added dropwise to a solution of 4-(2-(2-(2-hydroxyethoxy)ethoxy)ethoxy)benzaldehyde (2.29 g, 9.0 mmol), triethyl amine (2.90 mL, 20.7 mmol) in CH_2Cl_2 (90.0 mL) at 0 °C. After complete addition, it was allowed to get ambient temperature and stirred at that temperature for overnight. After completion of the reaction, it was quenched with water

and diluted with CH_2Cl_2. The organic layer was washed with water, brine and dried over $MgSO_4$. After removal of the solvent under reduced pressure, the crude compound was purified by flash column chromatography (silica gel, CH_2Cl_2) to obtain the desired compound as a viscous liquid (2.77 g, 94 %). ^{1}H NMR (400 MHz, $CDCl_3$): δ = 9.88 (s, 1H, C*H*O), 7.83 (d, *J* = 8.8 Hz, 2H, Ar-*H*), 7.03 (d, *J* = 8.7 Hz, 2H, Ar-*H*), 6.44 (dd, *J* = 17.3 Hz, *J* = 1.4 Hz, 1H, CH=C*H*H), 6.15 (dd, *J* = 10.5 Hz, *J* = 17.4 Hz, C*H*=CH$_2$), 5.83 (dd, *J* = 1.4 Hz, *J* = 10.4 Hz, 1H, CH=CH*H*), 4.31 (t, 2H, C*H*$_2$), 4.21 (t, 2H, C*H*$_2$), 3.89 (t, 2H, C*H*$_2$), 3.74–3.72 (m, 4H, C*H*$_2$), 3.69 (t, 2H, C*H*$_2$). ^{13}C NMR (100 MHz, $CDCl_3$): δ = 190.8 (*C*HO), 166.1 (*C*O), 163.8 (*C*$_{Ar}$), 131.9 (2x*C*$_{Ar}$), 131.0 (*C*H=CH$_2$), 130.0 (*C*$_{Ar}$), 128.2 (CH=*C*H$_2$), 114.8 (2x*C*$_{Ar}$), 70.9 (*C*H$_2$), 70.6 (*C*H$_2$), 69.5 (*C*H$_2$), 69.2 (*C*H$_2$), 67.7 (*C*H$_2$), 63.6 (*C*H$_2$). MS (ESI Pos.) m/z: 309.2 [(M+H)$^+$], 331.2 [(M+Na)$^+$].

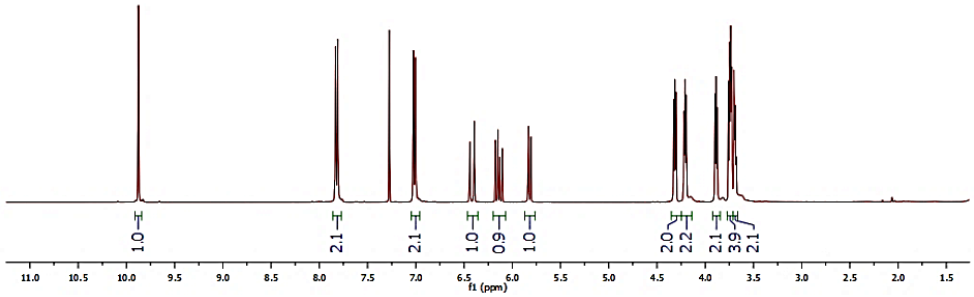

Figure S26 | ^{1}H NMR spectrum of 2-(2-(2-(4-formylphenoxy)ethoxy)ethoxy)ethyl acrylate (**A21**) in $CDCl_3$ at 25 °C.

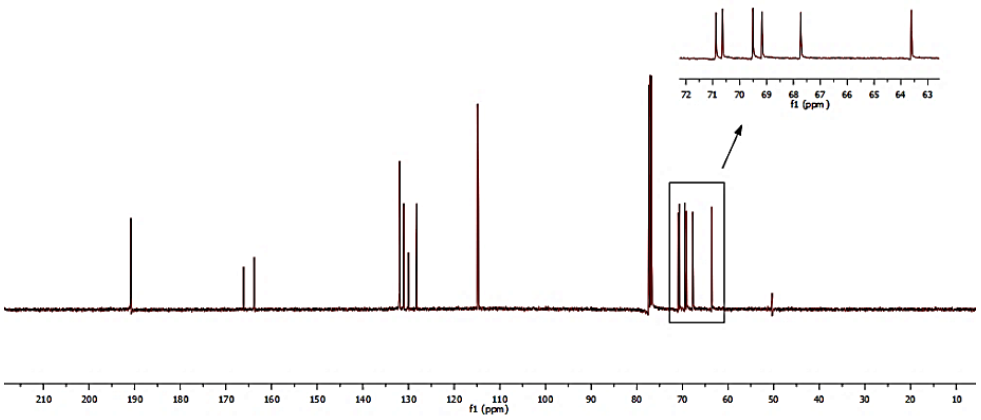

Figure S27 | ^{13}C NMR spectrum of 2-(2-(2-(4-formylphenoxy)ethoxy)ethoxy)ethyl acrylate (**A21**) in $CDCl_3$ at 25 °C.

2-(2-(2-(4-Formylphenoxy)ethoxy)ethoxy)ethyl 4-methylbenzenesulfonate (A22)

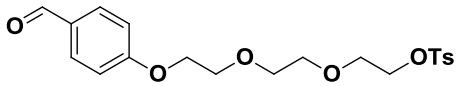

4-(2-(2-(2-Hydroxyethoxy)ethoxy)ethoxy)benzaldehyde (**A5**) (1.00 g, 3.9 mmol) was dissolved in CH_2Cl_2 (50.0 mL). *p*-Toluenesulfonyl chloride (1.13 g, 5.90 mmol) and triethyl amine (1.1 mL, 7.87 mmol) were added and the reaction mixture was stirred overnight at ambient temperature. After completion of the reaction (18 h and complete conversion was observed in ^{1}H NMR), the reaction mixture was concentrated under reduced pressure. The obtained residue was

diluted with CH_2Cl_2 (200.0 mL) and washed with an aqueous saturated $NaHCO_3$ solution, brine. The organic layer was dried over Na_2SO_4 and concentrated under reduced pressure yielding the desired compound (1.93 g, quantitative). **^{1}H NMR** (400 MHz, $CDCl_3$): δ = 9.85 (s, 1H, C*H*O), 7.80 – 7.77 (m, 4H, Ar*H*), 7.31 (s, 2H, Ar*H*), 7.00 (s, 2H, Ar*H*), 4.18-4.13 (m, 4H, CH_2), 3.84 (s, 2H, CH_2), 3.66-3.60 (m, 6H, CH_2), 2.41 (s, CH_3). **^{13}C NMR** (100 MHz, $CDCl_3$): δ = 190.8 (*C*HO), 163.8 (C_{Ar}), 144.8 (C_{Ar}), 132.9 (C_{Ar}), 131.9 (2xC_{Ar}), 130.0 (C_{Ar}), 129.8 (2xC_{Ar}), 127.9 (2xC_{Ar}), 114.8 (2xC_{Ar}), 70.8 (2x*C*H$_2$), 69.5 (*C*H$_2$), 69.2 (*C*H$_2$), 68.7 (*C*H$_2$), 67.7 (*C*H$_2$), 21.6 (*C*H$_3$).

4-(2-(2-(2-azidoethoxy)ethoxy)ethoxy)benzaldehyde (A23)

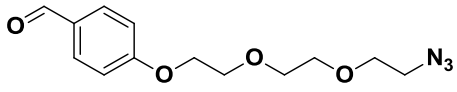

2-(2-(2-(4-Formylphenoxy)ethoxy)ethoxy)ethyl 4-methylbenzenesulfonate (8.03 g, 19.7 mmol) was dissolved in DMF (100 mL). Sodium azide (6.39 g, 98.3 mmol) was added and the reaction was stirred while heating to 60 °C. After stirring for 18 h the reaction mixture was allowed to cool down and concentrated under reduced pressure. The residue was dissolved in an aqueous 1M HCl solution (200 mL) and extracted with EtOAc (200 mL). The organic layer was washed with a saturated aqueous $NaHCO_3$ solution (200 mL) and brine (200 mL). The organic layer was dried over $MgSO_4$, filtered off and concentrated under reduced pressure. Purification using a flash column chromatography (silica gel, 0 % → 10 % MeOH in CH_2Cl_2) yielded the desired compound (5.04 g, 92 %) as a light-brown oil. ^{1}H NMR (400 MHz, $CDCl_3$): δ = 9.86 (s, 1H, C*H*O), 7.82 (d, *J* = 7.7 Hz, 2H, Ar-*H*), 7.02 (d, *J* = 7.8 Hz, 2H, Ar-*H*), 4.21 (m, 2H), 3.89 (m, 2H), 3.73 - 3.67 (m, 6H), 3.37 (m, 2H). ^{13}C NMR (100 MHz, $CDCl_3$): δ = 190.8 (*C*HO), 163.8 (C_{Ar}), 131.9 (2xC_{Ar}), 130.0 (C_{Ar}), 114.9 (2xC_{Ar}), 70.9 (*C*H$_2$), 70.7 (*C*H$_2$), 70.1 (*C*H$_2$), 69.5 (*C*H$_2$), 67.7 (*C*H$_2$), 50.6 (*C*H$_2$). MS (ESI Pos.) m/z: 280.4 [(M+H)$^+$].

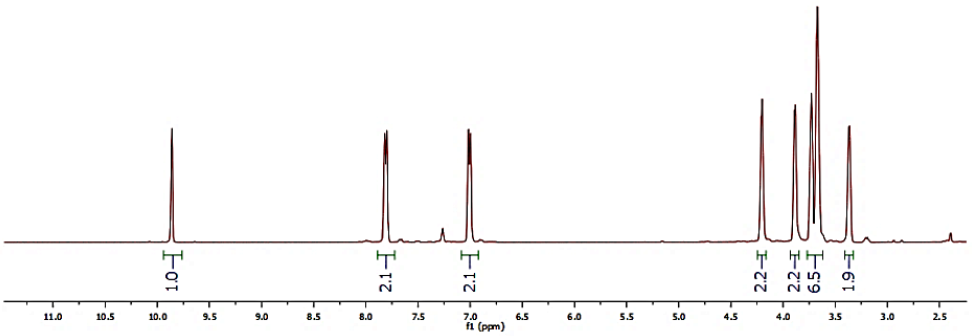

Figure S28 | ^{1}H NMR spectrum of 2-(2-(2-(4-Formylphenoxy)ethoxy)ethoxy)ethyl 4-methylbenzenesulfonate (**A23**) in $CDCl_3$ at 25 °C.

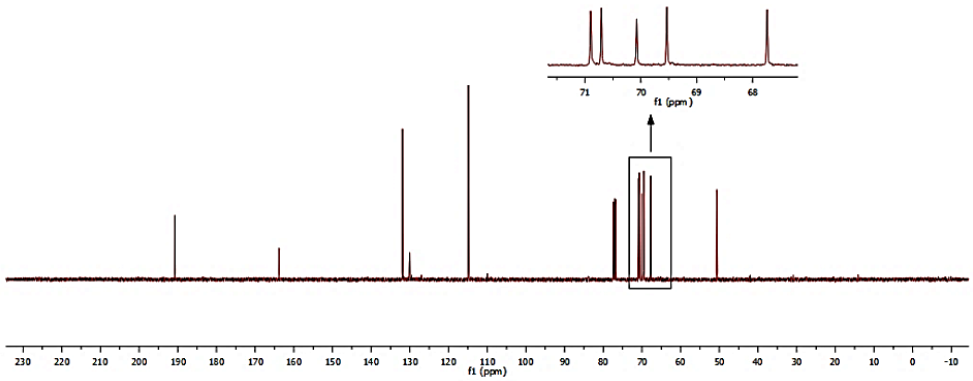

Figure S29 | ^{13}C NMR spectrum of 2-(2-(2-(4-Formylphenoxy)ethoxy)ethoxy)ethyl 4-methylbenzenesulfonate (**A23**) in $CDCl_3$ at 25 °C.

Aldehyde Labelled Mannose Acetate Derivative (A24)

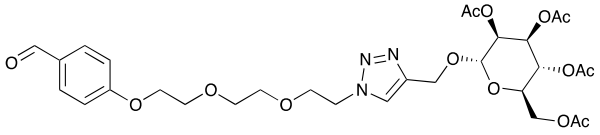

4-(2-(2-(2-Azidoethoxy)ethoxy)ethoxy)benzaldehyde (**A23**) (0.73 g, 2.62 mmol), 2,3,4,6-tetraacetylpropargylmannoside (1.01 g, 2.62 mmol) and triethyl amine (0.15 mL, 1.05 mmol) were added to a degassed mixture of CuI (0.05 g, 0.26 mmol) in CH_2Cl_2. The reaction mixture was stirred at ambient temperature for 3h. After completion of the reaction, it was concentrated under reduced pressure and the obtained residue was diluted with EtOAc. The organic layer was washed with satd. $NaHCO_3$ solution and brine, dried over $MgSO_4$. After concentration under reduced pressure, the obtained crude compound was purified by column chromatography (Silica gel, EtOAc) to obtain the desired compound as viscous oil (1.65 g, 95 %). R_f ($MeOH/CH_2Cl_2$ 1/4) = 0.8. ^1H NMR (400 MHz, $CDCl_3$): δ (ppm) = 9.86 (s, 1H, C*H*O), 7.82 (m, 3H, triazole-*H* and Ar-*H*), 7.01 (d, *J* = 7.9 Hz, 2H, Ar*H*), 5.29 (s, 2H, OCH_2), 5.21 (s, 1H, mannose-*H*), 4.92 (s, 1H, mannose-*H*), 4.79 (bs, 2H, mannose-*H*), 4.55 (m, 2H, OCH_2), 4.28 (m, 1H, mannose-*H*), 4.20 (t, 2H, OCH_2), 4.08 (m, 2H, OCH_2), 3.89 – 3.83 (m, 4H, OCH_2), 3.68 – 3.64 (m, 4H, OCH_2), 2.12 (s, 3H, OCOCH_3), 2.09 (s, 3H, OCOCH_3), 2.01 (s, 3H, OCOCH_3), 1.95 (s, 3H, OCOCH_3). MS (ESI Pos.) m/z: 688.4 [$(M+Na)^+$].

Aldehyde Labelled Mannose Derivative (A25)

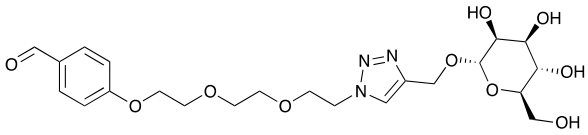

Sodium methoxide solution (0.01 mL, 0.01 mmol, 30 mol % in CH_3OH) was added dropwise to a solution of the acetate derivative (0.70 g, 1.05 mmol) in CH_3OH (5.0 mL). After complete addition, it was stirred at room temperature while the solution turned greenish gradually. After completion of the reaction, it was concentrated under reduced pressure and then acidified with an ion exchange resin (eluent: CH_2Cl_2/MeOH 1/1) to obtain

the desired compound as a pale yellow viscous liquid (0.50 g, 96 %). R_f (MeOH/CH_2Cl_2 1/4) = 0.4. ^{1}H NMR (400 MHz, CD_3OD): δ (ppm) = 9.84 (s, 1H, C*H*O), 8.05 (s, 1H, Triazole-*H*), 7.88 (d, *J* = 7.9 Hz, 2H, Ar*H*), 7.11 (d, *J* = 7.1 Hz, 2H, Ar*H*), 4.83 (s, 1H, mannose-*H*), 4.77 (d, 1H, mannose-*H*), 4.62 (s, 1H, mannose-*H*), 4.57 (t, 2H, OCH_2), 4.22 (t, 2H, OCH_2), 3.89 (t, 2H, OCH_2), 3.83 (m, 3H, OCH_2 & mannose-*H*), 3.77 – 3.72 (m, 2H, OCH_2), 3.67 – 3.54 (m, 7H, OCH_2 & mannose-*H*). ^{13}C NMR (100 MHz, CD_3OD): δ (ppm) = 192.80 (*C*HO), 165.58 (C_{Ar}), 145.10 ($C_{Triazole}$), 133.14 (C_{Ar}), 131.46 ($C_{Triazole}$), 126.15 (C_{Ar}), 116.07(C_{Ar}), 100.74 ($C_{Mannose}$), 74.99 ($C_{Mannose}$), 72.53 ($C_{Mannose}$), 72.03 ($C_{Mannose}$), 71.73 ($C_{Mannose}$), 71.47 (OCH_2), 70.58 (OCH_2), 70.28 (OCH_2), 69.09 (OCH_2), 68.60 (OCH_2), 62.98 (OCH_2), 60.64 (OCH_2), 51.45 (NCH_2). MS (ESI Pos.) m/z: 520.4 [$(M+K)^+$].

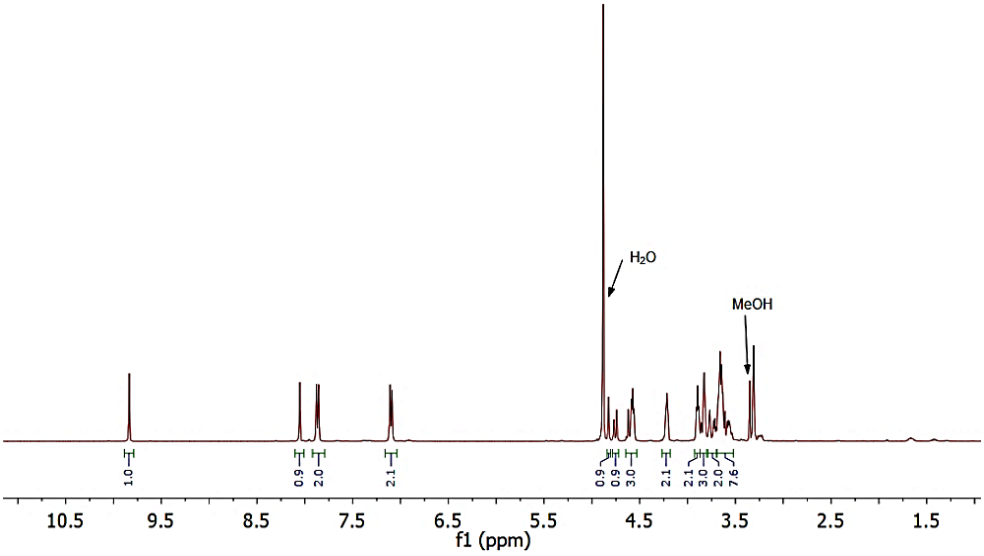

Figure S30 | ^{1}H NMR spectrum of aldehyde labelled mannose derivative (**A25**) in CD_3OD at 25 °C.

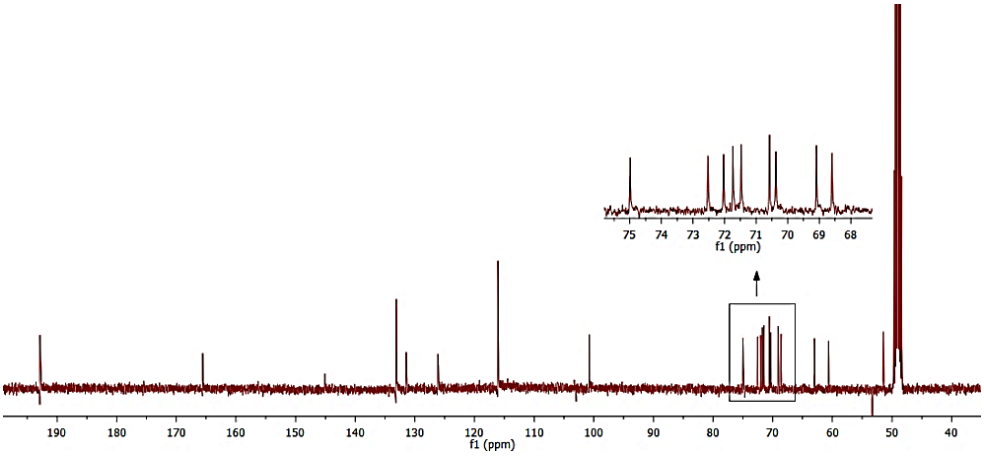

Figure S31 | ^{13}C NMR spectrum of aldehyde labelled mannose derivative (**A25**) in CD_3OD at 25 °C.

References

1. Han, M. *et al. Eur. J. Org. Chem.* **2011,** 7271–7277 (2011).
2. Poolman, J. M. *et al. Nat. Protoc.* **9,** 977–988 (2014).
3. Boekhoven, J. *et al. Nat. Chem.* **5,** 433–437 (2013).
4. León, E. I., Martín, Á., Pérez-Martín, I., Quintanal, L. M. & Suárez, E. *Eur. J. Org. Chem.* **2012,** 3818–3829 (2012).
5. Gromov, S. P. *et al. Eur. J. Org. Chem.* **2010,** 2587–2599 (2010).
6. Mason, S. J., Hake, J. L., Nairne, J., Cummins, W. J. & Balasubramanian, S. *J. Org. Chem.* **70,** 2939–2949 (2005).
7. Furuta, T., Watanabe, T., Tanabe, S., Sakyo, J. & Matsuba, C. *Org. Lett.* **9,** 4717–4720 (2007).
8. Li, L. *et al. Angew. Chem. Int. Ed.* **53,** 3835–3839 (2014).
9. N. Del Cid, L. Shen, J. Belleisle and M. Raghavan, *PloS one*, 2012, **7**, e41727.
10. S. I. Van Kasteren, H. B. Kramer, D. P. Gamblin and B. G. Davis, *Nat. Protoc.*, **2**, 3185-3194 (2007).
11. J. C. M. Van Hest, K. L. Kiick and D. A. Tirrell, *J. Am. Chem. Soc.*, **122**, 1282-1288 (2000).
12. S. I. van Kasteren, H. B. Kramer, H. H. Jensen, S. J. Campbell, J. Kirkpatrick, N. J. Oldham, D. C. Anthony and B. G. Davis, *Nature*, **446**, 1105-1109 (2007).
13. M. M. Bradford, *Anal. Biochem.*, **72**, 248-254 (1976).
14. J. **Boekhoven, C. M.** Rubert, S. Sur, A. Worthy, S. I. Stupp, *Angew. Chem. Int. Ed.*, *52*, *12077-12080 (2013).*
15. Ishmuratov, G. Y. *et al. Chem. Nat. Compd.* **45,** 465–469 (2009).
16. Astorga, C., Rebolledo, F. & Gotor, V. *Synthesis* **1993,** 287–289 (1993).
17. Yi, W. *et al. Eur. J. Med. Chem.* **45,** 639–646 (2010).
18. McFarland, J. M. & Francis, M. B. *J. Am. Chem. Soc.* **127,** 13490–13491 (2005).
19. Standley, S. M. *et al. Bioconjug. Chem.* **15,** 1281–1288 (2004).
20. Berg, S. *et al.* New compounds. 35 (2003). at <http://worldwide.espacenet.com/publicationDetails/biblio?FT=D&date=20030703&DB=EPODOC&locale=en_EP&CC=WO&NR=03053330A2&KC=A2&ND=7>
21. Jain, R., Standley, S. M. & Fréchet, J. M. J. *Macromolecules* **40,** 452–457 (2007).
22. Nielsen, C. B. *et al. J. Org. Chem.* **70,** 7065–7079 (2005).

Tunable hydrogel network properties through chemical crosslinking using functionalized PEG polymers

5

Abstract

We demonstrate that functionalized PEG crosslinkers improve mechanical properties of the hydrazone LMWG system. The presence of the polymer in the gel network significantly improves the storage modulus. Also the gels obtained are much more transparent. The combination of LMWGs and crosslinkers allows us to make gels with tailored mechanical properties.

Introduction

LMWGs are very popular for producing materials such as electronic devices and biomedical applications.[1,2] Gelator molecules form aggregates in the form of fibres which eventually entangle into a network and keep the solvent in place. The driving forces behind the self-assembly process are the non-covalent interactions which due to their reversibility allow for responsive or adaptive behaviour in smart materials.

However, the general problem with LMWGs is poor mechanical performance.[3] The assemblies based on non-covalent interactions cannot match the mechanical properties of polymer gels which are generally based on covalent interactions.

Over the past few years there has been an increasing interest in combining these two gel structures.[4] The major motive behind this synergetic approach of polymer gels and LMWGs is to obtain better mechanical performance while simultaneously keeping the responsive properties.[5]

Various strategies of combining LMWGs with polymers have been demonstrated.[4] For example, a combination of a pyridine-based gelator with polyacrylic acid was created yielding a gel with acid-base interactions between the two networks. The cooperation resulted in increased entanglement and improved gel strength.[6] Otto et al. presented a similar case of dithiol-based fibres reinforced with sulphate containing polymers. The interactions between the positively charged hydrogel and the negatively charged sulphate yielded a positive impact on the G' value.

Rowan et al. created crosslinks by covalently linking the polymer to a guanosine monomer on each end. Hydrogels were prepared from guanosine-containing helical assemblies and crosslinked with polydimethylacrylate polymers. This also led to an improved storage modulus.[7]

The examples described above provide us with an interesting approach as well as results which are very interesting for our own purposes. In prior studies, we have shown the ability to introduce chemical functionalizations into a hydrazone hydrogel network by means of mixing in different aldehyde compounds.[8] This approach can be extrapolating to polymers and should allow us to introduce chemical crosslinks by incorporating functionalized polymers into our hydrogel network.

Here, we present the addition of covalent crosslinks to a hydrazone-based hydrogel system **(Fig. 1)**. The addition of crosslinks improves the mechanical properties and also results in a decrease in CGC. Also, the synthetic methods used provide an easy approach in designing crosslinks of different length.

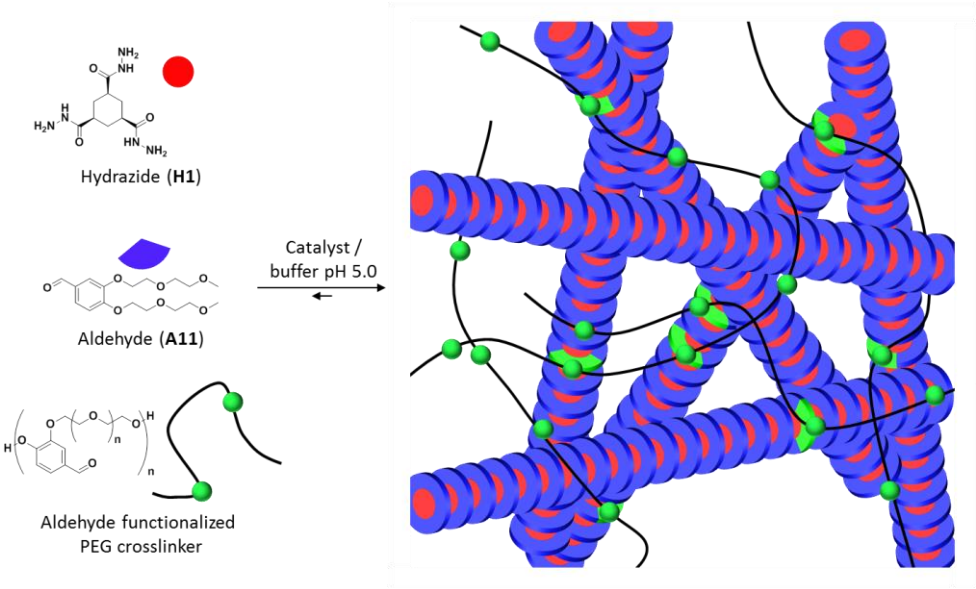

Figure 1 | Concept of a covalently crosslinked hydrazone gel system. Based on the hydrazone gelator system, a functionalized polymer is introduced as one of the soluble building blocks of the hydrogel creating chemical crosslinks between the hydrogel network fibres.

Results and discussion

In previous work we have proved the ease of tuning our system with functionalized aldehydes decorated with probes and reactive groups.[8] The same method enables us to introduce water-soluble polymers into the hydrogelator system. Poly (ethylene glycol) (PEG) shares a highly similar structure with the short tailed ethylene oxide benzaldehydes which we use in our current hydrogel system. Also, PEG is a widely used water-soluble polymer well known for its many applications making it a suitable candidate in the synthesis of our crosslinker molecules. By combining PEG with benzaldehyde functional groups a design is obtained which imitates the small molecule aldehyde building block (**A11**), but also with the ability of binding multiple hydrazides to a single polymer chain. The addition of benzaldehyde functional groups in order to bind to the hydrazide core (**H1**) should yield a functional crosslinkers in only a few synthetic steps.

Two different designs for the PEG-based crosslinkers were proposed (**Fig. 2**). The first approach is a terminal functionalization of PEG (**P1**), the second approach creates an alternating co-polymer of PEG and benzaldehydes (**P2**). The **P1** design creates a simple crosslinker with a defined length, whereas the **P2** design creates an alternating structure of benzaldehydes and PEG with a larger expected size distribution. The two designs resemble a trade-off, namely the control over the polymer size vs the degree of functionalization. The probability of a crosslinker binding to the gel fibre depends on these characteristics. Both

designs should improve the gel network by creating chemical crosslinks and with that yield a hydrogel with improved mechanical properties.
Both polymers started from the mesylation of commercial PEG which creates good leaving groups for the next synthetic step, followed by Williamson ether synthesis which introduces the benzaldehyde group.

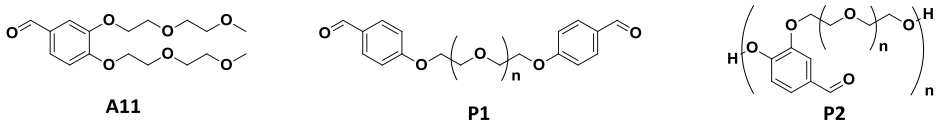

Figure 2 | Proposed designs of functionalized PEG crosslinkers. Original aldehyde (**A11**) exhibiting many similarities to the proposed designs: Functionalized PEG crosslinker (**P1**) represents a straight-forward design very closely related to the original aldehyde with two terminal functional groups. PEG crosslinker (**P2**) exhibits a more complex alternating design and contains more reactive groups with the aim of increasing the probability of chemically binding to a hydrazide group.

Both crosslinkers were prepared in a similar fashion, starting from the appropriate hydroxybenzaldehyde and commercial PEG (**Fig. 3**). Commercial PEG was subjected to mesylation of both terminal positions which provided mesylate **P0**. Contrary to reported literature procedure, tosylation with *p*-toluenesulfonyl chloride or chlorination with thionyl chloride were both unsuccessful as chain cleavage was observed in either case upon analysis of the final product.[9,10] In order to prevent chain cleavage a large excess of triethyl amine was favoured.[11] Williamson ether synthesis with 4-hydroxybenzaldehyde and 3,4-dihydroxybenzaldehyde (or the potassium salt[10,12]) yielded the respective final products **P1** and **P2**. The versatility of the synthetic route allowed us to investigate crosslinkers of different lengths. Therefore, different lengths of the **P1** design were synthesized ranging from 300, 2000, 10.000 and 35.000 Da, named **P1-300**, **P1-2000**, **P1-10.000** and **P1-35.000**. **P2** was determined to have an M_w of 180.000 Da using GPC and ^{1}H NMR.

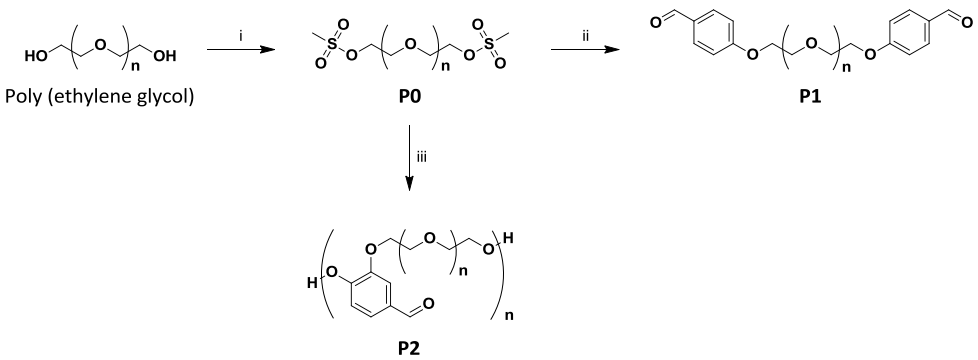

Figure 3 | Synthetic route towards functionalized PEG crosslinkers. Reagents and conditions (i) MsCl, Et_3N, THF, 0°→ RT, 48 h, 70-89%; (ii) 4-Hydroxybenzaldehyde, K_2CO_3, DMF, 72 h, 130°C, 40%; (iii) 3,4-Dihydroxybenzaldehyde, K_2CO_3, DMF, 120 h, 130°C, 79%.

Critical gel concentration (CGC) tests were performed in order to determine the effect of the functionalized PEG crosslinkers on the gel network. We replaced a small fraction of the original aldehyde with modified PEG crosslinkers, retaining the total amount of functional aldehyde groups.

Of the **P1** series, **P1-300** showed very poor solubility in water which did not allow us to perform any CGC experiments. **P1-2000** and **P1-10.000** both showed an increase of the CGC upon addition of 1% of crosslinker and higher. **P1-35000** showed a decrease of the CGC, with a minimum of 1.25 mM upon addition of 4% of crosslinker. When more than 20% of **P1-35000** was added clear solutions instead of gels were obtained.

The insolubility of **P1-300** came as a surprise. With an average of 6 to 7 ethylene oxide units and 2 benzaldehyde units, the crosslinker was expected to be soluble enough. The structure contained a similar ratio of hydrophobic and hydrophilic groups as some of the short-tailed aldehydes described in our previous work.[8] The negative effect of both **P1-2000** and **P1-10.000** could possibly be explained due to the contraction of the fibres by the crosslinkers. Subsequent bundling would lead to precipitation which explains the poor performance of the crosslinkers which we observed. The positive effect of **P1-35000,** being the only beneficial crosslinker, could be explained by its length. Namely, the length of **P1-35000** could be long enough to form crosslinks but the bulkiness might prevent bundling.

Rheology measurements were performed in order to study the change in material properties (**Fig. 4a-b**). Since **P1-35000** was the only crosslinker to yield a beneficial result in the CGC test, we decided to focus our measurements on this crosslinker. Gel samples were prepared at 20 mM of compound **3** in order to increase gelation speed and thereby reduce measurement time.

Upon addition of **P1-35000** a steady increase of the maximum storage modulus (G') was observed with maximum value of 270 kPa at 7.5% of **P1-35000**. Further addition resulted in a sharp decrease of G'.

For the CGC test, a decrease in the CGC was observed upon addition of 6% of **P1-35000**, followed by an increase upon further addition. Above 20%, we obtained vials containing clear solutions instead of gels.

Comparing behaviour of the CGC and rheology, we observe a turning point roughly around 6-7% of **P1-35000**. The storage modulus increases as the CGC decreases, which indicates that less gelator is needed to yield a gel. The observation of this optimum is probably due to the reinforcing effect of the crosslinkers on one hand but also the interference of the bulky PEG on the other hand.

Further visual inspection and mechanical frustration experiments yielded some illustrative insight. In a syringe plunger with an open end we were able to prepare free-standing cylindrical gel samples (**Fig. 4c-e**). We were able to cut the cylinder without losing structural integrity. It was also impossible to perturb gels containing **P1-35000** by means of vortex mixing or manual shaking whereas samples containing commercial PEG 35.000 would

collapse to a liquid state indicating a contribution of more than just physical crosslinks alone. Chemical crosslinks would have to be involved as well.

Increasing the addition of **P1** to 10% create an almost brittle and transparent material which could be manipulated as a solid. The other functionalized PEG chains were either poorly soluble (**P1-300**) or showed disruptive effects in the form of increased CGC values (**P1-2000**, **P1-10.000**). **P1-35.000** was deemed the most interesting polymer of its series.

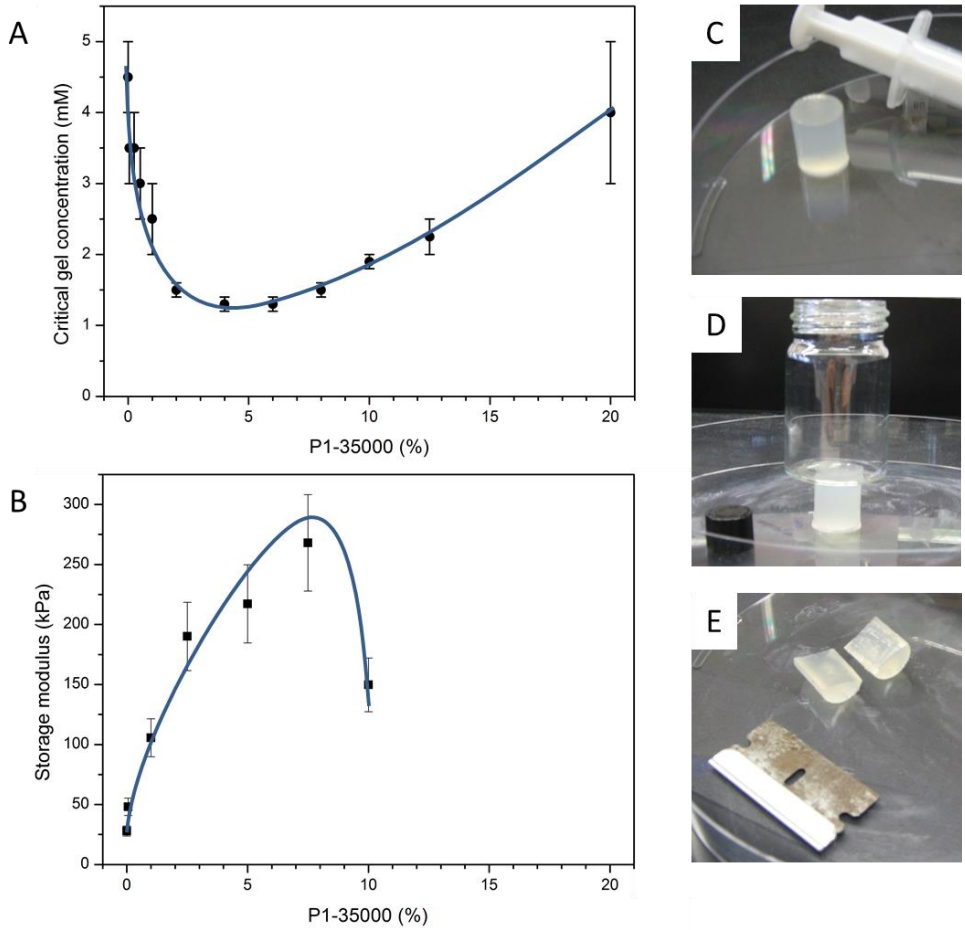

Figure 4 | CGC and storage modulus dependence on percentage of PEG crosslinker P1 added. (**a**) CGC test: dependence on the percentage of aldehydes linked to **P1**. (**b**) Gel formation measured by rheology: the effect of the percentage of aldehydes linked to the PEG crosslinker on the storage modulus. Errors are the standard deviation based on average of 15%; the lines are to guide the eye. The CGC drops drastically upon addition of **P1** (**a**) with a minimum at 4%. The storage modulus (**b**) shows a sharp increase upon addition of 7% of **P1** but shows a decrease upon further increase of crosslinker. (**c-e**) Free-standing gel sample of 20 mM (based on **H1**) (**c**), able to support small objects (**d**) and soft enough to cut with a razor-blade (**e**).

However, upon closer investigation we discovered that crosslinker **P1** was not fully functionalized. Determination of the degree of functionalization using ^{1}H NMR was performed revealing only 40-50% of functionalization on the terminal positions. This meant that not only partial conversion was obtained, but it was also highly likely to have a mixture of di-, mono- and unfunctionalized PEG.

P2 was expected to give different results due to its different structure. CGC tests were performed in order to determine which percentage of added **P2** would give the most interesting effects on the gel network (**Fig. 5**). **P2** was compared to PEG 200.000, a commercial polymer with a similar molecular mass.

A decreasing CGC value compared to pure hydrazone gel was observed, but when compared to a series of control experiments containing unfunctionalized PEG 200.000 there was no significant effect. Gels prepared with 1-3% of **P2** polymer added gave almost the same CGC values as gels prepared with an equal weight amount of PEG 200.000. The gels containing PEG 200.000 yielded weak gels just below these molarities indicating no significant effect. We hypothesized no significant effect was observed due to the ratio between the hydrazide and aldehyde functional groups (H:A ratio). The H:A ratio used in this experiment was 1:2, which we originally used in all previous experiments to ensure full conversion of hydrazide **H1** (**Fig. 5a**). In the case of addition of polymer **P2**, this was probably more of a disadvantage due to a difference in reactivity between the aldehydes on the PEG chain vs the small molecule aldehyde (**A11**). The excess of small molecule **A11** would exclude aldehydes polymer **P2** from reacting with hydrazide **H1.** Both **P2** and PEG 200.000 would only be able to create physical crosslinks, which would explain their similar CGC values.
The experiments were repeated with a H:A ratio of 1:1 in order to prevent exclusion of **P2** from reacting with hydrazide **H1** by the excess of **A11**. This change of strategy was a clear success, resulting in a striking difference between the control experiment and **P2** (**Fig. 5b**). **P2** showed a decrease in the CGC with a plateau value of 1.75 mM whereas the addition of unfunctionalized PEG 200.000 resulted in an increased CGC value.

Rheology experiments were performed at the values corresponding to the beginning of the plateau of the CGC which is around the first few percentages of **P2** (**Fig. 5c**). A decrease in storage modulus was observed with an extra sharp decrease around 1%. The linear visco-elastic region was sustained at higher percentages of strain upon addition of more **P2** meaning that the gels showed an increased elastic behaviour (**Fig. 5d**). This could be explained by the flexibility of the coil shaped PEG polymers which are able to reversibly stretch and relax which cannot be expected from their physically stacked counterparts.

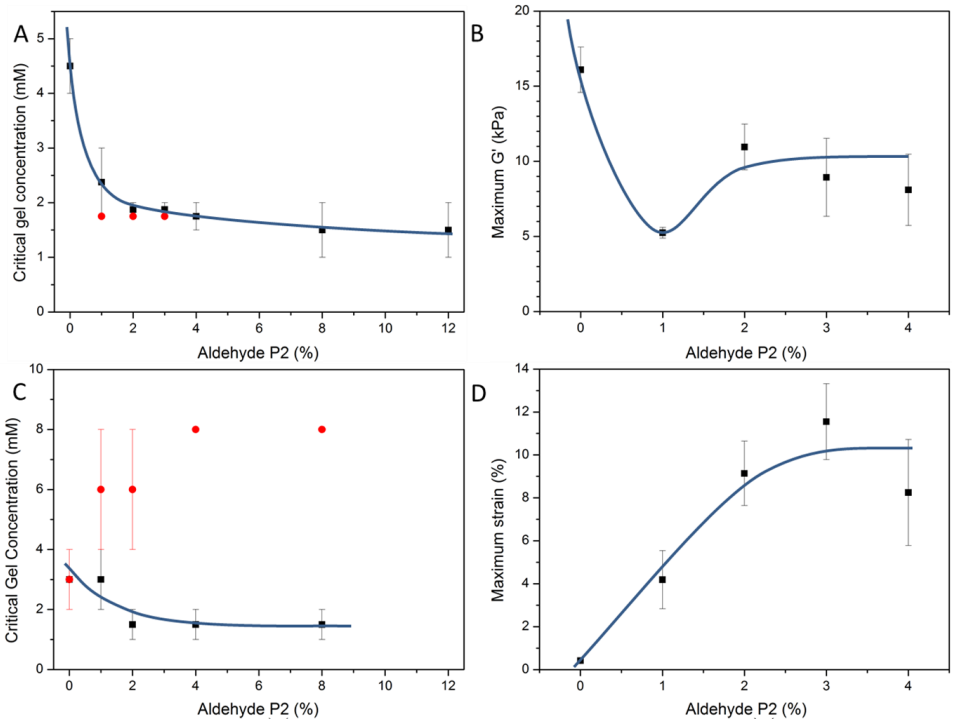

Figure 5 | Critical gel concentration and yield strain dependence on percentage of crosslinker P2 added. (**a,b**) Critical gel concentration test: dependence on addition of **P2** (squares) at 1:2 H:A ratio (**a**) and 1:1 H:A ratio (**b**). The red dots represent the CGC upon addition of an equal amount of unfunctionalized PEG 200.000 (circles). (**b,d**) Gel formation measured by rheology: the effect of the addition of **P2** on the storage modulus and yield strain at 1:1 H:A ratio. (**a**,**c**) The CGC drops drastically upon addition of **P2**, but the addition of **P2** only becomes significant compared to unfunctionalized PEG 200.000 when used in a 1:1 H:A ratio. The storage modulus (**b**) shows a sharp decrease upon minor addition of **P2** but shows some increase again upon higher addition suggesting a transition from a hydrogel to a polymer gel. The yield strain (**d**) is maintained at higher percentages of strain showing more elastic behaviour upon addition of **P2**. Errors are the standard deviation from duplicate experiments; the lines are to guide the eye.

Conclusion

We have synthesized functionalized PEG crosslinkers and introduced them into a hydrogel system which results in improved mechanical properties. The mechanical properties of the resulting gel depended on the ratio and structure of crosslinker that was added. The most successful crosslinker of the **P1** series, **P1-35000**, showed a fivefold increase in storage modulus. The **P2** crosslinker on the other hand increased the gel's yield strain. The method of synthesizing these crosslinkers also creates a wide range of possibilities in which many different chain lengths and degrees of functionalization can be applied. The fine-tuning of hydrogel networks can lead to improved tailored functional materials.

Experimental

General methods & materials

All reagents were purchased from commercials sources and used as provided unless stated otherwise. NMR spectra were recorded on a Bruker Avance-400 spectrometer (399.90 MHz for ^{1}H) at 298 K using residual protonated solvent signals as internal standard. (1H: δ($CHCl_3$) = 7.26 ppm. Gel permeation chromatography was performed using a Shimadzu system equipped with a LC-20AD high-precision solvent delivery unit, RID-10A Highly stable differential refractive index detector with dual temperature control and CTO-20A column oven containing 2 serial PL aquagel-OH MIXED-H columns with MilliQ water a solvent at a flow rate of 1 mL/min at 40°C. All samples were prepared at a concentration of 10 mg/mL in water and compared to PEO calibration standards. All experiments were performed using MilliQ water.

General procedure for PEG mesylate synthesis

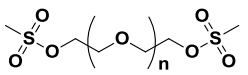

PEG 6000 (30 g, 5.0 mmol) was dissolved in DCM (200 mL) and cooled to 0°C using an ice bath. Triethyl amine (3.5 mL, 25 mmol) was added and the mixture was stirred. Methanesulfonyl chloride (1.9 mL, 25 mmol) was added dropwise to the reaction mixture. After all methanesulfonyl chloride was added the reaction mixture was allowed to warm to RT. After 2 days of stirring water was added (500 mL) and the layers were separated. The aqueous layer was extracted DCM (2 x 500mL). The organic layer were combined and dried over $MgSO_4$, filtered off and concentrated under vacuum. The concentrate was then precipitated in diethyl ether, filtered off and dried under vacuum yielding the PEG mesylate in 89% yield. ^{1}H NMR (400 MHz, $CDCl_3$) δ 4.15 (dd, J = 4.4, 4H, 2xSO_3CH_2), 3.77-3.30 (m, CH_2O), 2.98 (s, 6H, 2xCH_3).

General procedure for P1 crosslinker synthesis

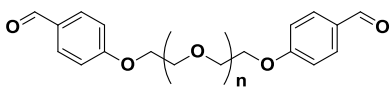

PEG mesylate (20.0 g) was dissolved in DMF (160 mL). 4-Hydroxybenzaldehyde potassium salt (3.93 g) was added and the reaction mixture was heated to 130°C. After consumption of the starting material was observed on ^{1}H NMR the reaction mixture was precipitated in Et_2O (1.5 L). The precipitate was dissolved in DCM (200 mL), filtered and precipitated two more times in Et_2O (2 x 1.5 L). The solid was dried under vacuum yielding **P1** as an off-white solid (10.0 g) in 50% yield. 1H NMR (400 MHz, $CDCl_3$) δ 9.84 (s, 2H, 2xCHO), 7.78 (d, *J* = 8.7, 4H, CH_{Ar}), 6.98 (d, *J* = 8.7, 4H, CH_{Ar}), 4.70 (t, *J* = 4.8, 4H, $PhOCH_2$), 3.88-3.38 (m, OCH_2CH_2).

General procedure for P2 crosslinker synthesis

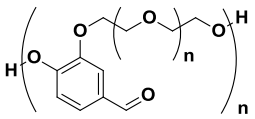

PEG mesylate (13.7 g) was dissolved in DMF (150 ml). To that 3,4-dihydroxybenzaldehyde (468 mg) and K_2CO_3 (1.50 g) were added. The reaction mixture was heated to 130ºC and stirred for five days. The reaction was allowed to cool to RT. The reaction was poured out in to an aqueous 1 M solution HCl (750 mL). The aqueous layer was extracted with DCM (3x 750 ml, 10 vol% ethanol). The organic layers were combined and extracted with water (750 ml) and an aqueous saturated solution of $NaHCO_3$ (750 ml). The organic layer was dried with $MgSO_4$, filtered off and evaporated until a dark brown solution remained. This solution was precipitated twice in Et_2O (2 x 2 L), filtered off and allowed to dry overnight under vacuum to provide the crosslinker (11.0 g, 79%) as a brown fluffy solid. 1H NMR (400 MHz, $CDCl_3$) δ 9.81 (s, 1H, CHO), 9.77 (s, 0.06H, CHO), 7.43 (m, 2H), 6.99 (d, *J* = 7.6, 1H), 4.23 (t, *J* = 4.8, 2H, *p*-$PhOCH_2$), 4.20 (t, *J* = 4.8, 2H, *m*-$PhOCH_2$), 3.90-3.43 (m, OCH_2CH_2).

General procedure for gel preparation

The procedure is explained for the **H1** and **A11** compounds but holds for any combination of hydrazides and aldehydes. Also, the functionalised gel samples were prepared using this procedure, including the desired functional aldehyde by replacing that amount of aldehyde **A11**. The trishydrazide (**H1**) (40 mM) and aldehyde (**A11**) (240 mM) derivatives were dissolved in aqueous 100 mM sodium phosphate buffer at pH 5. After mixing appropriate amounts of the two stock solutions, the resulting mixture was allowed to react overnight. All experiments were performed at room temperature. Depending on the type of crosslinker used gels were prepared in either a 1:2 (**P1**) or 1:1 (**P2**) functional group molar ratio of the hydrazide an aldehyde which means that there is an initial 1:6 (**P1**) or 1:3 (**P2**) molar ratio between **H1** and **A11**.

Rheology

Oscillatory experiments were performed using a AR-G2 rheometer from TA Instruments in a strain-controlled model the rheometer was equipped with a steel plate-and-plate geometry of 40 mm diameter and a water trap. The temperature of the plates was controlled at 25±0.2°C. Time sweep measurements were performed at a frequency of 1 Hz while applying 0.05% strain. The reported G' value is where G' reaches a plateau value. Frequency sweep measurements were performed at 0.05 % strain with frequency levels sweeping from 10^3-10^{-3} Hz. Strain sweep measurements were performed at a frequency of 1 Hz and strain levels sweeping from 0.05%-300%. The reported strain percentage is where G' begins its decrease from the plateau level. During measurements, the storage and loss moduli G' and G" were followed as a function of the time. Total volume – 1 mL and gelator concentration = 20 mM (20 mM of hydrazide derivative).

References

1. Hirst, A. R., Escuder, B., Miravet, J. F. & Smith, D. K. High-Tech Applications of Self-Assembling Supramolecular Nanostructured Gel-Phase Materials: From Regenerative Medicine to Electronic Devices. *Angew. Chem. Int. Ed.* **47,** 8002–8018 (2008).
2. Aida, T., Meijer, E. W. & Stupp, S. I. Functional Supramolecular Polymers. *Science* **335,** 813–817 (2012).
3. Yan, C. & Pochan, D. J. Rheological properties of peptide-based hydrogels for biomedical and other applications. *Chem. Soc. Rev.* **39,** 3528 (2010).
4. Cornwell, D. J. & Smith, D. K. Expanding the scope of gels – combining polymers with low-molecular-weight gelators to yield modified self-assembling smart materials with high-tech applications. *Mater Horiz* **2,** 279–293 (2015).
5. Mishra, S. B. & Mishra, A. K. in *Polymeric Hydrogels as Smart Biomaterials* (ed. Kalia, S.) 1–17 (Springer International Publishing, 2016).
6. Adhia, Y. J., Schloemer, T. H., Perez, M. T. & McNeil, A. J. Using polymeric additives to enhance molecular gelation: impact of poly(acrylic acid) on pyridine-based gelators. *Soft Matter* **8,** 430–434 (2012).
7. Way, A. E. *et al.* Enhancing the Mechanical Properties of Guanosine-Based Supramolecular Hydrogels with Guanosine-Containing Polymers. *Macromolecules* **47,** 1810–1818 (2014).
8. Poolman, J. M. *et al.* A toolbox for controlling the properties and functionalisation of hydrazone-based supramolecular hydrogels. *J Mater Chem B* **4,** 852–858 (2016).
9. Gothard, C. & Grzybowski, B. A Cost-Effective, Column-Free Route to Ethylene Glycol Oligomers EG6, EG10, and EG12. *Synthesis* **44,** 717–722 (2012).
10. Bayer, E., Zheng, H. & Geckeler, K. Functionalization of soluble polymers: 4. Synthesis of dichloro- and di(4-Formylphenyloxyethyl) poly(oxyethylene). *Polym. Bull.* **8,** (1982).
11. Harris, J. M. *et al.* Synthesis and characterization of poly(ethylene glycol) derivatives. *J. Polym. Sci. Polym. Chem. Ed.* **22,** 341–352 (1984).
12. Sayed, O. M., Mekky, A. E. M., Farag, A. M. & Elwahy, A. H. M. 3,4-Dimethyl-2,5-functionalized thieno[2,3- *b*]thiophenes: versatile precursors for novel bis-thiazoles. *J. Sulfur Chem.* **36,** 124–134 (2015).
13. Mitchell, P. *Tool and Manufacturing Engineers Handbook: Plastic Part Manufacturing*. (Society of Manufacturing Engineers, 1996).

Summary

Self-assembly is one of the most important processes taking place around us. Molecules work together to spontaneously form larger organised structures, such as molecular materials. The organisation of the structure in the end depends on the properties of the molecules at the start. These building blocks contain 'instructions' in the form of functional groups that have attractive and repulsive forces.

Especially in the field of hydrogels self-assembly is widely used technique. Building blocks in the form of hydrogelator molecules, assemble into fibres in water. Once the fibres are big enough they form a continuous network and keep the water in place.

However, making hydrogels brings forth a lot of unpredictability. Small changes in the building blocks may result in large changes such as different organisations or no organisation at all.

Besides, it is proven that reaction kinetics also play an important role in the formation of the organisation. The rate at which building blocks are provided determines the rate at which the final organisation is formed. This also affects the organisation and its properties. In order to bring this unpredictability to a minimum we must improve our understanding how the building blocks and the final organisation are related to each other. By improving our control over the structure and the self-assembly process, it will become easier to design molecular materials for certain purposes.

In this thesis we make use of a hydrogelator which is built up from smaller building blocks. A hydrazide core reacts with three aldehyde groups which form the final hydrogelator. Buy constructing the hydrogelator from smaller building blocks it becomes easier to modify the molecular structure. Also, the rate at which these building blocks react can be controlled by using a catalyst. We study the effects of the catalyst, but addition of other building blocks to the organisation and its mechanical properties.

First, we discuss elaborately how the hydrogels are discussed. The synthesis of the hydrazide as well as the aldehyde are discussed in a step-by-step procedure, followed by a series of analytical techniques, such as rheology and confocal laser scanning microscopy. The analytical procedures are described as such so they can be applied on any hydrogel. This chapter is a manual for fellow scientists from different fields who are interested in working with hydrogels.

Next, we discuss the properties of the hydrogelator system by hand of different catalytic conditions as well as functionalised building blocks. Three catalytic conditions have been studied, namely pH 5, pH 7 and pH 7 with aniline. The hydrogels show reduced gelation time, improved mechanical properties and lower critical gel concentration values at pH 5 and pH7 with aniline, 4.5 mM and 3.8 mM respectively. Microscopy reveals the formation of a homogeneous branched network of fibres under both conditions. Both catalytic conditions show a positive effect. However, at high concentrations of of aniline (>10 mM)

the mechanical properties deteriorated due to the formation of an aniline-byproduct. From all perspectives both catalysed gels showed better performance compared to the 'uncatalyzed' gel at pH 7.

After studying the catalytic conditions, we studied the addition of different functionalisations to the hydrogel. We studied a series of similar building blocks to see what the effect of the structure on the gelation was. By mixing hydrazides and aldehydes we obtained the hydrazone structure. The hydrazone structure would either form a gel, a precipitate or a solution. From these observations we concluded which structures of the hydrazones were to crystalline, hydrophobic or hydrophilic. Para-substituted aldehydes performed better than meta-substituted aldehydes in forming gels, but di-substituted aldehydes were too water-soluble. Also, the series of bishydrazides showed poor gelation when the carbon chain length was longer. Also, the bishydrazides with an odd carbon chain length performed worse compared to the bishydrazides containing an even carbon chain.

The hydrogels were functionalised by adding a small percentage of functionalised molecules, such as azides, thiols, and acetylene groups. On these molecules we attached fluorescent probes which made it possible to image the hydrogel network itself but also e.g. cells attached to the network. Using confocal laser scanning microscope, we were able to image the cells and the gel network orthogonally.

Finally, we added water-soluble polymers to the gel network. Functionalised PEG was used to form covalent bonds between the individual fibres in order to reinforce the network and improve the mechanical properties. Depending on the structure of the added crosslinker there was an increase in storage modulus or yield strain.

This hydrogelator shows us that we can obtain multiple properties using only one system. The desired properties can be obtained either by controlling the catalytic conditions or by choosing the right building blocks. By bringing these properties together in one single hydrogelator system we offer an extensive toolbox which can be used to improve the design of molecular materials.

Samenvatting

Zelf-assemblage is een van de belangrijkste processen dat om ons heen plaatsvindt. Moleculen werken samen om spontaan grotere georganiseerde structuren te vormen, zoals moleculaire materialen. De organisatie die de structuur uiteindelijk aanneemt hangt af van de eigenschappen van de moleculen aan het begin. Deze bouwstenen bevatten 'instructies' in de vorm van functionele groepen die bepaalde aantrekkende en afstotende krachten met zich meebrengen.

Vooral in de wereld van hydrogels is zelf-assemblage een veelgebruikte techniek. Bouwstenen, in de vorm van hydrogelatormoleculen, assembleren tot fibers in water. Zodra de fibers groot genoeg zijn vormen ze samen een continu netwerk en houden ze het water op zijn plaats.

Echter, het maken van hydrogels brengt veel onvoorspelbaarheid met zich mee. Kleine veranderingen aan de bouwstenen kunnen eindigen in grote veranderingen zoals hele andere organisatievormen of zelfs helemaal geen organisatie.

Daarnaast is bewezen dat reactiekinetiek een belangrijke rol speelt in de vorming van een organisatie. De snelheid waarmee bouwstenen worden aangeleverd bepaalt de snelheid waarmee uiteindelijke organisatie zich vormt. Dit heeft ook effect op de eigenschappen van de organisatie.

Om deze onvoorspelbaarheid zo klein mogelijk te maken moeten we beter leren begrijpen hoe de bouwstenen en de uiteindelijke organisatie in relatie tot elkaar staan. Door de structuur en de vorming van de zelf-assemblage beter te kunnen sturen wordt het makkelijker om moleculaire materialen voor een bepaald doel te ontwerpen.

In dit proefschrift maken we gebruik van een hydrogelator dat is opgebouwd uit kleinere bouwstenen. Een hydrazidekern reageert met drie aldehydegroepen waaruit de uiteindelijke hydrogelator gevormd wordt. Door de hydrogelator op te bouwen uit kleinere bouwstenen wordt het eenvoudiger om de molecuulstructuur aan te passen. Ook de snelheid waarmee de bouwstenen met elkaar reageren, kan door middel van een katalyator gestuurd worden. We bestuderen de effecten van de katalysator, maar ook de toevoeging van andere bouwstenen op de organisatie en de bijbehorende mechanische eigenschappen.

Eerst bespreken uitgebreid hoe de hydrogels zijn bereid. De synthese van zowel het hydrazide als het aldehyde worden in een stap-voor-stapprocedure behandeld. Daarna volgen een aantal analysetechnieken, zoals rheologie en confocale laserscanmicroscopie. De werkwijzen voor de analysetechnieken zijn dusdanig opgesteld dat deze op iedere hydrogel kunnen worden toegepast. Dit hoofdstuk is een handleiding voor medewetenschappers van buiten het veld die geïnteresseerd zijn in het werken met hydrogels.

Vervolgens bespreken de eigenschappen van het hydrogelatorsysteem aan de hand van zowel verschillende katalytische condities als gefunctionaliseerde bouwstenen. Drie katalytische omstandigheden zijn onderzocht, namelijk bij pH 5, pH 7 en pH 7 met aniline. De hydrogels vertonen kortere gelatietijden, betere mechanische eigenschappen en lagere kritieke gelconcentratiewaarden bij pH 5 en pH 7 met aniline, respectievelijk 4,5 en 3,8 mM. Microscopie toonde onder beide omstandigheden een homogeen vertakt netwerk van fibers aan. Beide katalytische omstandigheden hadden een gunstig effect. Echter, bij hoge concentraties aniline (>10 mM) namen de mechanische eigenschappen van de hydrogel af door het ontstaan van een aniline-bijproduct. Op alle fronten excelleerden de gekatalyseerde hydrogels ten opzichte van de 'ongekatalyseerde' gel bij pH 7.

Na de katalystische omstandigheden te hebben onderzocht zijn we begonnen met het bestuderen van de structuur en het toevoegen van diverse functionalisaties aan de hydrogel. We hebben een serie van vergelijkbare bouwstenen onderzocht om zo te zien wat het effect van de structuur op de gelatie is. Door de hydrazides en aldehydes met elkaar te mengen verkregen we de hydrazonstructuur. Vervolgens vormde deze hydrazonen een gel, een neerslag of een oplossing. Uit deze observaties concludeerden wij welke structuren van de hydrazonen te kristallijn, hydrofoob of hydrofiel waren. Zo bleken para-gesubstitueerde aldehydes beter te presteren dan meta-gesubstitueerde aldehydes in het vormen van hydrogels, maar waren di-gesubstitueerde aldehydes juist te goed oplosbaar in water. De reeks bishydrazides vertoonde slechte gelatie bij een langere koolstofstaart. Daarnaast presteerde de bishydrazides met een koolstofstaart van oneven lengte slechter dan de bishydrazides met een koolstofstaart van even lengte.

De hydrogels werden gefunctionaliseerd door kleine percentages gefunctionaliseerde moleculen toe te voegen, zoals azides, thiolen, of acetyleengroepen. Aan deze moleculen werden vervolgens weer fluorescente probes vastgezet wat mogelijk maakte om niet alleen het hydrogelnetwerk in beeld te brengen, maar ook cellen die op het netwerk waren gefixeerd. Met behulp van confocale laserscanmicroscopie waren we in staat de cellen en het gelnetwerk onafhankelijk van elkaar in beeld te brengen.

Tenslotte hebben we water-oplosbare polymeren aan het gelnetwerk toegevoegd. Gefunctionaliseerd polyethyleenglycol werd gebruikt om covalente bindingen te vormen tussen de individuele gelfibers met als doel om het netwerk te verstevigen en de mechanische eigenschappen te verbeteren. Afhankelijk van de structuur van de crosslinker die werd toegevoegd verhoogde de opslagmodulus of de vervormingsgrens van de hydrogels, wat inhoudt dat de gel bestendiger is tegen spanning en vervorming.

Deze hydrogelator laat zien dat met één systeem meerdere eigenschappen eenvoudig bereikbaar zijn. De gewenste eigenschappen kunnen bereikt worden door te sturen met de juiste katalytische omstandigheden of het kiezen van de juiste bouwstenen. Het samenbrengen van al deze eigenschappen in één gelatorsyteem biedt een uitgebreide gereedschapskist in het beter ontwerpen van moleculaire materialen.

Acknowledgements

Your colleagues are those that keep you sane during the day, so better hope you have good ones. During my time here, I spent time with more or less two 'generations' of colleagues. Even though some of them are long gone, I would still like to thank them for all the parties, dinners and our traditional Thursday nights going from E-cast to Minos to 't Klooster and somehow managing to cycle back home.

Jan, bedankt voor de mogelijkheid om te kunnen promoveren. Ik ben iets langer blijven plakken dan verwacht, zeker als je mijn masterstage er nog bij optelt. We hebben het nog aardig ver geschopt ondanks dat ik soms het idee had dat jij Grieks sprak en ik Latijn. Voortaan leg ik mijn voeten ook op het bureau.
Rienk, bedankt voor de wekelijkse begeleiding. Meestal wist jij door vragen met vragen te beantwoorden meer helderheid te scheppen. Echter, de vraag om om 9.00 uur achter mijn bureau te zitten weigerde ik uiteindelijk te beantwoorden. Deze uitdaging is voor de volgende werkgever.
Job, je bent het langst weg van allemaal, maar jij bent wel degene geweest die mij hier wegwijs heeft gemaakt. Bedankt voor wat je mij destijds hebt geleerd.
Christophe, bedankt voor jouw advies, en de studenten.
Wouter, als ik een euro kreeg voor iedere keer dat we een andere mening over iets hadden. Wij zijn samen lang de gangmakers geweest, hetzij om het lab op orde houden, hetzij om bier drinken. Bedankt voor alle gezelligheid en discussies, van beide was er een hoop.
Dainius, you're a riddle wrapped in a mystery inside an enigma. You were great company even though you didn't always speak out. Either that or you would say something so weird that would even puzzle me. I'll never forget you bragging about getting used to drinking special beers and not showing up for work the next day, or switching Job's brand new monitor with yours. You've demonstrated that chocolate croissants are the cornerstone of a scientist's breakfast.
Simge, you've shown us all that cooking skills range from the lab to the kitchen, from bright coloured molecules to plates full of dolma. No-one can resist your food. Turkish coffee was our daily ritual, even long after you left. Your synthetic advice was always valuable and unbreakable sunny attitude was most welcome.
Marta, my first neighbour in the lab, until the ceiling started to collapse. It was fun working next to you, showing your balls to everyone. It was also fun imitating you! Then again, we both had fun imitating others. Boz of zem!
Manu, our number one party girl. Your ability to take the lead in organising things together is something everyone appreciated. On Cyprus, you even managed to cram 9 holidays into 6. "I want to party hard" sums it up pretty well, just like "dancing with you was investment". Never a dull moment when you're around.

Roman, I believe we've used almost every anecdote against you that you brought from Georgia. Whether it was about the fact that wine comes from Georgia or the story about the chicken. I'm sure everyone is just jealous because you have real stories to tell. It was fun having you as a colleague, but I'm sure we will run into each other plenty of times.
Eszter, if there's a student in our group that deserves notice, it's definitely you. Even though you were a master student, you joined all the parties, drinks, and even the group trip. You were definitely one of us. I still have your Hungarian beer coaster dictionary and you will probably recognize the last sentence of this book. I knew it would be of good use!
Jerre, grappig genoeg bleken zowel onze werk- als uitgaanssfeer aan elkaar te grenzen, evenals onze muzieksmaken. WOB WOB WOB! Wij zijn nog niet van elkaar af.
Elena, glad you brought back the party vibe to the group while you were here. Don't let Germany make you too serious. SCHMETTERLING! Either you will laugh in Spanish or agree in German now.
Chandan, there's no better way to surprise your colleagues than by becoming a father. We didn't expect you were expecting. Hope everything is fine!
Emma, I believe you're the most senior PhD now. I'm sure you will show your best behaviour towards the other PhD's at all times, just like I did. Sorry about all the Ikea jokes, but they were so easy to put together.
Lars, eindelijk geen discussie meer over de muziek op het lab! Gelukkig konden we wel samen avonden aan elkaar draaien in Paard van Troje. Wat dat betreft ben je ben wel de meest random persoon met de meest random hobby's. Van DJ'en en motorrijden tot tuinhuisjes bouwen, je bent van alle markten thuis totdat het cool wordt natuurlijk.
Matija, master from a to z, or should I say from alcohol to zen. Nothing gets you stressed or scared. I believe you know very well what is most important in life, like keeping it simple. I'm sure we'll have another drink sometime.
Serhii, the silent driving force within our group. I bet your patience has been tested a lot through the years. Either, waiting for dextran to dissolve or with the rest of us in Barcelona. Thanks for your help, especially on working with these bloody polymers.
Fanny, groot voorstander van bier drinken, alleen moest je steeds sporten. Mocht ik nog een keer moeten budgetteren dan wil ik het graag van jou leren.
Susan, "Ow god, wat heeft hij nou over mij geschreven?". Waarschijnlijk moet je nu al lachen, Haha! Wat ik wil zeggen is: laat je vooral niet gek maken, dan komt het wel goed.
Sang-Jae, energie voor twee en een planning voor drie. Ze zeggen dat de meeste studenten tijd kosten maar in jouw geval was dat gelukkig niet zo. Bedankt voor jouw bijdrage. Loop jezelf vooral niet voorbij, daar weet ik zo onderhand alles van.
Sander, iedere dag forensde jij je de pleuris om bij mij op kantoor te zitten. Ik doe het je niet na. Bedankt voor alle nuttige en leuke discussies. Het hield me zowel van als aan het werk.

Frank, aangezien sarcasme op papier moeilijk overdraagbaar is moet ik hier maar iets serieus schrijven. Het was leuk om met jou samen te werken. Discussiëren met jou hielp goed in het snel werken naar een concreet resultaat.
Vincent, met 3 beeldschermen maakte je altijd veel indruk. Vermoedelijk had je op één scherm altijd een internetmeme openstaan. Ik weet nog steeds niet hoeveel kleuren All Stars jij hebt. Vuurbal, jongûh!
Vasu, master in showmanship. You don't often see the combination of being an artist and an exact scientist. Speaking of combinations, you could actually filibuster through your defence by singing. Your ability to flood every conversation with facts is quite remarkable. Too bad you don't drink for you could win the pub quiz.
Cansel, dearest of all my colleagues. You've made the lab colourful again with your HBCs. It was great having you around, in good times as well as bad. Who knows, maybe I'll buy you dinner someday.
Tomasz, finally someone who appreciates board games. Glad you were here for the last couple of months. We finally managed to play Secret Hitler and some more Cards against Humanity. Drive safely now!
Angie, or was it Maria? I still think you should switch places for a day, just to confuse everyone. Good luck! I'm sure you'll manage.
Kai, always laughing and in a good mood. Good effort for drinking a few beers with us even though you're not used to it.
Yiming, thanks for all the nice discussions in the office.
Qian and Bowen, last but not least. Good luck!
Marcel, Ben, Louw, Mieke, Eduardo, Ger en Stephen, jullie ook bedankt voor alle hulp, gevraagde en ongevraagde adviezen, en natuurlijk de gezellig sfeer, vooral om 15.00 uur bij de koffie.

Credits gaan naar mijn baancode en het geld dat erop stond. TCWB53, first come, first serve!

Natuurlijk wil ook mijn familie, Pa, Ma, Pepijn, Merijn en Caroline bedanken voor alle steun.

Tenslotte bestaat er ook een leven buiten het werk en daarom wil ik al mijn vrienden bedanken waarmee ik die tijd heb doorgebracht. Jullie hielden mij geestelijk op de been wanneer ik weer eens uit de rails dreigde te lopen. Ondanks al mijn grappen lopen jullie nog steeds niet van mij weg:
Ben, Brian, Rico, Emmy, Judith, Willem-Pieter, Sterre, Christel, Lisanne, Larissa, Thomas B, Rik, Sanne P, Artjom, Sanne M, Donya, Thierry, Thomas S, Berry, Chris, Elian, Jelle, Sjors, Joelle, Dennis, Rogier, Renske, Bart, Michael, Annelous, Ricardo, Daniela, Natalie, Natan, Karin, Artie, Imelda, Renée, Rowan, Thijs, Astrid, Maikel, Ines, Floris, Petra, Maarten, Sijmen, Martine, Linda, Sabrina, Jelena, Martijn, Ronald, Alex, Niels, Nathalie, Renate, Fiona, Ceylo, Joe, Ian, Roderick en Salome.

About the author

Jos was born on the 31st of August 1988 in the city of Schiedam. In 2004, he received his HAVO-diploma and decided to study the chemistry bachelor's degree (HLO) at the Hogeschool Rotterdam with a specialization in organic chemistry. His first internship took place at Leiden University in the bio-organic synthesis group where he worked on the SAWU-multicomponent (Staudinger/Aza-Wittig/Ugi) reaction for the synthesis of iminosugars. A final internship took place at Organon N.V. in Oss where he explored an alternative synthetic route for the production of Etonogestrel, an active pharmaceutical ingredient used in various contraceptives. After obtaining his bachelor degree in 2008 he returned to Leiden University to study a master's degree in chemistry with a specialization in design & synthesis. During his first internship in the bio-organic synthesis group he worked on conformationally restricted ceramide analogues as potential glucosyl ceramide inhibitors. His final internship took place at the Delft University of Technology in the research group of prof. dr. Jan van Esch and covered the synthesis of crosslinkers for the modification of low-molecular-weight hydrogels. After graduating in 2011, Jos continued at the Delft University of technology as a PhD-student which resulted in the thesis you are currently reading.

List of publications

Unbiased Tracking of the Progression of mRNA and Protein Synthesis in Bulk and in Liposome-Confined Reactions

Pauline van Nies, Zohreh Nourian, Maurits Kok, Roeland van Wijk, Jonne Moeskops, Ilja Westerlaken, Jos M. Poolman, Rienk Eelkema, Jan H. van Esch, Yutetsu Kuruma, Takuya Ueda and Christophe Danelon

Chembiochem **14,** 1963–1966 (2013)

Catalytic control over supramolecular gel formation

Job Boekhoven, Jos M. Poolman, Chandan Maity, Feng Li, Lars van der Mee, Christophe B. Minkenberg, Eduardo Mendes, Jan H. van Esch and Rienk Eelkema

Nature Chemistry **5,** 433–437 (2013)

Variable gelation time and stiffness of low-molecular-weight hydrogels through catalytic control over self-assembly

Jos M. Poolman, Job Boekhoven, Anneke Besselink, Alexandre G. Olive, Jan H. van Esch and Rienk Eelkema

Nature Protocols **9,** 977–988 (2014)

A toolbox for controlling the properties and functionalisation of hydrazone-based supramolecular hydrogels

Jos M. Poolman, Chandan Maity, Job Boekhoven, Lars van der Mee, Vincent A.A. le Sage, G.J. Mirjam Groenewold, Sander I. van Kasteren, Frank Versluis, Jan H. van Esch and Rienk Eelkema

Journal of materials chemistry B **4,** 852–858 (2016)

Catalysis of supramolecular hydrogelation

Fanny Trausel, Frank Versluis, Chandan Maity, Jos M. Poolman, Matija Lovrak, Jan H. van Esch and Rienk Eelkema

Accounts of chemical research **49,** 1440-1447 (2016)

Negatively charged lipid membranes catalyze supramolecular hydrogel formation

Frank Versluis, Daphne M. van Elsland, Serhii Mytnyk, Dayinta L. Perrier, Fanny Trausel, Jos M. Poolman, Chandan Maity, Vincent A. A. le Sage, Sander I. van Kasteren, Jan H. van Esch and Rienk Eelkema

Journal of the American chemical society **138,** 8670-8673 (2016)

Crosslinker-Induced Effects on the Gelation Pathway of a Low Molecular Weight Hydrogel

Willem E.M. Noteborn, Damy N.H. Zwagerman, Victorio Saez Talens, Chandan Maity, Lars van der Mee, Jos M. Poolman, Serhii Mytnyk, Jan H. van Esch, Alexander Kros, Rienk Eelkema and Roxanne E. Kieltyka

Advanced Materials (2017)

Activation of an organocatalyst by a chemical signal

Fanny Trausel, Chandan Maity, Jos M. Poolman, Davey S.J. Kouwenberg, Antonio M. Grande, Frank Versluis, Jan H. van Esch, Rienk Eelkema

Submitted to *Nature Communications*

List of abbreviations

Ac	acetyl
APT	attached proton test
AU	arbitrary units
bs	broad singlet
CCD	charge-coupled device
CGC	critical gel concentration
CLSM	confocal laser scanning microscopy
ConA	concanavalin A
Cryo-TEM	cryo-transmission electron microscopy
Cy5	cyanine 5
d	doublet
DAPI	4',6-diamidino-2-phenylindole
DCM	dichloromethane
DMEM	Dulbecco's modified Eagle medium
DMF	N,N-dimethylformamide
DMSO	dimethylsulfoxide
DNA	deoxyribonucleic acid
EDTA	ethylenediaminetetraacetic acid
EG	ethylene glycol
ESI	electron spray ionization
Et	ethyl
et al.	et alii (and others)
FITC	fluorescein isothiocyanate
FBS	foetal bovine serum
Fmoc	9H-Fluoren-9-ylmethoxycarbonyl
G'	storage modulus
G"	loss modulus
H:A	hydrazide : aldehyde ratio
HOSu	N-hydroxysuccinimide
HPLC	high-performance liquid chromatography
IPTG	isopropylthiogalactoside
J	coupling constant
kPa	kilopascal
LMWG	low-molecular-weight gel
m	multiplet
M	molar
Me	methyl
MeOH	methanol
MHz	megahertz
mM	millimolar
µM	micromolar
MS	mass spectrometry
NMR	nuclear magnetic resonance
Ova	ovalbumin
PBS	phosphate-buffered saline
Pd/C	palladium (10%) on activated carbon
PDMS	polydimethylsiloxane
ppm	part per million
PTFE	polytetrafluoroethylene
q	quartet
rt	room temperature
s	singlet
SEM	scanning electron microscopy
t	triplet
Ts	para-toluenesulfonyl
UV-Vis	ultraviolet-visible

“Viszlát, minden idök legfiatalabb örült tudósa!”

-Eszter Makkos